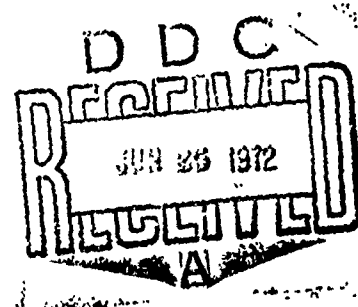# NAVAL POSTGRADUATE SCHOOL
Monterey, California

THESIS

INLET DISTORTION, VORTICITY, AND STALL

IN AN AXIAL-FLOW COMPRESSOR

by

Clinton Jefferson Farmer

Thesis Advisor: A. E. Fuhs

March 1972

Approved for public release; distribution unlimited.

14. KEY WORDS	LINK A		LINK B		LINK C	
	ROLE	WT	ROLE	WT	ROLE	WT
turbomachinery						
axial-flow compressors						
vorticity						
turbulence						
secondary flows in axial-compressors						
compressor stall						
compressor stall margin						
inlet flow distortion						
inlet pressure fluctuations						
inlet turbulence						
inlet vorticity in axial compressors						
stall-inducing flow distortion						
distortion factor						
distortion tolerance						

DD FORM 1473 (BACK)
1 NOV 65

S/N 0101-807-6821

139

Security Classification

A-31409

DOCUMENT CONTROL DATA - R & D

(Security Classification of title, body of abstract and indexing annotation must be entered when the overall report is classified)

1. ORIGINATING ACTIVITY (Corporate author)	2a. REPORT SECURITY CLASSIFICATION
Naval Postgraduate School Monterey, California 93940	Unclassified
	2b. GROUP

3. REPORT TITLE

Inlet Distortion, Vorticity, and Stall in an Axial-Flow Compressor

4. DESCRIPTIVE NOTES (Type of report and inclusive dates)

Master's Thesis; March 1972

5. AUTHOR(S) (First name, middle initial, last name)

Clinton Jefferson Farmer

6. REPORT DATE	7a. TOTAL NO. OF PAGES	7b. NO. OF REFS
March 1972	139	74

8a. CONTRACT OR GRANT NO.	9a. ORIGINATOR'S REPORT NUMBER(S)
b. PROJECT NO.	
c.	9b. OTHER REPORT NO(S) (Any other numbers that may be assigned this report)
d.	

10. DISTRIBUTION STATEMENT

Approved for public release; distribution unlimited.

11. SUPPLEMENTARY NOTES	12. SPONSORING MILITARY ACTIVITY
	Naval Postgraduate School Monterey, California 93940

13. ABSTRACT

A new approach to defining inlet distortion factors for axial-flow compressors is presented. A summary of past analyses of inlet distortion, along with a brief review of flow-distortion definition and compressor performance, provides a background for the proposed theory. Inlet flow-distortion in terms of total-pressure fluctuations at the compressor face is converted to vorticity. The effects of vorticity on the internal aerodynamics of the compressor are investigated with some approximate calculations included to indicate the validity of this approach. Refinements and alternate solutions to the theory which could lead to definition of a more comprehensive and reliable definition of stall-inducing inlet distortion are included. ( ) ≃ʄ .

DD FORM 1473 (PAGE 1)
1 NOV 65

S/N 0101-807-6811

A-31408

Inlet Distortion, Vorticity, and Stall

in an Axial-Flow Compressor

by

Clinton Jefferson Farmer
Lieutenant, United States Navy
B.S., United States Naval Academy, 1966

Submitted in partial fulfillment of the
requirements for the degree of

MASTER OF SCIENCE IN AERONAUTICAL ENGINEERING

from the

NAVAL POSTGRADUATE SCHOOL
March 1972

Author _____

Approved by: _____
Thesis Advisor

_____
Chairman, Department of Aeronautics

_____
Academic Dean

ABSTRACT

A new approach to defining inlet distortion factors for axial-flow compressors is presented. A summary of part analyses of inlet distortion, along with a brief review of flow-distortion definition and compressor performance, provides a background for the proposed theory. Inlet flow-distortion in terms of total-pressure fluctuations at the compressor face is converted to vorticity. The effects of vorticity on the internal aerodynamics of the compressor are investigated with some approximate calculations included to indicate the validity of this approach. Refinements and alternate solutions to the theory which could lead to definition of a more comprehensive and reliable definition of stall-inducing inlet distortion are included.

TABLE OF CONTENTS

LIST OF TABLES

LIST OF FIGURES

ACKNOWLEDGEMENTS

I. INTRODUCTION

Engine stall has always been a problem of varying magnitude in jet powered aircraft employing axial-flow compressors. At present aircraft gas turbine performance is largely limited by flow separation and surge in the compressor. Generally, highest compressor efficiencies occur near the point of flow breakdown (stall), and so the design margin between normal operation and stall is kept to a practical minimum. A compressor's ability to remain below this stall limit is significantly affected by the amount and degree of distortion in its inlet flow. Inlet flow distortion has been called by many names, all of which basically describe variations in total-pressure, total-temperature, or velocity over the inlet cross-section. Previously, inlet flow distortion has been at a level which the compressor could handle without a serious degradation in performance. However, with the greater speeds and performance demanded of today's high-specific-energy turbomachines, inlet distortion at the compressor face can alone be great enough to cause compressor stall and surge. One prominent source of distortion has been traced to shock-wave/boundary-layer interactions within the inlet. Others are steam ingestion, pressure transients due to afterburner light-off, ordnance discharges, etc. The magnitude of the problem in some recent aircraft designs has caused much research to be conducted in this area, specifically correlating maps of total-pressure variations at the compressor face to engine surge. The results of this work have yielded an immense amount of empirical data. However, reduction of these data has yet to provide a technique which adequately describes the distortion accommodation of a given engine-inlet configuration over its entire

range of operation.   In contrast to empirical correlations yielding a
statistical yes-no answer to the question of whether or not the engine
will stall, methods are needed which link stall criteria for a blade
element to distortion patterns.   This paper presents a new approach to
analyzing already existing data and provides evidence of a better
insight into the actual fluid mechanics involved in the problem.

II. STATEMENT OF PROBLEM

A. AXIAL COMPRESSOR PERFORMANCE[1]

The performance of an axial-flow compressor such as found on aircraft turbojet engines is best described by its steady-state performance map. Figure 1 illustrates a typical compressor map. "Pressure ratio" is exit total-pressure to inlet total-pressure and "corrected airflow" is engine mass-flow rate corrected for total-temperature and total-pressure.
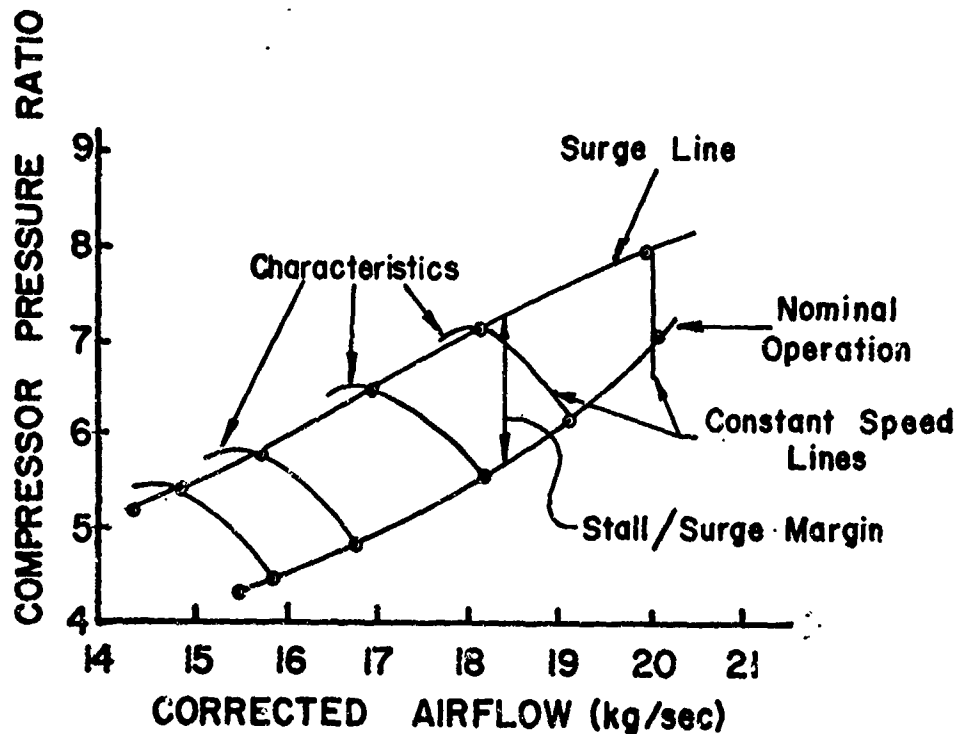
FIG. I   COMPRESSOR PERFORMANCE MAP
J85- GE- 13 [adapted from Ref.2]

---

[1]The information and examples in this section were adapted from a report by Brimelow [Ref. 1].

The surge line defines the maximum pressure ratios which the compressor can achieve throughout its range of rotor speeds. Operation above this line is accompanied by a drastic reduction in pressure ratio. This is called "surge," and it is caused by excessive aerodynamic blade stall.

The stability of a system is determined by the slope of its pressure ratio/flow characteristic. Consider steady operation at point M_1 of Fig. 2.
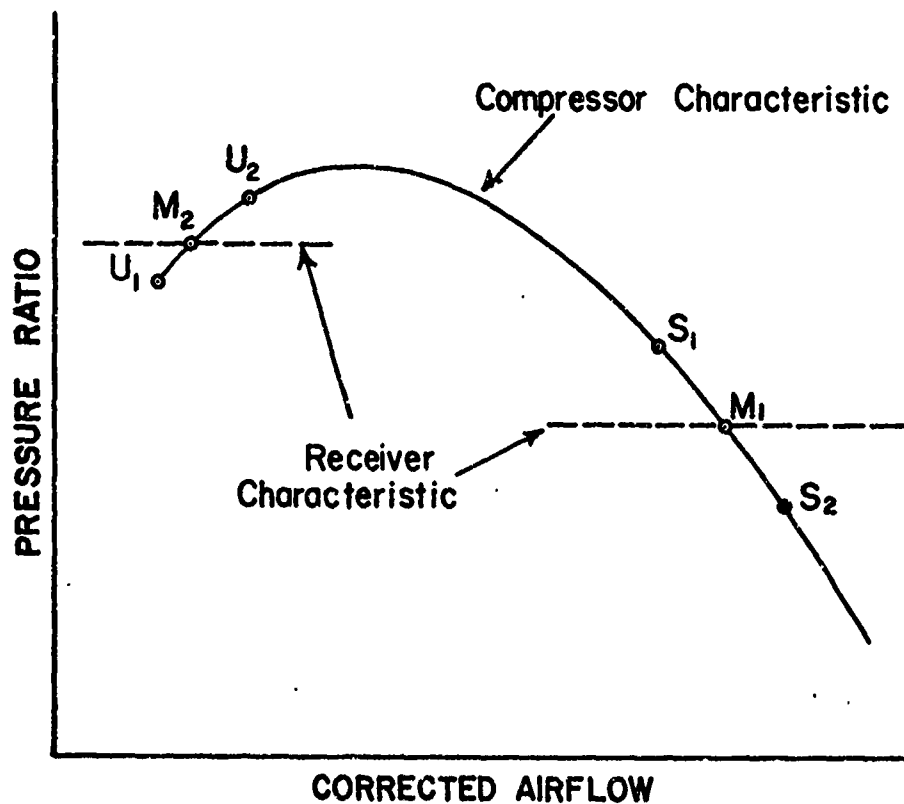
FIG. 2   COMPRESSOR / RECEIVER MATCHING CHARACTERISTICS

Now if the flow became unsteady and a perturbation were to cause a reduction in airflow to point S_1 (constant speed), the compressor would be delivering an instantaneous pressure greater than that in the

receiver. Effectively the compressor back-pressure has been lowered, and the flow would increase until a match is again reached. Similarly for an increase in flow to point S_2, the increased back-pressure would cause a return to stable operation at point M_1. However, if the compressor is matched on the positive slope of the characteristic, by the same reasoning, unsteady conditions exist and perturbations are aggravated to "surge."

A stall margin, defined as the vertical distance between the nominal (design) operating line and the surge line, can be thought of as a measure of the compressor's ability to accommodate flow transients which instantaneously load the machine. This margin is dictated by overall engine-inlet design and is affected by many different phenomena. Unfortunately the point of maximum efficiency in a compressor is just prior to stall or just below the surge line on the performance map, and therefore a trade-off between efficiency and surge margin is required. The expected flow transients which the compressor must be able to accommodate will affect the design efficiency.

Flow transients initiated within the engine system are normally caused by power level (throttle) movement. Transients can also be initiated by flow distortion at the compressor face. Of the various flow distortion parameters, Brimelow [Ref. 1] states that inlet total-pressure and total-temperature have been identified as having the greatest effect on engine stability, which is to a large extent the compressor's ability to remain below the surge line. Total-pressure variations can be steady-state spatial distortion, time-varying spatial distortion, in-phase pulsations which are spatially uniform over the compressor face, or a combination of these. Low frequency spatially uniform (planar)

pressure fluctuations (on the order of 20 CPS) do not affect the compressor but do have a detrimental effect on the inlet and engine control systems. High frequency planar fluctuations (more than one per revolution) affect compressor stability much like time-varying spatial distortion.

Spatial distortions can be further segregated into radial and circumferential inlet flow distortion. This separation into circumferential and radial distortion was arbitrary, somewhat motivated by geometric simplicity. A radial total-pressure distortion such as shown in Fig. 3(a) produces very little variation in inlet static pressure. The net result is a low velocity in the low pressure region and a high velocity in the high pressure region.

(a)

(b)
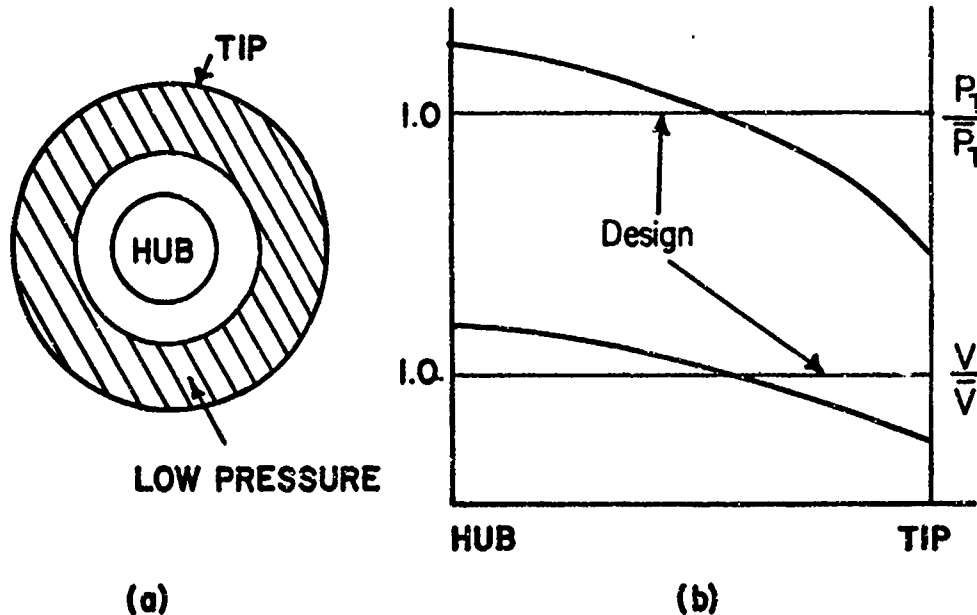
FIG. 3   RADIAL PRESSURE DISTORTION
[adapted from Ref. 1]

In the low velocity region the blades will operate at higher incidences and higher total-pressure ratios. The net result will be a reduction in the compressor stall margin.

For the circumferential type distortion shown in Fig. 4(a), the associated surge line reduction is a function of the basic stage-match of the compressor, the axial spacing between blade and vane rows, and the unsteady response of the rotor blades. Since the blade rows restrict circumferential redistribution of flow, each circumferential segment performs essentially independently.

(a)

(b)
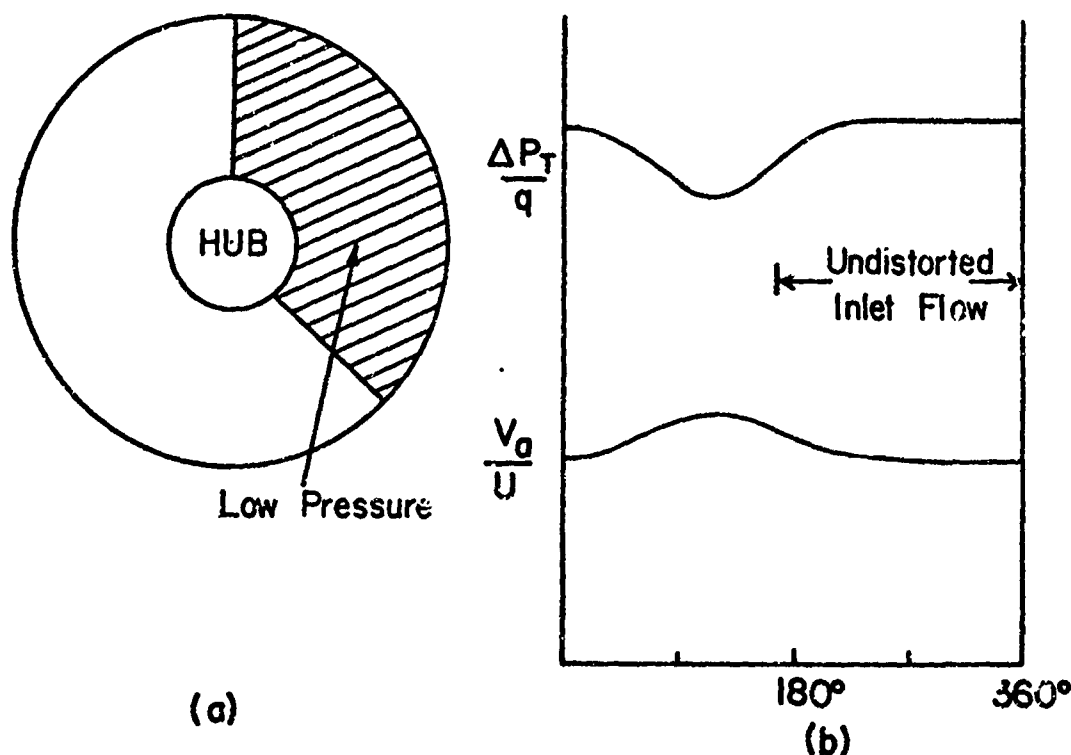
FIG. 4   CIRCUMFERENTIAL   DISTORTION
[adapted from Ref.1]

All segments are required to deliver the same exit static pressure so that in the area of low inlet pressure there is a high pressure ratio and vice-versa. Correspondingly, the high pressure ratio forces a low

axial velocity in this area and a high velocity in the segment of high inlet pressure. These variations in velocity, produced less than one duct-diameter upstream of the compressor, result in static pressure fluctuations at the compressor face. This mechanism of varying velocities (incidences) can induce surge when the average pressure ratio of the distorted flow is less than the surge pressure ratio for undistorted inlet flow. The effects of circumferential pressure pulses on a TF-30 engine are presented in Ref. 3. It was found here that the amplitude of a pulse necessary to stall the engine varied inversely with pulse duration and that the engine was most sensitive to distorted sectors of 180 to 240 degrees.

The distortions which are encountered in actual compressor applications such as jet aircraft inlets are neither radial nor circumferential but a combination of the two. Furthermore the magnitude, location, shape, and duration of these pressure variations change continually. It is virtually impossible to evaluate precisely the effect that these distortions have on engine stability because there are so many distortion patterns significant to each compressor surge. Therefore it has been necessary through experimental programs to develop generalized correlations between pattern characteristics and corresponding effects on compressor stability. Correlating the shape, location, spatial extent, and magnitude of the inlet distortion requires analyzing many radial and many circumferential patterns and relating the overall picture to engine stability. From this is generated a distortion factor which is a measure of the associated loss in stability-margin for that given propulsion system. Because compressor geometry and blading are not considered in arriving at this parameter, the result cannot be applied to other systems.

For a more detailed and complete analysis of this subject, consult Brimelow's excellent work in Ref. 1.

B. PRESENT STATE OF INLET DISTORTION ANALYSES

Until a few years ago, engine-inlet compatibility limits were successfully determined by evaluating an engine's tolerance to steady-state distortion. Normally this was done with screens or similar obstructions placed in the inlet and the compressor face instrumented with low-response pressure probes. The engine was operated under all conditions of interest, and by comparing pressure data at the compressor face with the engine's performance, distortion factors were derived. It was known that unsteady flow was being produced by these test devices, but no attempt was made to evaluate its effect. However, when this technique was applied to the TF-30 turbofan engine during the F-111A flight test program, the data did not correlate well nor was the method found valid for other fan type engines at that time. An improved steady-state distortion factor, K_{d2}, was developed, but it too fell short of providing the needed total evaluation of inlet distortion. It was becoming more evident that there was another significant variable involved, namely turbulence. Turbulence can be described as flow with random pressure fluctuations and can be quantified as a fluctuation in RMS total-pressure, $(\Delta P_{RMS})/(P_T)$. With increased aircraft speeds, turbulence has taken on greater importance since there is a significant amount of turbulent flow associated with the boundary-layer/shock-wave interaction within supersonic inlets. It was felt that steady-state distortion indexes were still of value, but a correlation with turbulence was necessary. One such empirical relation showing a decrease in distortion tolerance, K_{d2}, with increasing turbulent energy is depicted in Fig. 5.

18
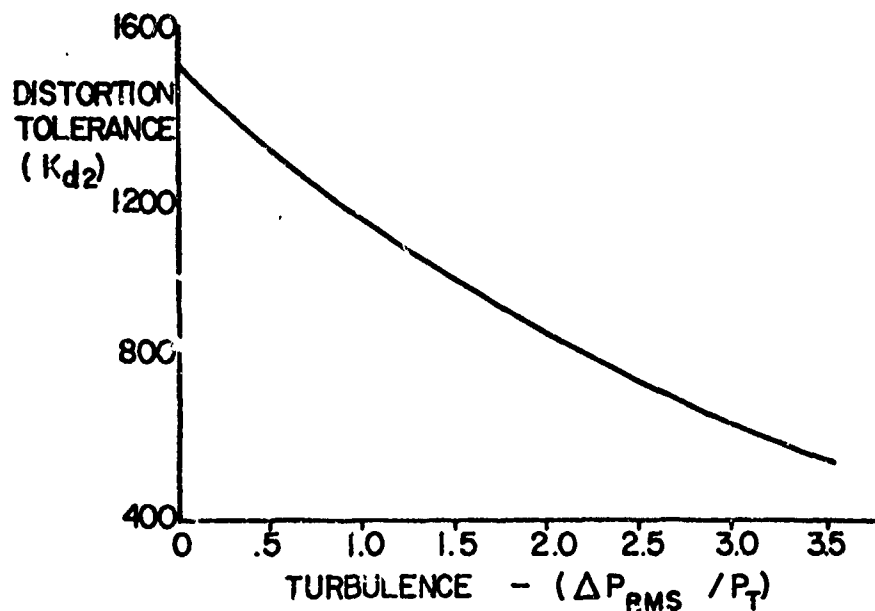
FIG. 5   LOSS IN STEADY-STATE DISTORTION
TOLERANCE WITH TURBULENCE
[adapted from Ref. 4]

Turbulence has two primary effects on axial compressor performance. First, turbulent inlet flow causes a reduction in compressor surge line, its sensitivity being a function of turbulent frequency and amplitude. Second, a reduction in flow capacity accompanies inlet turbulence. These two phenomena were observed in tests performed by Brimelow and Plourde [Ref. 5] on a TF-30 turbofan engine. This all led to the development of new distortion indexes such as the K_{DA} and K_{DM} parameters of Ref 6. However, lack of correlation caused Burcham and Hughes to raise doubt as to the usefulness of the conventional turbulence definition, $(\Delta P_{RMS})/(P_T)$. Bellman and Hughes [Ref. 7] found no consistent relationship at all between turbulence factors and surge, and in some cases surge was experienced as turbulence level was decreasing. Therefore it was concluded here that peak-to-peak pressure fluctuations at key areas of the compressor face are more important in surge prediction than are turbulence levels.

19

Also extensive experimental data have been obtained from a J85-GE-13 turbojet placed in a supersonic wind-tunnel running at Mach numbers close to 2.5. By varying the characteristics of the engine inlet duct, a desired level of time variant flow distortion was produced through internal shock interactions [Ref. 2]. Calogeras, Burstadt and Coltrin found for this J85 configuration that time-averaged distortion could be well below a stall-inducing value while instantaneous peaks exceeded this value. In addition, severe pressure fluctuations could result in an instantaneous distortion of a type quite different from the time-averaged distortion.

Of these few representative programs discussed, there are two striking similarities worthy of note: (1) Each is dedicated to using inlet flow distortion described by raw total-pressure data to predict compressor surge. No attempt at determining the cause or nature of the stall is made. (2) There is much uncertainty and disagreement associated with the present methods of predicting distortion induced stall. A universal distortion parameter has not been agreed upon.

Obviously a better understanding of the internal fluid dynamics, while a difficult task at best, would nonetheless allow a more comprehensive generation of a stall-inducing distortion parameter. Total-pressure is the easiest and perhaps the only flow parameter which can be measured at the compressor face with sufficient accuracy and frequency response to gain meaningful data. The vast amount of pressure data available due to the previously mentioned programs provides an extensive empirical data base with which to treat this problem. In evaluating these data, inclusion of time and temperature dependence could only improve the usefulness of the results. Therefore it is proposed that vorticity become the basis of a "universal distortion

factor." This thesis will show how existing total-pressure maps along with total-temperature and time data can be transformed into vorticity maps, Analysis of the resulting vorticity maps will provide evidence as to the flexibility of this method.

Vorticity is more closely related to fluid dynamics than is total pressure alone. Compressor stall and engine surge are flow-separation phenomena; therefore the key to understanding their causes lies in the internal dynamical situation.

C. VORTICITY APPROACH

1. Compressor Stall

The most significant phenomenon affecting the performance of an axial-flow compressor is stall. If the flow rate through a compressor blade row is decreased while the rotor speed is maintained constant, angles of attack on the blades will increase and eventually flow separation will occur. This condition is called stall and is similar in some respects to the stall of an isolated airfoil; differences are due to the adjacent blading in a cascade. Stalled operation of a compressor is accompanied by a drastic decrease in efficiency and excessive oscillating blade loads capable of causing structural failure. Stall occurs in the range of unstable compressor operation and hence can trigger surge. Usually a compressor stalls in an asymmetric manner; that is, well defined regions of the annulus are stalled while the remaining area is unstalled; see Fig. 6. The flow through these stalled patches is severely restricted in accordance with the decrease in total flow-rate through the compressor, thus the flow is diverted around this blockage. Effectively this increases blade angle-of-attack on one side of the restriction while decreasing it on the other side. In Fig. 7 blade No. 1
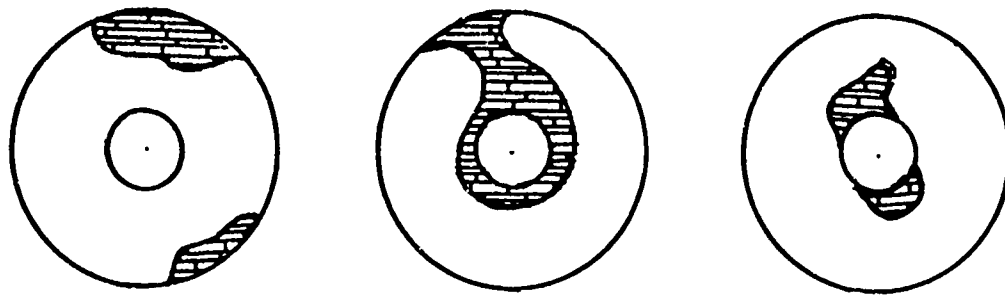
FIG. 6   TYPICAL   STALL   PATTERNS

Decreasing
Angle- of – Attack

Increasing
Angle- of -Attack
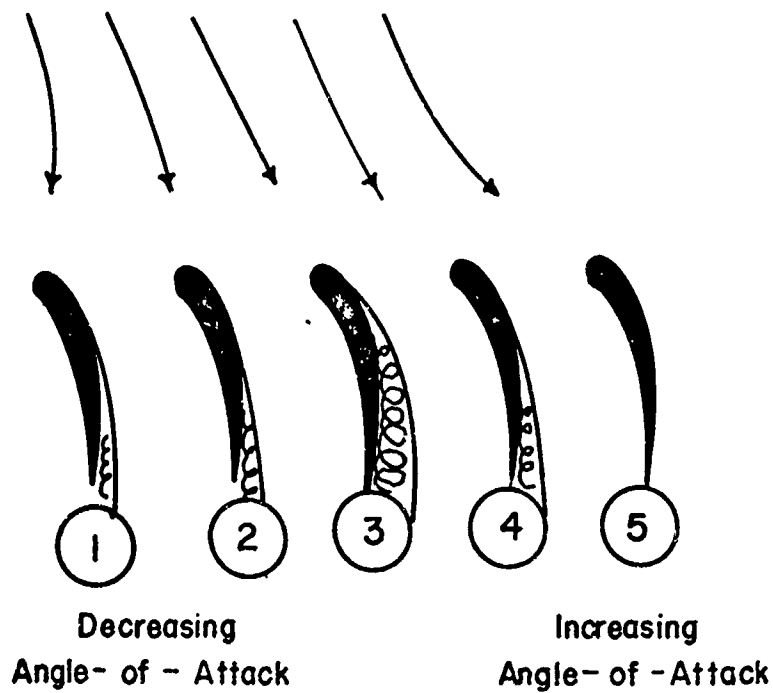
FIG. 7   STALL CELL   GROWTH AND
ROTATION IN A BLADE ROW

·will soon become unstalled while at blade No. 5 flow separation will commence. This condition is termed "rotating stall" since it propagates circumferentially in a direction opposite to rotor rotation. In an absolute frame of reference this speed of circumferential propagation is 30-60 per cent of the rotor speed [Ref. 8]. When these conditions become severe enough to cause net flow-rate fluctuations with time, the situation is called "surge." This describes operation in the unsteady area of the compressor performance map in Fig. 1. Valensi [Ref. 9] has made a thorough investigation into these phenomena with some excellent photographic results. Of the various analytical methods available for predicting compressor stall, the most generally accepted employs the limiting-blade-loading criteria of Lieblein, Schwenk, and Broderick [Ref. 10]. Their "limiting diffusion factor," D, is a function of the velocity relative to the blade and the circulation about the element. If a constant axial velocity assumption is made, this simplifies to a function involving the flow turning angle and cascade solidity. For design purposes where such stage parameters may not be available, Lieblein [Ref. 11] has derived an equivalent diffusion ratio, D_{eq}, which is based on inlet and outlet conditions to the compressor and the type of blading installed. Unlike a single airfoil where angle-of-attack is used to predict stall, the critical variable for a cascade of blades is the flow turning-angle. The exit-flow angle as well as the inlet angle must now be considered.

2. Secondary Flows in Axial Compressors

Returning now to normal compressor operation, flow patterns based on axisymmetric flow distribution and an infinite number of blades have been described quite well in the literature. However, it is necessary

to consider a finite number of blades since there are wall boundary-layer interactions, tip clearance leakages, blade boundary-layers, and centrifugal effects which are not represented adequately by assuming axisymmetric flow. Although these asymmetric phenomena have been studied independently for reasons of simplicity, it must be remembered that their effects are not necessarily additive (non-linear) and may have strong interactions.

Figure 8 illustrates the various secondary flows which have been found to exist in axial-flow turbomachines as a result of the above mentioned viscous and three-dimensional effects. Lakshminarayana and Horlock [Ref. 12] have made a thorough review of secondary flows in axial-flow turbomachines and have indicated where in the literature more specific information can be found. Woods [Ref. 13] presents the current state of the art in analytical treatment of secondary flows and associated losses in axial-flow turbomachines.

The induced velocities caused by secondary flows are considered losses since only a small part of their kinetic energy is recoverable downstream. Secondary velocities may perturb the exit flow angle from a blade row. Near annulus walls where lies the origin of the central vortex in Fig. 8, the induced exit flow angle can cause local blade stall. Much work has been performed in analyzing these phenomena, and some analytical methods for predicting three-dimensional exit flow angles have been proved valid through experimental results [Refs. 14 and 15].

Another source of strong secondary flows in blade passages lies in non-uniform inlet flow such as described previously. Treating inlet flow distortion as vorticity provides a natural basis from which to

Fluid

Cascade
Secondary
Flow

Tip Leakage Flow

Scraping Effects

Tip Leakage
Vortex

Scraping
Vortex

Radial Flows

Cascade
Secondary
Vortices

Trailing
Vortex

Rotation

Trailing Vortices = Shed
Vortices + Trailing Fila-
ment Vortices
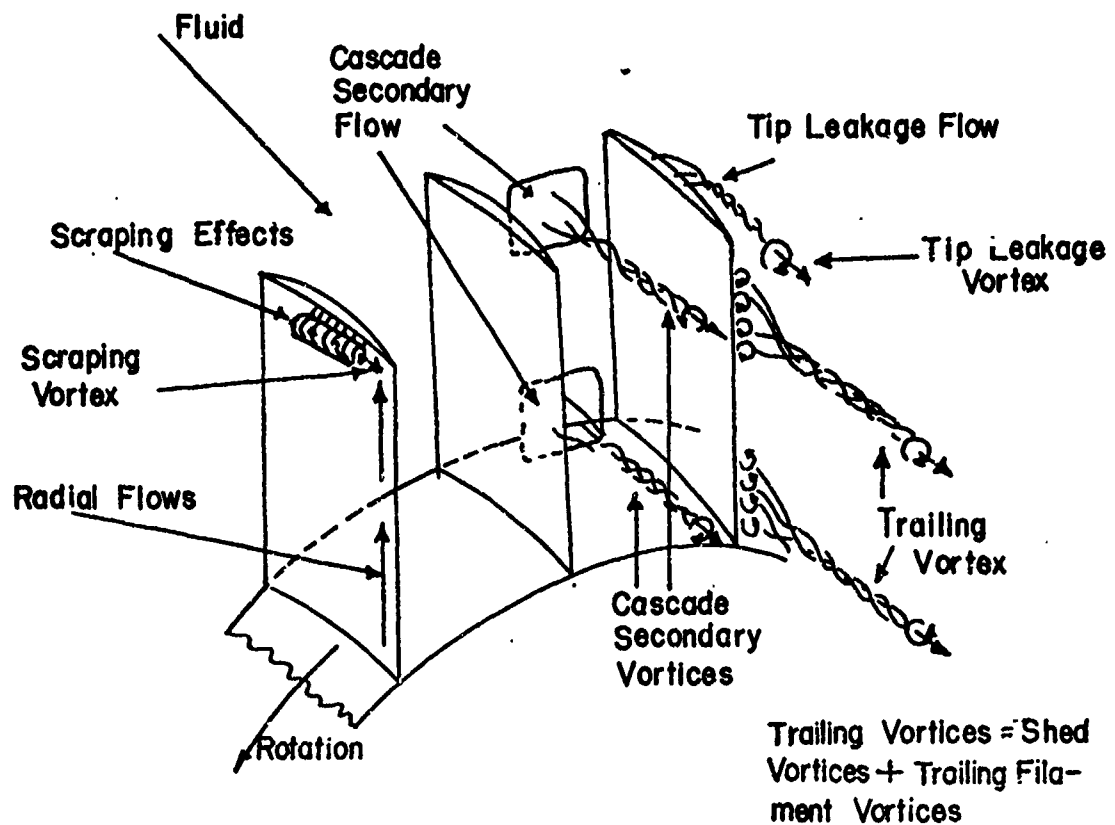
**FIG. 8   SECONDARY FLOW AND VORTICES IN AN AXIAL
FLOW   COMPRESSOR   ROTOR [adapted from Ref. II]**

compute resultant secondary circulation at the exit plane. The effects
of this secondary flow on cascade performance can be studied analogously
to boundary-layer induced circulation. Comparison with an appropriate
blade-loading criterion may predict the compressor's unstable operation.

3. <u>The Theory of Vorticity Analysis</u>

The thermodynamic properties which are significant in compressor
performance are total-pressure (velocity), total-temperature (enthalpy),
specific heat, and molecular weight. Variation of any one or combination
of these properties with time and/or position at the compressor face

constitutes inlet flow distortion and should be an integral part of any universal distortion parameter. To date distortion factors dealing only with one inlet property at a time have been reported, i.e. total-temperature variation $\rightarrow K_T \rightarrow K_T(\text{stall})$ or total-pressure fluctuation $\rightarrow K_p \rightarrow K_p(\text{stall})$. This type of piecemeal approach, while providing satisfactory results for certain restricted applications, cannot be expected to remain valid under all conditions. In reality, an aircraft engine will encounter all of these fluid distortion properties at one time or another. A partial list of causes of these is: inlet characteristics, environmental conditions, rocket exhaust from ordnance, hot runway operation, steam catapult launches, and the normal operating envelope of the aircraft. There is definitely need for a more realistic or universal distortion parameter, one which accounts for the total inlet distortion. It is the intent of this work to show that a distortion parameter based on vorticity would be more flexible and yield more comprehensive surge prediction criteria than present methods.

Crocco's Theorem provides a versatile means of converting existing inlet distortion maps to vorticity in that pressure, temperature, and time are all available as desired for inclusion in the transformation. As indicated previously, time is an important parameter in such an analysis, the aspects of steady-state versus turbulence induced stalls being quite distinct. Hawthorne [Refs. 16 and 17], Preston [Ref. 18], and Horlock [Ref. 15] all deal with the passage of vorticity through a cascade. Horlock and Hawthorne calculate induced exit flow angles which involves a solution to Poisson's Equation. Calculating appropriate exit circulation and comparing it with blade-lift circulation is a far simpler process that yields a qualitative feel for the relative size of this

26

effect. Comparison of this secondary circulation with that caused by three-dimensional effects should also be made in order to look for possible interactions.

The effect of inlet distortion on blade angle-of-attack must also be considered since this is the other "half" of the flow turning angle. This effect is much less subtle and can be dealt with in a more straight-forward manner. Areas of low pressure represent lower axial velocity, hence higher angles-of-attack. The unsteady response of the blades must be considered, particularly for circumferential inlet distortion where blade passing frequency is a factor.

III. CONVERSION OF PRESSURE TO VORTICITY MAPS

A. CROCCO'S THEOREM

In general form, Crocco's Theorem can be written as

$$T \text{ grad } S + u \times \text{curl } u = \text{grad } H + \frac{\partial u}{\partial t} \tag{1}$$

which holds in unsteady flow [Ref. 19]. From basic Thermodynamics

$$\frac{S_2 - S_1}{R} = -\text{Ln}\left(\frac{P_{T2}}{P_{T1}}\right) + \frac{\gamma}{\gamma - 1} \text{Ln}\left(\frac{T_{T2}}{T_{T1}}\right) \tag{2}$$

Combine Eqns. (1) and (2), assuming H = Constant

$$\frac{-RT}{P_T} \text{ grad } P_T \stackrel{+}{\cdot} u \times \text{curl } u = \frac{\partial u}{\partial t} \tag{3}$$

The following development will apply to the system defined in Fig. 9.
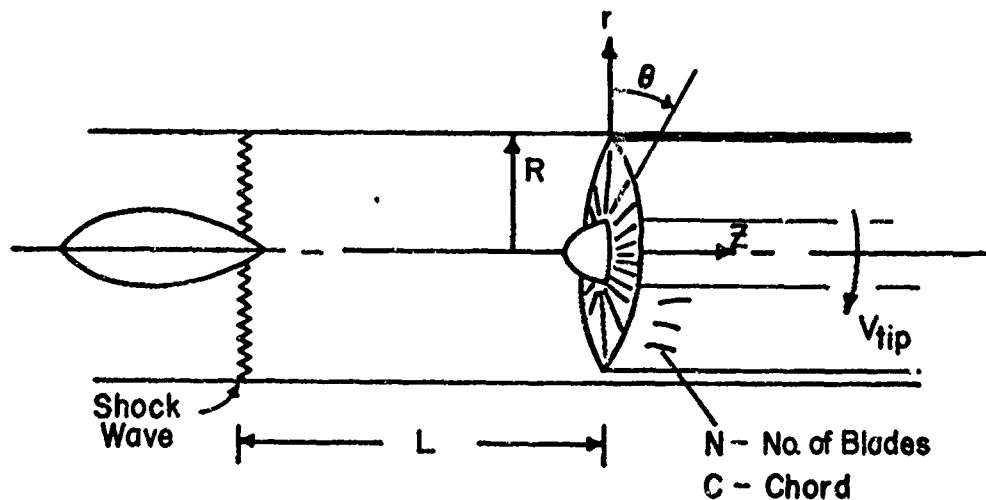
FIG. 9   NOMENCLATURE

Writing Eqn. (3) in component form using cylindrical coordinates yields

$$\frac{-RT}{P_T}\frac{\partial P_T}{\partial r}\hat{e}_r + (u_\theta \omega_z - u_z \omega_\theta)\hat{e}_r = \frac{\partial u_r}{\partial t}\hat{e}_r \tag{4}$$

$$\frac{-RT}{P_T}\frac{1}{r}\frac{\partial P_T}{\partial \theta}\hat{e}_\theta + (u_z \omega_r - u_r \omega_z)\hat{e}_\theta = \frac{\partial u_\theta}{\partial t}\hat{e}_\theta \tag{5}$$

$$\frac{-RT}{P_T}\frac{\partial P_T}{\partial z}\hat{e}_z + (u_r \omega_\theta - u_\theta \omega_r)\hat{e}_z = \frac{\partial u_z}{\partial t}\hat{e}_z \tag{6}$$

The following reference quantities taken at the compressor face will be used to non-dimensionalize the equations. Refer to Fig. 9.

$P_T = P'\bar{P}_T$ $\bar{P}_T$ = Average Stagnation Pressure

$u = u'\bar{a}$ $\bar{a}$ = Average Speed of Sound

$r = r'\frac{D}{2}$ D = Compressor Diameter

$z = z'\frac{D}{2}$

$\omega = \omega'\frac{2\bar{a}}{D}$ ω = Fluid Vorticity

Table I lists some of the characteristic times available. Blade passing frequency will be used in this development, since most available data include compressor speed; then

$$t = t'\frac{2\pi R}{V_{TIP}N}$$

The numerical value of the reduced frequency for stall is based on the work of Carta [Ref. 20]. For values less than approximately 0.1, blade

29

TABLE I   CHARACTERISTIC TIMES

BLADE PASSING FREQUENCY

$$\frac{V_{TIP}N}{2\pi R} = \frac{(1500)(36)}{(6)(2)} = 4500 \text{ Hz}$$

ONCE-PER-REV

$$\frac{V_{TIP}}{2\pi R} = \frac{1500}{(6)(2)} = 125 \text{ Hz}$$

WAVE PROPAGATION

RADIAL $\quad \frac{a}{2R} = \frac{1200}{4} = 300 \text{ Hz}$

LONGITUDINAL $\quad \frac{a \pm u}{L} = 60,180 = 120 \text{ Hz}$

STALL TIME

REDUCED FREQUENCY $\quad = \frac{\pi f c}{U} \leq 0.1$

$$f \leq \frac{(0.1)(1200)}{(3)(0.2)} = 200 \text{ Hz}$$

stall is essentially equivalent to steady-state stall. For a reduced frequency larger than 0.1, stall is suppressed due to dynamic effects. Other work in this area has been performed by Carta [Ref. 22]. The paper by Ericssen and Reding [Ref. 21] is a survey of dynamic stall.

Rewriting the component equations in non-dimensional form and canceling terms yields

$$-\frac{1}{\gamma P'}\frac{\partial P'}{\partial r'} + \frac{\overline{a}^2}{a^2}(u_\theta'\omega_z' - u_z\omega_\theta') = \frac{V_{TIP}N\overline{a}}{2\pi a^2}\left(\frac{\partial u_r'}{\partial t'}\right) \tag{7}$$

$$-\frac{1}{\gamma P'r'}\frac{\partial P'}{\partial\theta} + \frac{\overline{a}^2}{a^2}(u_z'\omega_r' - u_r'\omega_z') = \frac{V_{TIP}N\overline{a}}{2\pi a^2}\left(\frac{\partial u_\theta'}{\partial t'}\right) \tag{8}$$

$$-\frac{1}{\gamma P'}\frac{\partial P'}{\partial z'} + \frac{\overline{a}^2}{a^2}(u_r'\omega_\theta' - u_\theta'\omega_r') = \frac{V_{TIP}N\overline{a}}{2\pi a^2}\left(\frac{\partial u_z'}{\partial t'}\right) \tag{9}$$

Equations (7), (8), and (9) are exact. Orders of magnitude of various terms will be examined to ascertain whether or not complexity can be reduced in a logical and consistent manner.

B. ORDER OF MAGNITUDE ANALYSIS

Figure A-2[2] represents an inlet-flow distortion map at the face of a J85-GE-13 turbojet. This distortion map triggered surge. The map of Fig. A-3 is a similar situation in a TF-30 turbofan engine. These

---

[2]Reference to figures and equations labeled with a letter/number combination nave more detailed explanations which are contained in the Appendix.

maps will be considered representative of stall-inducing flow distortion
for purposes of making an order-of-magnitude analysis on Eqns. (7), (8),
and (9).

Establish an order of magnitude, ϵ, such that

$$\frac{\overline{P}_T - P_T}{\overline{P}_T} \approx 1 - P' \equiv O(\epsilon)$$

From Figs. A-2 and A-3

$$-0.2 \leq \epsilon \leq 0.2$$

Between 12 and 5 o'clock, Fig. A-2, $\partial P'/\partial r'$ is a maximum. Refer to
Appendix A for all numerical values.

$$\frac{\partial P'}{\partial r'} = \frac{\partial(P_T/\overline{P}_T)}{\partial(2r/D)} \simeq \frac{1.17 - .97}{(7.1 - 6.05)(2/16.1)} = 1.53$$

From Fig. A-3 at the 12:30 o'clock position

$$\frac{\partial P'}{\partial r'} \simeq \frac{1.04 - .96}{(2.15 - 1.8)(2/6)} = .685$$

$$-0.7 \leq \frac{\partial P'}{\partial r'} \leq 1.5$$

Between 5 and 7 o'clock, Fig. A-2, a maximum value of $\partial P'/\partial \theta$ exists such
that $\quad \dfrac{\partial P'}{\partial \theta} \simeq \dfrac{1.20 - .95}{.6 \text{ rad}} = .416$ per radian

Similarly from Fig. A-3 at 1 o'clock

$$\frac{\partial P'}{\partial \theta} \simeq \frac{1.04 - .92}{.35 \text{ rad}} = .343 \text{ per radian}$$

$$\frac{\partial P'}{\partial \theta} \simeq .4$$

A discussion of the term $\partial P'/\partial z'$ is contained in Appendix A, Part II. An acoustic analysis taken at the compressor face yields Eqn. (A-2) which allows a magnitude estimation of $\partial P'/\partial z'$.

$$\left. \frac{\partial P_T}{\partial z} \right|_{face} = \left(\frac{1}{\overline{u}_z + \overline{a}} \right) \left. \frac{\partial P_T}{\partial t} \right|_{face} \qquad (A-2)$$

$$\frac{\partial P'}{\partial z'} = \frac{D}{\overline{P}_T} \frac{\partial P_T}{\partial z}$$

$$\frac{\partial P'}{\partial z'} = \frac{D}{\overline{P}_T} \left(\frac{1}{\overline{u}_z + \overline{a}} \right) \frac{\partial P_T}{\partial t}$$

From Figs. A-3 through A-8 at the point "$\blacksquare$", the following data are available.

$P' = .92 \qquad P_T = P'\overline{P}_T = 1480 \text{ psf}$

$P' = .96 \qquad P_T = 1545 \text{ psf}$

$$\overline{u}_z = \frac{(P_T - P_S)}{\rho/2}^{1/2} = \frac{(1610 - 1440)}{.0015/2}^{1/2}$$

$$= 475 \text{ ft/sec}$$

$$\overline{a} = \overline{u}/M = 475/.4 = 1190 \text{ ft/sec}$$

$$\frac{\partial P'}{\partial z'} = \left(\frac{3 \text{ ft}}{1610 \text{ lbs/ft}^2} \right) \left(\frac{1 \text{ sec/ft}}{475 + 1190} \right) \left(\frac{1545 - 1480 \text{ lbs/ft}^2}{6 \text{ Fig} \times .2 \times 10^{-3} \text{ sec/Fig}} \right)$$

$$\frac{\partial P'}{\partial z'} = .05$$

33

An average value of u_z' for the J85 can be obtained from data in Appendix C.

$$u_z' \cong \frac{\overline{u_z}}{\overline{a}} \approx \frac{460}{1110} = .415$$

A maximum value would be

$$P' = 1.17 \qquad u_z \approx \frac{(P_T - P_S)}{\rho/2}^{1/2} = 750 \text{ ft/sec}$$

$$u_z' \approx \frac{750}{1110} = .675$$

$$u_z' \approx .7$$

Data with which to estimate the magnitudes of u_r' and u_θ' or their partial derivatives are not available. However, an upper bound of order ϵ can be definitely established by considering the consequences of u_r' or $u_\theta' \approx 0(\epsilon^0)$. A radial velocity component of order unity is not possible within a duct. Any u_r' components present at the compressor face are caused solely by turbulent fluctuations and are probably of order ϵ^2; however an upper bound of ϵ will be assumed. A velocity component such as u_θ', called pre-rotation, is often generated intentionally as a means of establishing a desired angle-of-attack on the first blade row. The magnitude of this velocity should be smaller than u_z' and certainly not larger. A velocity in the circumferential direction of order ϵ^0, about equal to the axial velocity, is unrealistic; and if it were present, the engine would just not run. For the case under consideration there is no pre-rotation so that any u_θ' which does exist is caused also by turbulent fluctuations and is probably of order ϵ^2. Again an upper bound of ϵ will be assumed.

Therefore

$$u_\theta' \doteq u_r' < u_z'$$

Partial derivatives of u_θ' and u_r' with respect to time can also be given only a bound with respect to u_z'.

$$\frac{\partial u_\theta'}{\partial t'} \approx \frac{\partial u_r'}{\partial t'} < \frac{\partial u_z'}{\partial t'}$$

There are two phenomena causing a time dependency. One is due to the motion of the rotor. For patterns of large extent on the P_T map, the appropriate frequency is once-per-rev. For patterns of limited extent, blade passing frequency is appropriate. Unsteady aspects of the flow cause a time dependency also.

Continuing, the magnitude of ω_r' will be assessed.

$$\omega_r' \equiv \frac{\omega_r D}{2\bar{a}} \approx \left(\frac{\partial u_z}{\partial \theta} + \frac{\partial u_\theta}{\partial z} \right) \frac{D}{2\bar{a}}$$

From Fig. A-2 between 8 and 9 o'clock, and data from Appendix C

$$P' \approx .97 \qquad u_z \approx \left(\frac{P_T' - P_S}{\rho/2} \right)^{1/2} = 400 \text{ ft/sec}$$

$$P' = 1.17 \qquad u_z = 750 \text{ ft/sec}$$

$$\Delta\theta = 30° \approx .52 \text{ radians}$$

$$\omega_r' = \frac{(350 \text{ ft/sec})(1.34 \text{ ft})}{(.52 \text{ rad})(.605 \text{ ft})2(1110 \text{ ft/sec})} = .814 \text{ per radian}$$

$$\omega_r' \approx .8$$

35

Similarly, approximating $\omega_\theta{}'$ yields

$$\omega_\theta{}' \equiv \frac{\omega_\theta D}{2\bar{a}} = \left(\frac{\partial u_r}{\partial z} - \frac{\partial u_z}{\partial r}\right) \frac{D}{2\bar{a}}$$

From Fig. A-2 between 12 and 5 o'clock

$$\omega_\theta{}' \approx \left(\frac{-(750 - 400)\ \text{ft/sec}}{.06\ \text{ft}}\right) \frac{1.34\ \text{ft}}{2(1110\ \text{ft/sec})} = -3.52$$

$$\omega_\theta{}' \approx 3.5$$

For the axial component of vorticity

$$\omega_z{}' \approx \frac{\omega_z D}{2\bar{a}} = \left(\frac{\partial u_\theta}{\partial r} + \frac{\partial u_r}{\partial \theta}\right)\ \frac{D}{2\bar{a}}$$

Since both partial derivatives are really unkown in size, this term will be evaluated later.

The magnitude of $\partial u_z{}'/\partial t'$ in Eqn. (9) can be estimated by again referring to the point "B" in Figs. A-3 through A-8.

$$P' = .92 \qquad u_z = \left(\frac{(P_T - P_S)}{\rho/2}\right)^{1/2} = \left(\frac{(.92)(1610 - 1440)}{.0015/2}\right)^{1/2}$$

$$u_z = 231\ \text{ft/sec}$$

$$P' = .96 \qquad u_z \approx 374\ \text{ft/sec}$$

$$\Delta t = (6\ \text{figs.}) \times (.2 \times 10^{-3}\ \text{sec/fig.})$$

$$\frac{\partial u_z{}'}{\partial t'} = \frac{\pi}{\bar{a}\ \text{RPS}\ N}\left(\frac{\Delta u_z}{\Delta t}\right) = \frac{3.14}{(1190)(166)}\left(\frac{374 - 231}{1.2 \times 10^{-3}}\right)$$

$$\frac{\partial u_z{}'}{\partial t'} = .06$$

Entropy can be expressed as

$$\frac{S - \bar{S}}{R} = - Ln\left[\frac{P}{\bar{P}}\right] + \frac{\gamma}{\gamma - 1} Ln\left[\frac{T}{\bar{T}}\right]$$

where P and T are static values at the compressor face. Assuming $P = \bar{P}$, combination of this equation with Eqn. (2) yields

$$\left(\frac{a}{\bar{a}}\right)^2 = \frac{T}{\bar{T}} = (P')^{\frac{\gamma-1}{\gamma}} = 1 + (\epsilon)^{\frac{\gamma-1}{\gamma}}$$

$$= 1 + \frac{\gamma-1}{\gamma} \epsilon \approx 1 + \epsilon^2$$

The deviation of local speed of sound from average speed of sound is less than the deviation of local stagnation pressure from average stagnation pressure. Therefore $\bar{a}/a$ will be set equal to 1.

Table II is a summary of these established relative magnitudes in terms of ϵ. The velocities, u_θ' and u_r', are placed at their absolute upper bounds and ω_z' is set equal to ϵ^0 for later verification.

TABLE II	RELATIVE	ORDERS	OF	MAGNITUDE

ϵ^2	ϵ	ϵ^0	ϵ^{-1}
$\frac{\partial P'}{\partial Z'}$		P' $\frac{\partial P'}{\partial \theta}$ $\frac{\partial P'}{\partial r'}$	
$\frac{a - \bar{a}}{\bar{a}}$	u_r' u_θ'	u_z'	
		ω_r' ω_θ' ω_z'	
$\frac{\partial u_r'}{\partial t'}$ $\frac{\partial u_\theta'}{\partial t'}$	$\frac{\partial u_z'}{\partial t'}$		

Now Eqn. (7) can be written

$$-\frac{1}{\gamma P'}\frac{\partial P'}{\partial r'} + \left(u_\theta'\omega_z' - u_z'\omega_\theta'\right) = \frac{V_{TIP}}{2\pi}\frac{N}{a}\frac{\partial u_r'}{\partial t'} \qquad (7a)$$

$$\epsilon^0 \quad \epsilon^0 \qquad \epsilon \;\; \epsilon^0 \qquad \epsilon^0 \; \epsilon^0 \qquad \epsilon^0 \qquad \epsilon^2$$

Dropping terms of order ϵ

$$-\frac{1}{\gamma P'}\frac{\partial P'}{\partial r'} - u_z'\omega_\theta' = 0 \qquad (10)$$

$$\omega_\theta' = \frac{-1}{\gamma P'u_z'}\left(\frac{\partial P'}{\partial r'}\right)$$

Similarly for Eqn. (8)

$$-\frac{1}{\gamma P'r'}\frac{\partial P'}{\partial\theta} + (u_z'\omega_r' - u_r'\omega_z') = \frac{V_{TIP}}{2\pi}\frac{N}{a}\frac{\partial u_\theta'}{\partial t'} \qquad (8a)$$

$$\epsilon^0 \quad \epsilon^0 \qquad \epsilon^0 \; \epsilon^0 \qquad \epsilon \;\; \epsilon^0 \qquad \epsilon^0 \quad \epsilon^2$$

$$\omega_r' = \frac{1}{\gamma P'u_z'r'}\left(\frac{\partial P'}{\partial\theta}\right) \qquad (11)$$

The size of ω_z' was assumed to be of order ϵ^0 although at this point it
is, in fact, unknown. In arriving at Eqns. (10) and (11), ω_z' is
multiplied by small terms (u_r' and u_θ'); therefore little if any error
should be introduced here. Subsequent analysis establishes the size of
ω_z'. From Eqn. (9)

$$-\frac{1}{\gamma P'}\frac{\partial P'}{\partial z'} + \left(u_r'\omega_\theta' - u_\theta'\omega_r'\right) = \frac{V_{TIP}}{2\pi}\frac{N}{a}\frac{\partial u_z'}{\partial t'} \qquad (12)$$

$$\epsilon^0 \quad \epsilon \qquad \epsilon \;\; \epsilon^0 \qquad \epsilon \;\; \epsilon^0 \qquad \epsilon^0 \quad \epsilon$$

Equation (12) contains most of the terms whose magnitudes were generally uncertain. All terms are of the order ϵ so no consisten$^+$ simplification can be made. This equation will not be used in the subsequent transformations from P_T to vorticity.

C. APPLICATION OF RESULTS

Equations (10) and (11) are the required relations for transforming total-pressure maps to circumferential and radial vorticity maps respectively. The procedure, as applied to the J85 map, is outlined below.

The expressions $\partial P'/\partial r$; in Eqn. (10) and $\partial P'/\partial \theta$ in Eqn. (11) are obtained in a similar fashion from Fig. A-2. For one particular radial line, values of P' are plotted against r', the slope at any point being the local value of $\partial P'/\partial r'$. This is done for sufficient radials to adequately cover the entire map. Local values of P' can be taken directly from the P_T map, and from these u_z' can be calculated (assuming constant static pressure). Similarly in Eqn. (11), for one discrete radius, values of P' at a position, θ, are taken at intervals through 360 degrees. These values are plotted, the local slopes being numerically equal to $\partial P'/\partial \theta$. Other values necessary to compute ω_r' can be taken directly from the map or readily computed. See Appendix B for the calculations outlined above.

The results of these calculations, depicted in Figs. 10 and 11 as ω_r' and ω_θ' contour maps, present a two-dimensional picture of conditions at the compressor face. Since $\nabla \cdot (\nabla \times \omega) = 0$, it follows from Gauss' Divergence Theorem that

$$\iint_A (\vec{\omega} \cdot \vec{r}) \, dA = \iiint_V (\vec{\nabla} \cdot \vec{\omega}) \, dV = 0$$

Application of this theorem to the maps of ω_r' and ω_θ' contours yields a quantitative estimate of the axial vorticity, ω_z', which is reflected in Table II. These calculations are contained also in Appendix B, and the resulting map is given as Fig. 12.

Radial and circumferential vorticity maps for the TF-30 total-pressure data in Fig. A-10 have also been generated. They are Figs. 13 and 14.
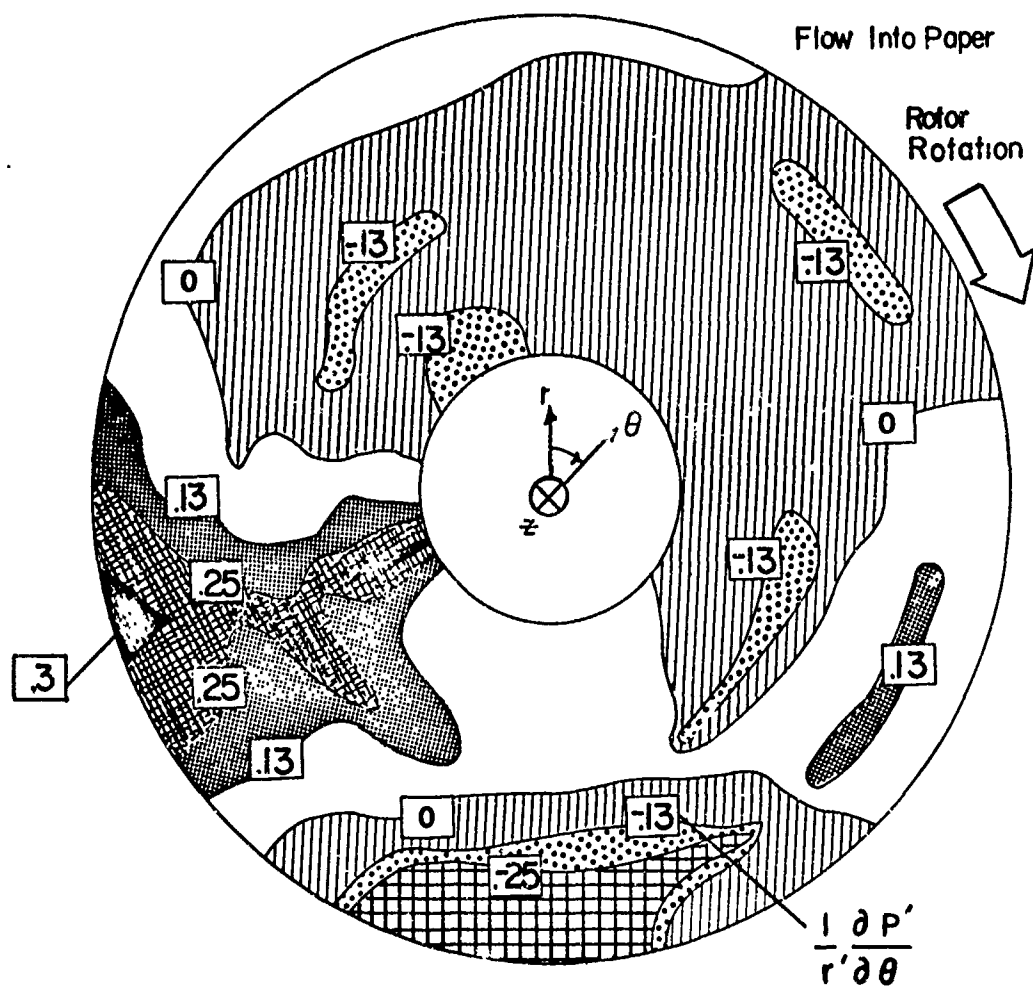
FIG. 10   RADIAL VORTICITY CONTOURS,   J85

41
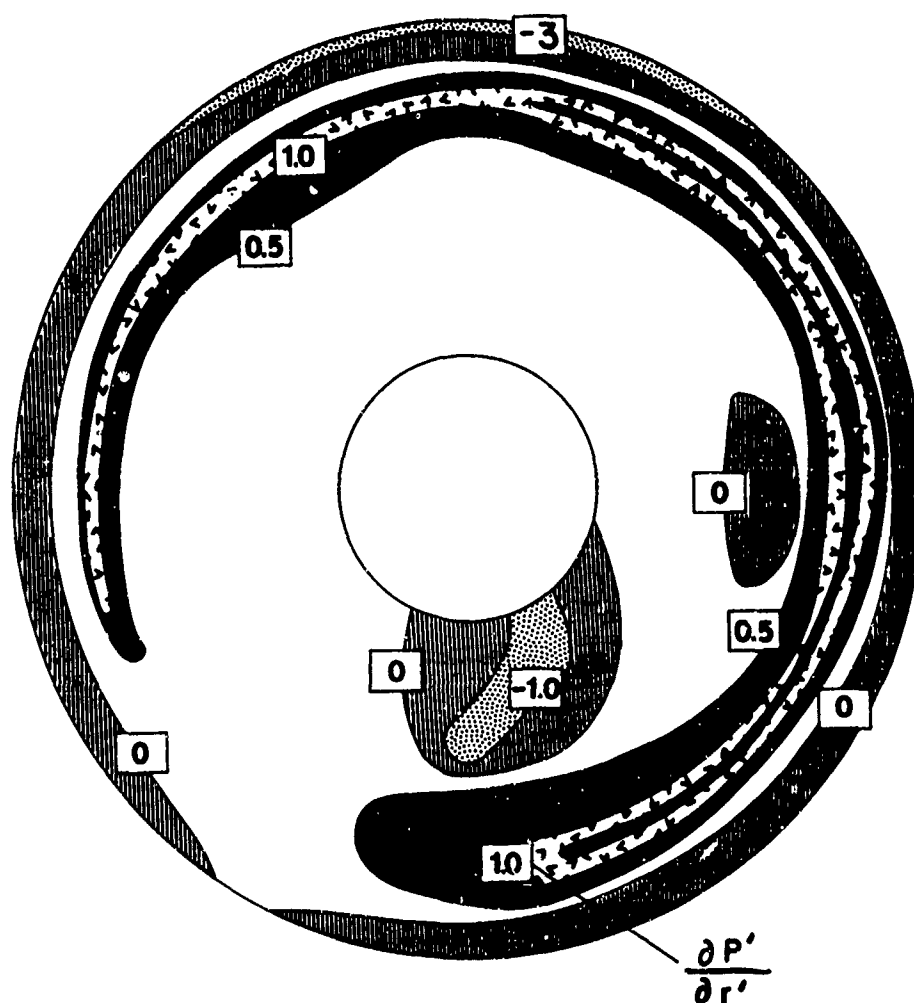
FIG. II CIRCUMFERENTIAL VORTICITY CONTOURS, J85
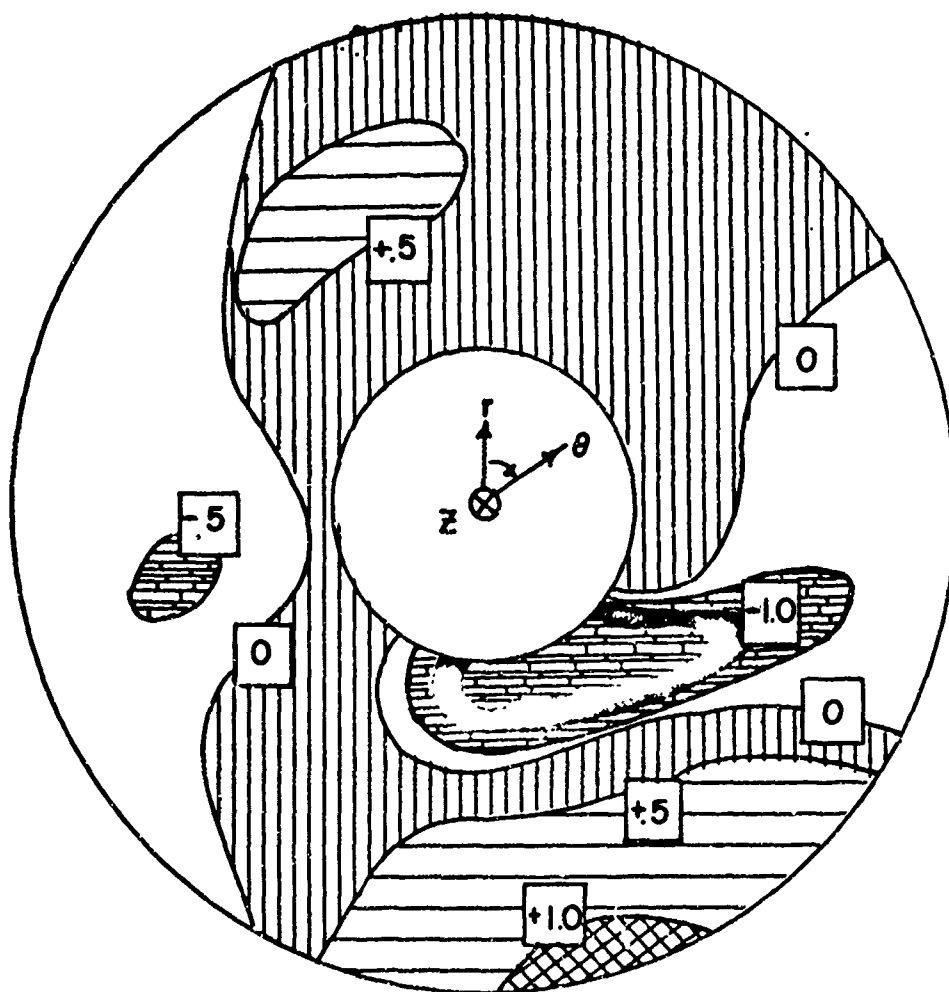
FIG. 12   CONTOURS OF NET FLUX
OF ω'_z FOR J85

$$\frac{1}{r^1} \frac{\partial P^1}{\partial \theta}$$
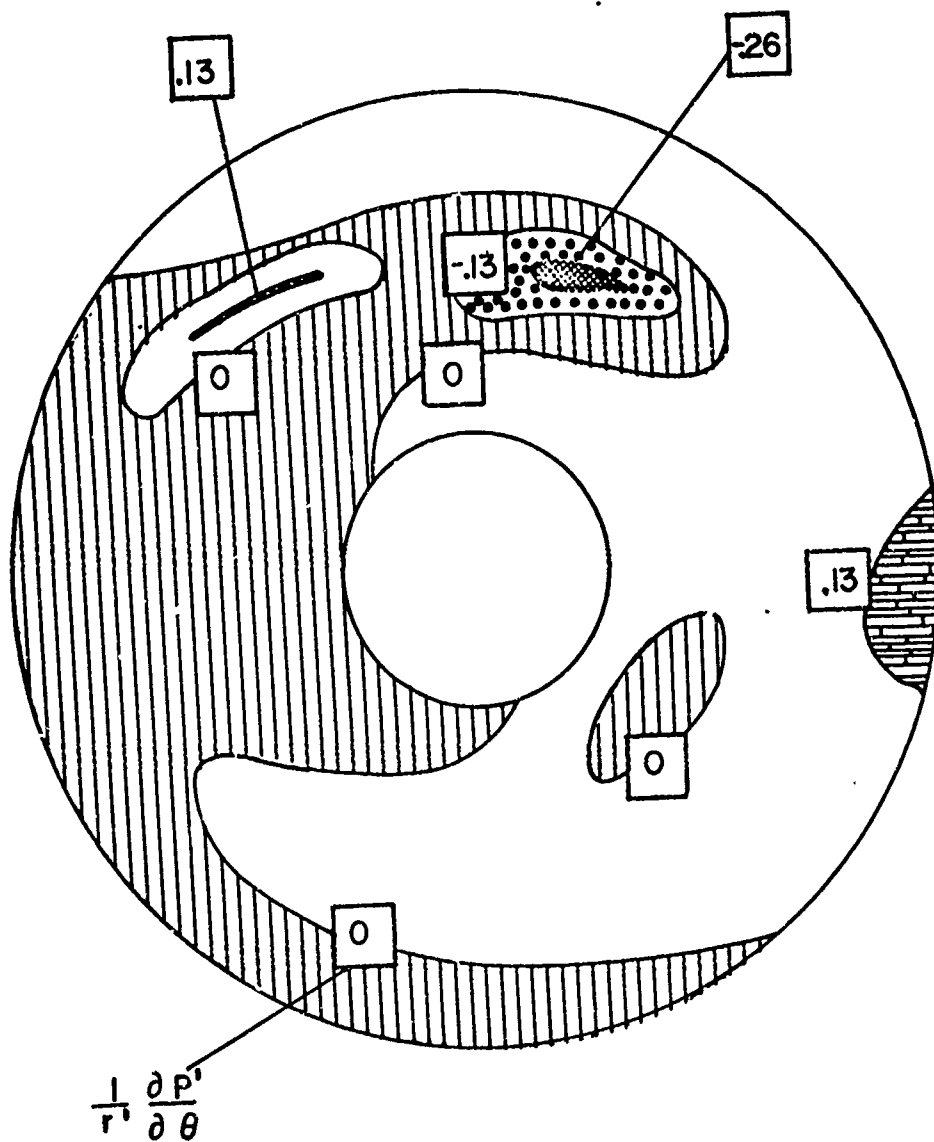
FIG. 13   RADIAL   VORTICITY   CONTOURS,   TF-30
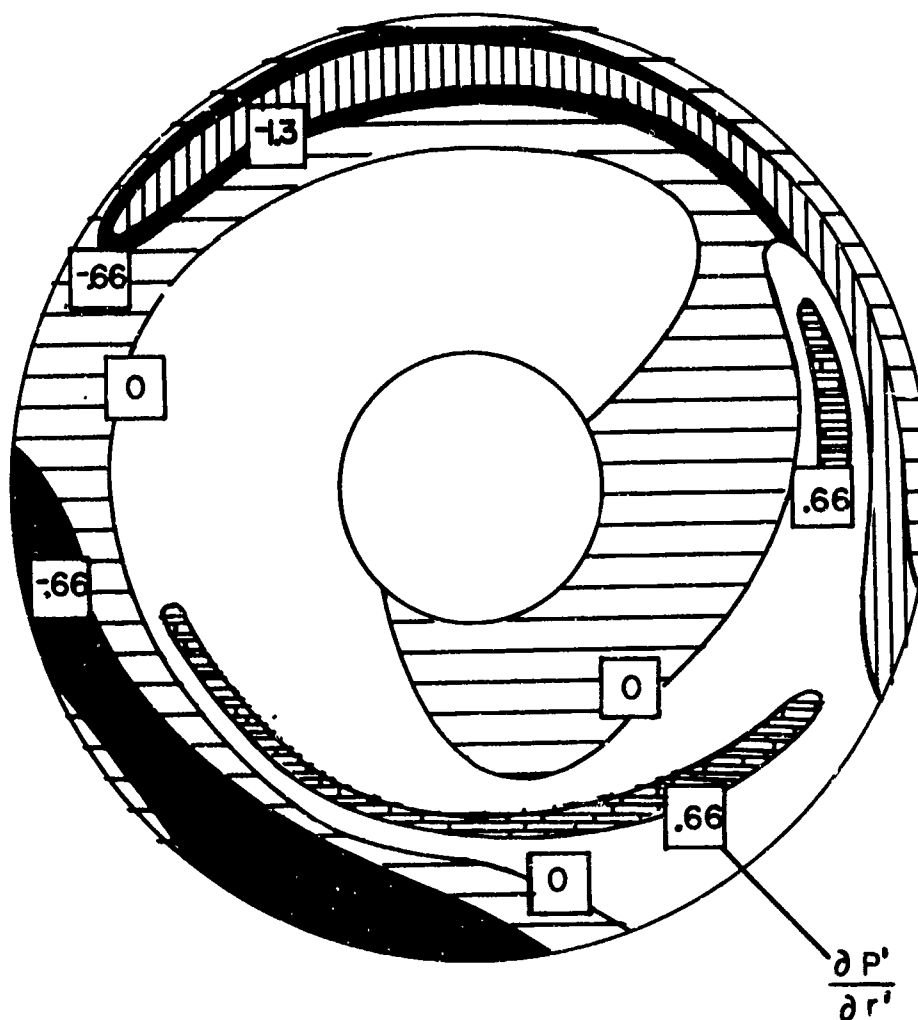
FIG. 14   CIRCUMFERENTIAL   VORTICITY
CONTOURS,   TF – 30

IV. ANALYSIS OF VORTICITY MAPS

A. RADIAL VORTICITY INLET EFFECTS

In vector notation radial vorticity is aligned parallel to local blade spans of the compressor, $+\omega_r$ pointing outward radially according to the right-hand rule. The vorticity in Fig. 10 is concentrated in two areas, $-\omega_r$ between 5 and 7 o'clock and $+\omega_r$ at 8 o'clock. In analyzing the effects of these local concentrations it must be noted that four distinct situations can be represented by a vorticity map such as this. These are listed in Table III. Vortex-sheets are aligned parallel with the flow and vortex filaments are convected with the flow.

TABLE III   Possible Combinations for Radial Inlet Vorticity

Case	Vortex	Blades	Flow
I	Sheet	Stator	Steady
II	Sheet	Rotor	Unsteady
III	Filament	Stator	Unsteady
IV	Filament	Rotor	Unsteady

Case I

A continuous sheet of vortex filaments passing through a stationary blade row (stator) is a steady-state problem. According to the Biot-Savart Law, velocities are induced in the fluid which cause changes in local blade incidences, Fig. 15. In a cascade Γ is the circulation about a blade.

$$\Gamma = S(V_{u1} - V_{u2}) \tag{13}$$

and

$$L = \rho V_{\infty} \Gamma \tag{14}$$

Then

$$\frac{\Delta L}{L} = \frac{\Delta \rho}{\rho} + \frac{\Delta V_{\infty}}{V_{\infty}} + \frac{\Delta \Gamma}{\Gamma} \tag{15}$$
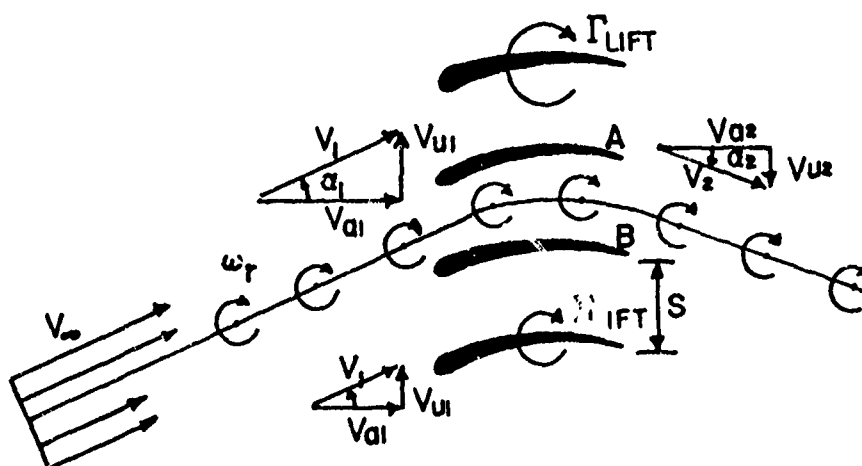
FIG. 15   RADIAL VORTEX - SHEET PASSING
THROUGH A STATOR

Therefore blades in region "A" where $\Delta\Gamma/\Gamma$ is positive are more heavily loaded.

The first stator row is behind a rotor so Figs. 10 and 13 cannot be applied here without knowing the influence of the rotor on ω_r'. This case could be applied directly to inlet guide-vanes however.

Case II

A steady vortex-sheet passing through a rotating blade row is an unsteady problem due to the relative motion between particle paths and

47

the rotor. Again, induced velocities cause variations in the absolute
velocity, V_1, which result in $\Delta\beta_1$ (relative inlet flow angle) and hence
$\Delta\Gamma$ and ΔL. W is relative velocity in Fig. 16. As blade "A" passes
through the vortex-sheet to position "B", it experiences a decrease in
lift which is represented by a smaller Γ_{lift}. This results in shed
circulation equal in direction to Γ_{lift} and a resultant decrease in
strength of the trailing vortex-sheet. Dynamic response of the blading
is a factor which must be considered in this case.

For a rotating cascade, circulation associated with blade lift is a
function of the peripheral velocity, W_u. For the circuit abcd in Fig.
16 this is

$$\Gamma_{lift} = S(W_{u1} - W_{u2}) \qquad (16)$$

The corresponding lift on this blade is

$$L = \rho\Gamma W_\infty = \rho S(W_{u1} - W_{u2})W_\infty \qquad (17)$$
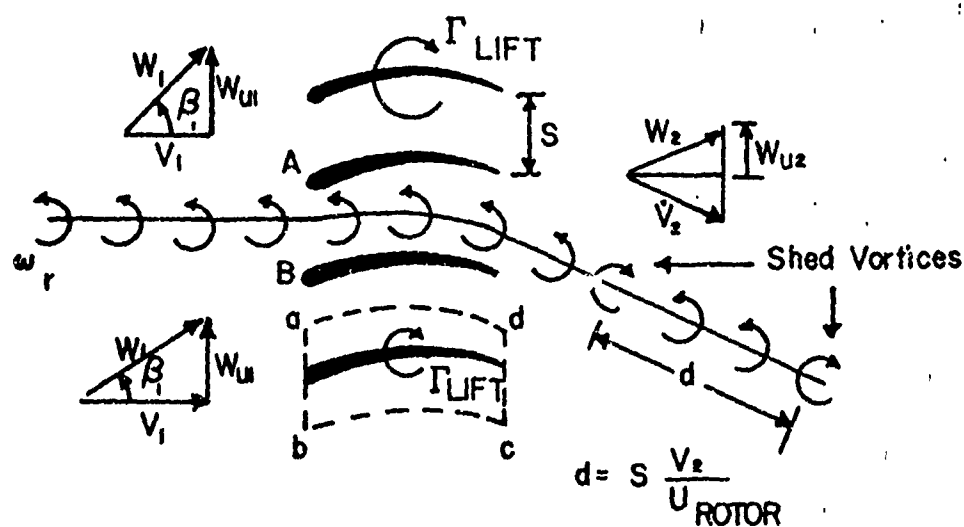
FIG. 16   RADIAL VORTEX-SHEET PASSING
            THROUGH A ROTOR

48

For our sign convention, $-\omega_r$ causes blade unloading while $+\omega_r$ increases the local incidence. Comparison of circulation causing blade lift to that associated with inlet distortion (Γ_{dist}) from Fig. 10 should give a feel for the relative strength of this effect. For brevity, all mean quantities will be used and the dynamic response of the blading will be neglected. From data in Appendices C and D, for the J85

$$W_{u1} = 650 \text{ ft/sec}$$

$$W_{u2} = 321 \text{ ft/sec}$$

$$\text{Blade Gap } (S_m) = \frac{1.095}{12} \text{ ft}$$

$$\text{Blade Chord } (C) = \frac{1.05}{12} \text{ ft}$$

$$\Gamma_{lift} = S(W_{u1} - W_{u2}) \tag{16}$$

$$\underline{\Gamma_{lift} = 30 \text{ ft}^2/\text{sec}} \qquad \text{(Relative)}$$

$$\Gamma_{dist} = \omega_r CS \tag{18}$$

$$\omega_r = \frac{2854.9}{P'\sqrt{9.17P' - 8.17}} \quad \frac{1}{r'}\left(\frac{\partial P'}{\partial \theta}\right) \tag{D-1}$$

From Fig. A-2 at 8 o'clock

$$P'_{avg} \simeq 1$$

From Fig. 10 at 8 o'clock

$$\frac{1}{r'}\left(\frac{\partial P'}{\partial \theta}\right) \simeq + .13$$

Therefore $\qquad \omega_r = + 372 \text{ sec}^{-1} \qquad$ (absolute)

and $\qquad \Gamma_{dist} = 2.97 \text{ ft}^2/\text{sec} \qquad$ (absolute)

The ratio of circulations becomes

$$\frac{\Gamma_{lift}}{\Gamma_{dist}} \approx \frac{30}{2.97} = 10$$

which is about 10 per cent. It must be remembered that this is occurring at blade passing frequency, and any induced stall would be dynamic stall.

$$\text{Blade Passing Frequency} = \left(\frac{14,200}{60} \frac{Rev}{Sec}\right)\left(31 \frac{Blades}{Rev}\right) = 7.3 \frac{Blades}{ms.}$$

Case III

Unsteady vortex filament motion through a stator is a more complex problem since time dependency of the fluid motion as well as the unsteady response of the blading must be considered. This situation can be pictured as the passage of a vortex filament or a local concentration of vorticity passing through a cascade. In a similar problem, Crimi and Reeves [Ref. 25] calculated sizable lift fluctuations as a helicopter rotor blade passed over a spanwise oriented vortex. Ward [Ref. 26] observed dynamic stall of a rotor blade which he asserted was caused by a radial vortex passing beneath the blade. Figure 17 depicts this situation in a cascade.
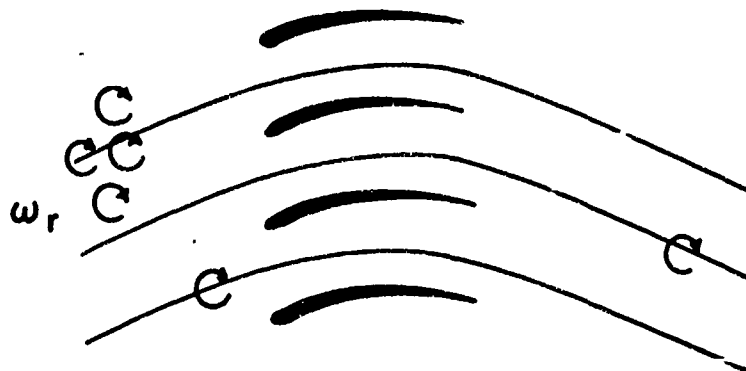
FIG. 17   RADIAL VORTEX FILAMENTS
PASSING THROUGH A STATOR

<u>Case IV</u>

It follows that a vortex filament approaching a rotating blade row is also an unsteady problem. Figure 18 shows basically how W_{u1} is affected by ω_r.
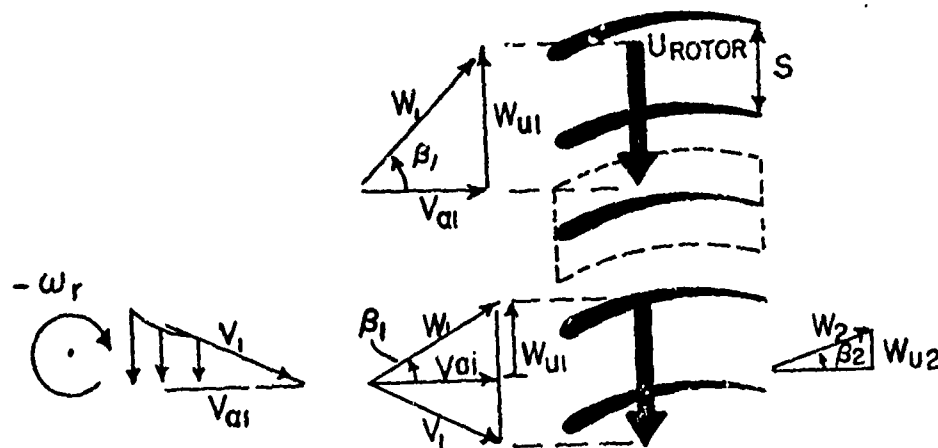
FIG. 18   RADIAL VORTEX FILAMENT
APPROACHING A ROTOR

B. CIRCUMFERENTIAL VORTICITY INLET EFFECTS

Circumferential vorticity taken vectorially is positive in the clockwise direction. Due to the signs in Eqn. 10, the positive gradients in Figs. 11 and 14 represent $-|\omega_\theta'|$. The circumferential vorticity map for the J85 in Fig. 11 shows a strong concentration of vorticity at the outer radii extending through about 300 degrees. Figure 14 shows a similar characteristic for the TF-30 although it is weaker and less extensive. As in the case of ω_r', four basic situations can exist for possible analysis. These are listed in Table IV.

TABLE IV   Possible Combinations for Circumferential Inlet Vorticity

Case	Vortex	Blades	Flow
I	Sheet	Stator	Steady
II	Sheet	Rotor	Steady
III	Filament	Stator	Unsteady
IV	Filament	Rotor	Unsteady

Case I

Circumferential vorticity is oriented perpendicular to the local
blade spans of the compressor. A sheet of ω_θ approaching a stationary
blade row is pictured in Fig. 19.
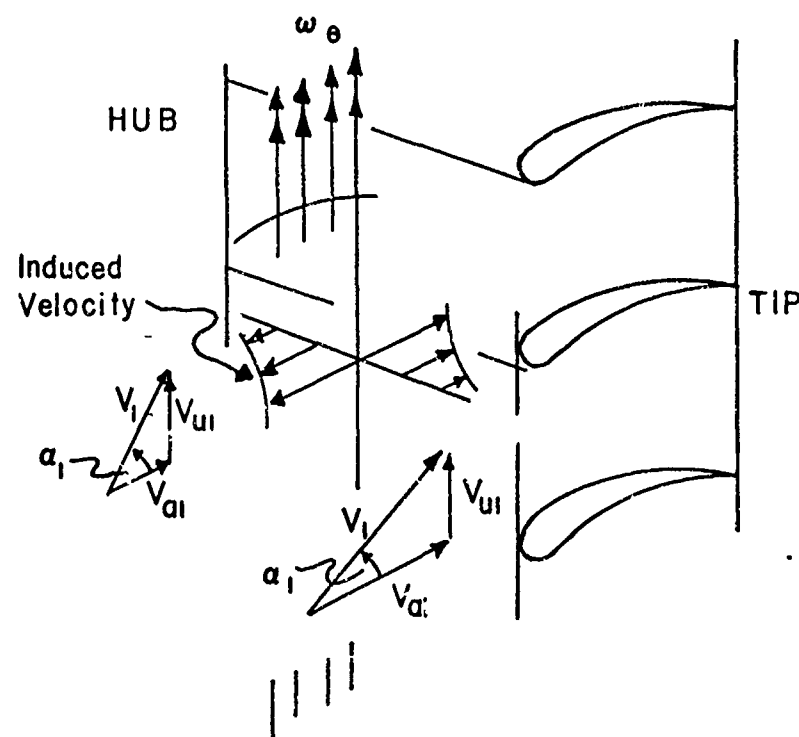
FIG. 19   CIRCUMFERENTIAL VORTEX- SHEET
APPROACHING A STATOR

52

Induced velocities according to the Law of Biot-Savart cause V_{a1} and hence α_1 to change ahead of the cascade. This results in variable lift along the blade spans which produces shed vorticity downstream. Shed vorticity will be dealt with in more detail later when considering secondary flows.

Case II

A circumferential vortex sheet approaching a rotating blade row presents two problems for analysis. Relative motion between the particle paths and the rotor gives rise to a streamwise component of vorticity as well as a component perpendicular to the blade spans, Fig. 20.
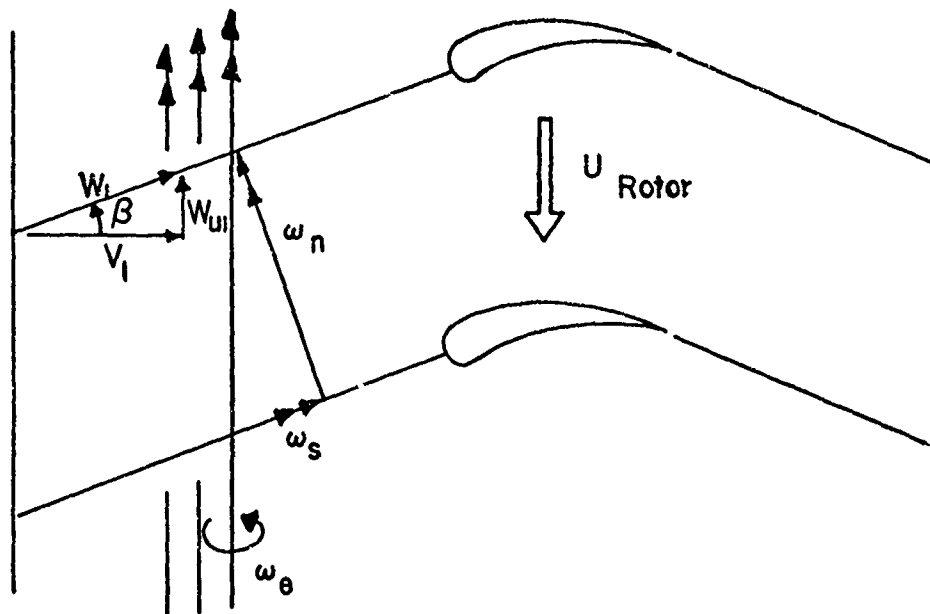
FIG. 20   COMPONENTS OF CIRCUMFERENTIAL
            VORTEX-SHEET APPROACHING A ROTOR

The concentration of ω_θ' at the outer radius in Fig. 11 is essentially constant for about 300 degrees of angular displacement. The life time of one particular characteristic such as this can be as long as the time

for one revolution. The series of TF-30 P_T maps in Appendix A shows a life-time of close to 1/4 revolution. The significance of this is that one blade can experience the same velocity distortion for up to 250 degrees of revolution which allows a steady-state analysis. Induced velocities caused by the normal component of this sheet are those shown in Fig. 19. Velocities induced by the streamwise component are pictured in Fig. 21.
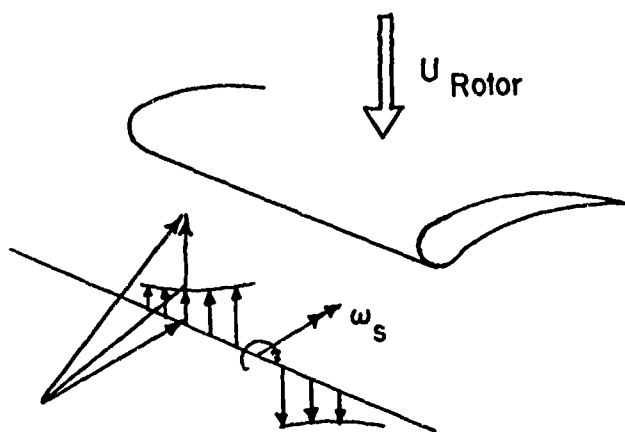
FIG. 21   STREAMWISE COMPONENT OF A CIRCUMFERENTIAL VORTEX-SHEET AT A ROTOR

The streamwise component causes the typical variations in lift along the blade span, but it also passes through the blade row and affects the exit flow angle. This will be discussed later. The normal component also causes a spanwise variation in lift as shown in Fig. 19.

For ω_θ of small circumferential extent, the situation is unsteady due to relative motion between particle paths and the rotor.

Case III

A circumferential vortex filament approaching a stator is an unsteady problem. The effect of the associated entry velocity perturbations shown in Fig. 22, a function of the dynamic response of the blading, would probably be negligible. However, as this filament passes through the blade passage, a streamwise component develops which can interact with existing secondary flows. This phenomenon will be discussed in the next section.
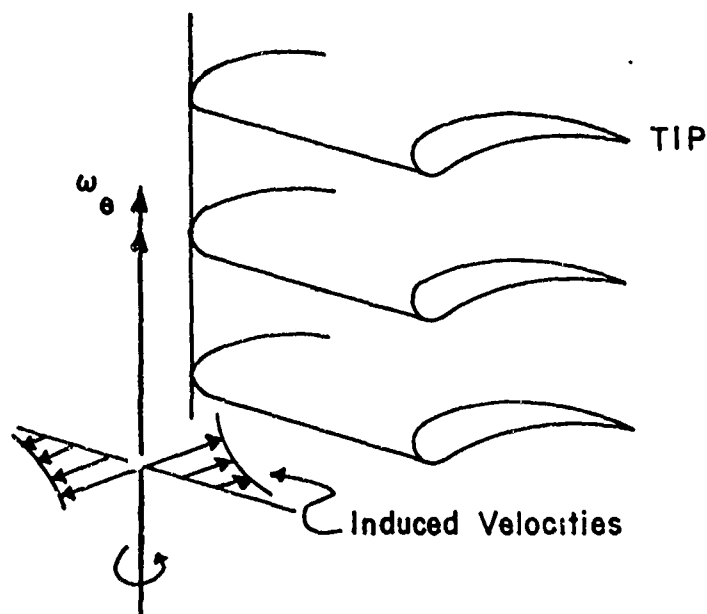
FIG. 22   CIRCUMFERENTIAL VORTEX FILAMENT
           APPROACHING   A   STATOR

Case IV

A circumferential vortex filament approaching a rotor is different than the previous case only because a streamwise component of the filament is present ahead of the blades. Again unsteady response of the blades is a factor to consider.

C. PASSAGE AND EXIT EFFECTS

Several authors have treated the problem of turning a non-uniform flow in a cascade of airfoils. Squire and Winter's method for calcu-. lating secondary flows downstream of a cascade [Ref. 27] has been used extensively in the literature. Preston [Ref. 18], using a more simpli- fied approach, also treates the generation of streamwise vorticity which gives rise to secondary flow after a cascade. However, Preston assumes that in addition to the components of vorticity present in the original vortex filament, a change in circulation about the blade will cause circulation to be shed into the stream. Hawthorne [Ref. 16 and 17] attempts an analytical proof of the existence of these different com- ponents of vorticity in nonuniform flow, and he obtains reasonable agreement with experimental results.

Consider an isolated vortex filament in a sheet normal to the flow direction as it passes through a cascade of stationary airfoils; see Fig. 23. Due to the difference in flow velocity over the suction and pressure surfaces of the blades, this filament will be turned and stretched as it passes through the cascade. Downstream of the cascade, segment ab' gives rise to a "distributed streamwise vorticity" through- out the passage exit plane. This description applies not only to a filament as shown here but also to a vortex-sheet. Squire and Winter's well known expression for this distributed vorticity is

$$\xi_{dist} = -2\epsilon \frac{du}{dz} \tag{19}$$

where ξ is streamwise vorticity, ϵ is the deflection angle, and Z is the spanwise position.
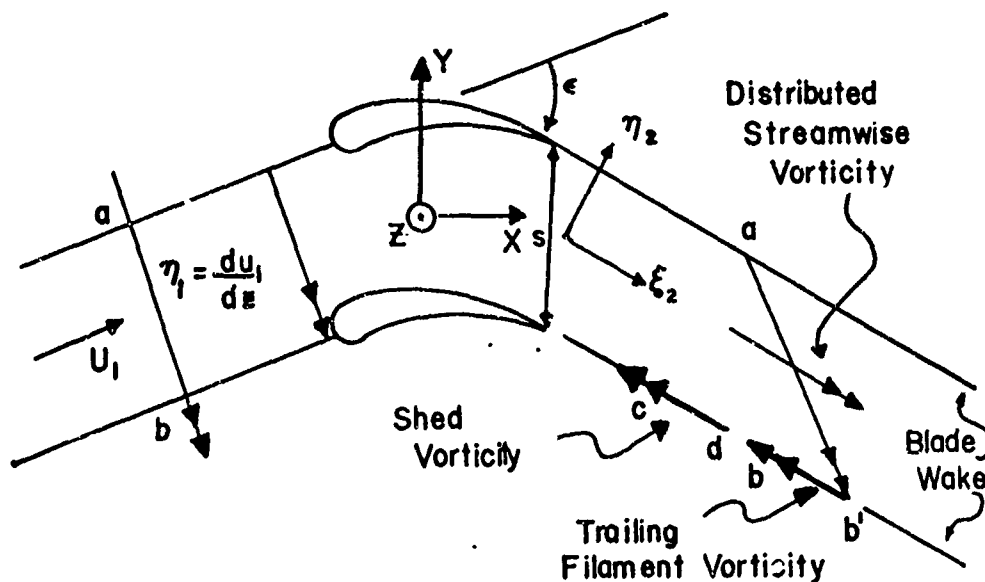
FIG. 23   VORTEX FILAMENT PASSAGE THROUGH A CASCADE

Segment b-b', part of the original filament a-b in Fig. 23, lies along the stagnation streamline and in considering the spanwise direction, this becomes a "vortex-sheet." This is called "trailing filament" vorticity. A third component of exit vorticity, "shed circulation" caused by variable spanwise lift due to the asymmetric inlet flow, also lies along the stagnation streamline and gives strength to the trailing vortex-sheet. This component is labeled c-d in Fig. 23.

Preston's simple analytical expressions for these secondary components of circulation, as applied to Fig. 23, are as follows.

Distributed Secondary Circulation:

$$d\Gamma_1 = \xi_2 \; S \cos \left(\tfrac{\epsilon}{2}\right) dz$$

And replacing ξ_2 with Squire and Winter's expression for distributed secondary vorticity, Eqn. (19), yields

$$d\Gamma_1 = -2\epsilon\left(\frac{du_1}{dz}\right) S \cos \left(\tfrac{\epsilon}{2}\right) dz \tag{20}$$

57

Trailing Filament Circulation:

$$d\Gamma_2 = \left(\frac{du_1}{dz}\right) 2 \ S \sin \left(\frac{\epsilon}{2}\right) \ dz \tag{21}$$

Trailing Shed Circulation:

$$d\Gamma_3 = \left(\frac{du_1}{dz}\right) 2 \ S \sin \left(\frac{\epsilon}{2}\right) \ dz \tag{22}$$

Trailing shed circulation is equal in magnitude and direction to $d\Gamma_2$.
The net circulation associated with the trailing vorticity in one blade
passage and from one airfoil in the form of a "vortex sheet" is the sum
of these three components.

$$d\Gamma = d\Gamma_1 + d\Gamma_2 + d\Gamma_3$$

$$d\Gamma = \left(\frac{du_1}{dz}\right) \left[4 \ S \sin \left(\frac{\epsilon}{2}\right) - 2 \ \epsilon \ S \cos \left(\frac{\epsilon}{2}\right) \right] dz \tag{23}$$

From this exit secondary circulation the change in mean exit flow angle
can be calculated. This total circulation is not uniformly distributed
over the exit area [Ref. 18].

Investigations into changes in deflection due to cascade secondary
flows have generally taken two lines of thought. Values of induced
deflection at the lifting line were derived from the induced velocities
calculated solely from the strength of the vortex sheets by Carter
[Ref. 28] and Hausmann [Ref. 29] to mention a few. These methods neglect
the effects due to distributed passage vorticity and hence are unlikely
to provide satisfactory agreement with experiment [Ref. 12].

Hawthorne [Ref. 30], Smith [Ref. 31], and others have considered
secondary motions to be induced by the distributed vortices within the
passages. It is assumed that the flow downstream behaves as if each

blade passage were separated from its neighbor by the blade wakes, i.e.
vortex sheets. The secondary velocities in the blade passages, v
circumferentially and w spanwise, are defined by a stream function, ψ,
such that

$$w = - \frac{\partial \psi}{\partial y} \qquad v = \frac{\partial \psi}{\partial z}$$

The stream function satisfied continuity for this steady secondary motion
superposed on the main flow.

$$\frac{\partial w}{\partial y} + \frac{\partial v}{\partial z} = 0$$

Substituting the stream function into the vorticity equation (ω = curl u)
and setting it equal to Squire and Winter's expression for the distributed
vorticity, Eqn. 19, yields Poisson's Equation.

$$\frac{\partial^2 \psi}{\partial y^2} + \frac{\partial^2 \psi}{\partial z^2} = -\xi_2 = -2\epsilon \frac{du_1}{dz} \tag{24}$$

Solutions to Eqn. (24) are tedious but have been accomplished by a series
method [Refs. 27 and 30], by relaxation techniques [Ref. 17], and by
electrical analogs [Ref. 32]. The latter reference considers variable
spanwise deflection which causes Eqn. (24) to become

$$\nabla^2 \psi = -2\epsilon \frac{du_1}{dz} + u_1 \frac{d\epsilon}{dz} \tag{25}$$

An exit flow solution for a parabolic inlet profile similar to the case
at hand is given by Honda [Ref. 33].

59

Once secondary velocities, v and w, have been determined, local changes in the exit flow angle, $\Delta\alpha_2$, can be computed. V_2 is the mainstream exit velocity for uniform inlet flow with exit angle α_2.

$$\Delta\alpha_2 = \text{Tan}^{-1}\left(\frac{v}{V_2}\right)$$

The exit flow angle for distorted inlet flow then becomes

$$\alpha_{2_{dist}} = \dot{\alpha}_2 + \Delta\alpha_2$$

Comparison of $\alpha_{2_{dist}}$ with appropriate blade loading criteria [Ref. 10 and 11] could explain the compressor's unstable operation.

Another method of dealing with secondary velocities, v and w, obtained from solving Poisson's Equation was used by Hawthorne [Ref. 17]. Again the assumption of blade passages extended downstream by vortex-sheets trailing the blades is made. There are no normal velocities at the vortex-sheets. The strength of these sheets can be determined by calculating Δw, the change in spanwise secondary velocity across them. As mentioned before, these sheets of fluid leaving the trailing edges are vortex-sheets composed of trailing shed and trailing filament vorticity; see Fig. 24. If the trailing filament vorticity is estimated and subtracted from the total strength of the sheet, the trailing shed ˌ circulation remains. From this can be calculated the variation in lift on the blade since shed circulation and blade lift are related by

$$\Delta L = \rho u \Gamma_3$$

Hawthorne's expression for this trailing filament circulation is

$$d\Gamma_2 = S\left(\frac{du_1}{dz}\right)\left[\frac{1}{2}\frac{\sin 2\alpha_2 - \sin 2\alpha_1}{\cos \alpha_1} - 2\epsilon\cos(\alpha_4)\right] \quad (26)$$
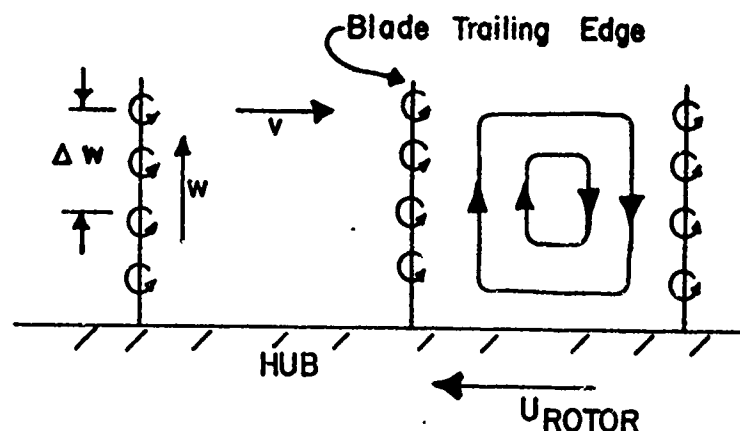
FIG. 24 SECONDARY FLOW DOWNSTREAM OF A BLADE ROW [adapted from Ref. 17]

which is the same as Preston's formula given as Eqn. (21) except for different inlet/exit flow angles. Hawthorne's predicted shed circulation agreed quite well with an experimentally determined spanwise lift variation.

D. CALCULATION OF SECONDARY CIRCULATION

A calculation of these components of secondary circulation as caused by the circumferential vorticity in Fig. 11 was performed in order to quantitatively evaluate the effect of such distortion on a compressor. The analysis was made assuming steady-state conditions which means Case II of Table IV, a circumferential vortex-sheet passing through a rotor. The following terms require definition.

V - Absolute Velocity

W - Relative Velocity

U - Rotor Peripheral Velocity

61

ω - Absolute Fluid Vorticity

ζ - Relative Fluid Vorticity

Ω - Rotor Angular Speed

α - Absolute Flow Angle

β - Relative Flow Angle

$\rightarrow$ - Velocity Vector

$\twoheadrightarrow$ - Vorticity Vector

Subscripts; see Fig. 25

r,θ,z - Absolute Coordinate Direction

s,n - Natural or Streamline Coordinates

s - Streamwise

n - Normal to Streamlines

0 - Upstream of Compressor

1 - Compressor face (entry to blade row)

2 - Blade-row exit plane
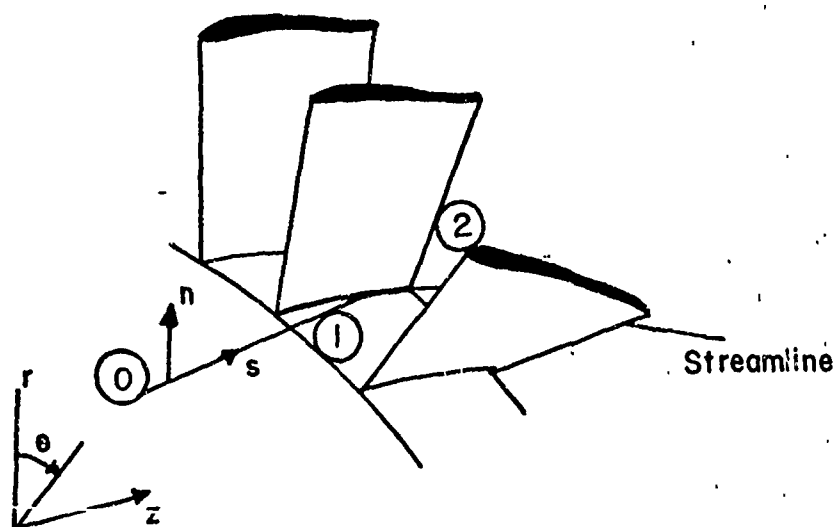
FIG. 25   NOMENCLATURE

Horlock's method [Ref. 15] of treating the passage of a vortex filament through a rotating blade-row results in the following vector transformation. Figure 26(a) is the velocity diagram ahead of the rotor which is convecting the vortex filament, ω_θ (one of many in a sheet). The absolute velocity is axial so that $W_{\theta 1} = -U_{rotor}$. Figure 26(c) is the inlet __absolute__ vorticity combined with rotor rotation to give the inlet __relative__ vorticity. Equations (27) and (28) are the corresponding analytical expressions for these components of relative vorticity in terms of ω_θ.

$$\zeta_{s1}' = +2\,\Omega\cos\beta_1 - \omega_\theta\sin\beta_1 \tag{27}$$

$$\zeta_{n1} = -2\,\Omega\sin\beta_1 - \omega_\theta\cos\beta_1 \tag{28}$$

The approach of a vortex filament to a rotating cascade and the resultant secondary relative vorticity at the passage exit are pictured in Fig. 27. This figure is similar to Fig. 23 except it applies to a rotor while Fig. 23 is for a cascade.

Combining inlet streamwise vorticity which passes through the cascade unaffected with the exit vorticity of Eqn. (19) yields the total distributed vorticity in the blade passage exit plane.

$$\zeta_{s2} = \zeta_{s1} - 2\,\epsilon\,\zeta_{n1} \tag{29}$$

Substituting Eqns. (27) and (28)

$$\zeta_{s2} = (2\Omega\cos\beta_1 - \omega_\theta\sin\beta_1) - 2\epsilon(-\omega_\theta\cos\beta_1 - 2\Omega\sin\beta_1) \tag{30}$$

Since this exit vorticity is in the direction of the flow, multiplying it by the blade passage exit area normal to the direction of flow yields exit distributed circulation.
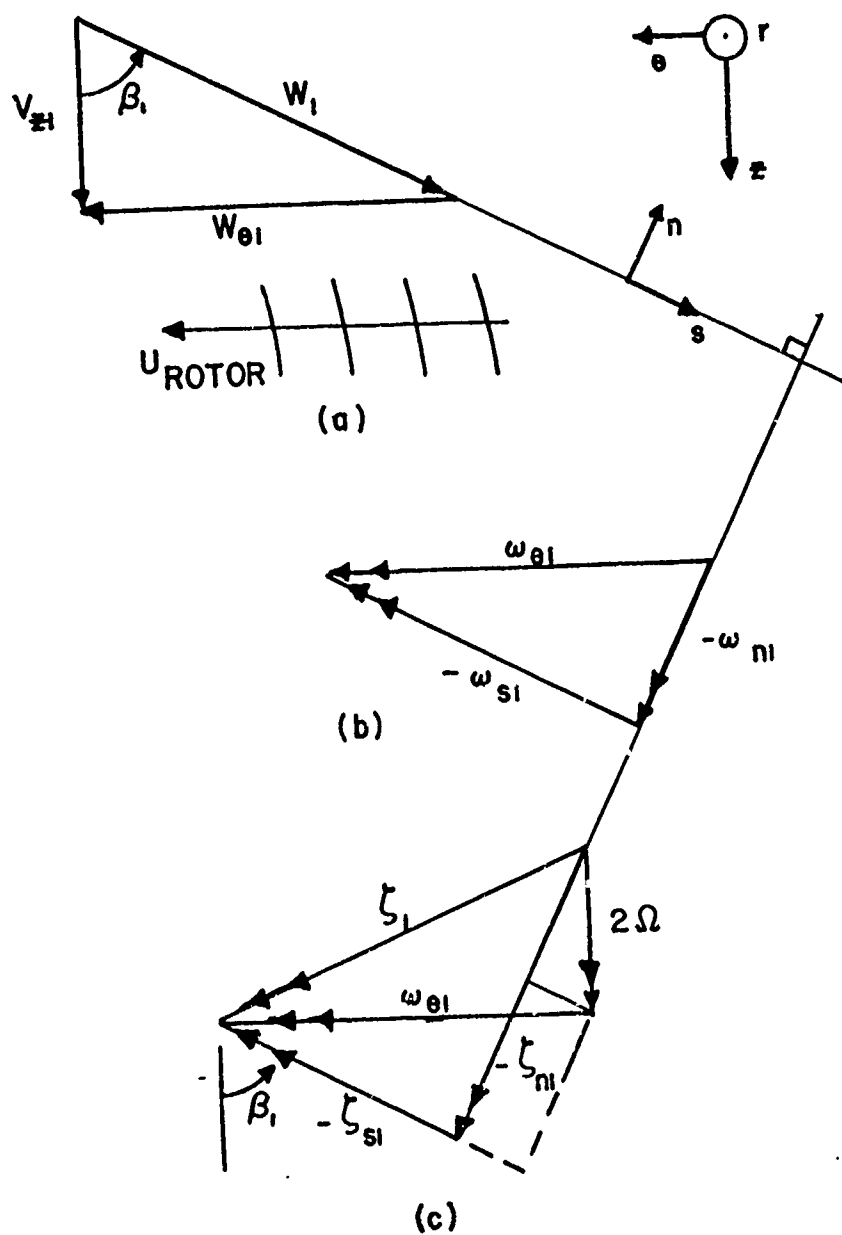
FIG. 26   VECTOR TRANSFORMATION FROM
ABSOLUTE TO RELATIVE VORTICITY
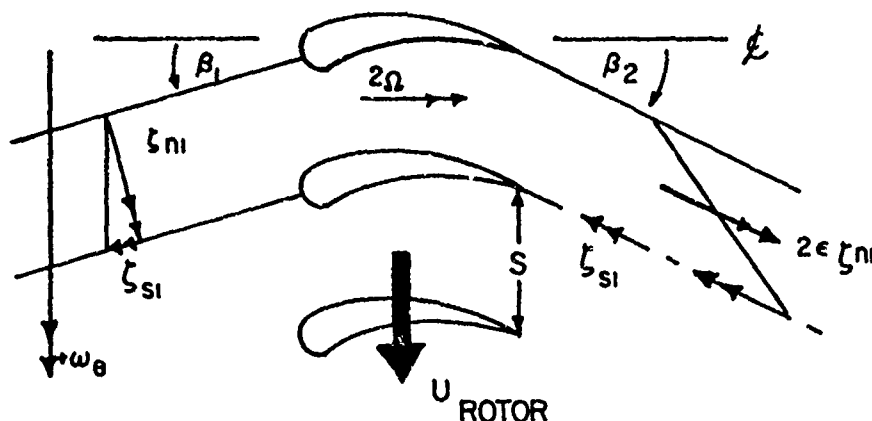
FIG. 27   PASSAGE   OF   A   VORTEX   FILAMENT
            THROUGH   A   ROTATING   CASCADE

$$\frac{d\Gamma_1}{dr} \,. = \, \zeta_{s2} \, S \, \cos \beta_2 \tag{31}$$

When transformed from absolute to relative coordinates, Hawthorne's
expression for trailing filament circulation given previously as Eqn.
(26) becomes

$$\frac{d\Gamma_2}{dr} = S \, \zeta_{n1} \left(\frac{1}{2} \, \frac{\sin 2\beta_2 - \sin 2\beta_1}{\cos \beta_1} - 2\varepsilon \cos \beta_2 \right) \tag{32}$$

Assuming two-dimensional flow, Hawthorne's equation for shed circulation
is

$$\frac{d\Gamma_3}{dr} = -S \cos \beta_1 \, \zeta_{n1} (\tan \beta_2 - \tan \beta_1) \tag{33}$$

A simplified application of these equations to the circumferential
vorticity and total-pressure maps for the J85 (Figs. 11 and A-2) was

made by assuming an average radial distribution of $\partial P'/\partial r'$ and P' to exist for a circumferential segment of the face. Equation D-2 was applied to radials at the three circumferential positions shown in Fig. 28. (Appendix D)

$$\omega_\theta = \left(\frac{-2854.9}{P'\sqrt{9.17P' - 8.17}} \right) \frac{\partial P'}{\partial r'} \quad sec^{-1} \qquad (D-2)$$

Now using Eqns. (27), (28), and (29), the various components of relative vorticity were calculated for a sufficient number of radial positions see Appendix E. Figure 29 shows the relative sizes of these components for circumferential position I.
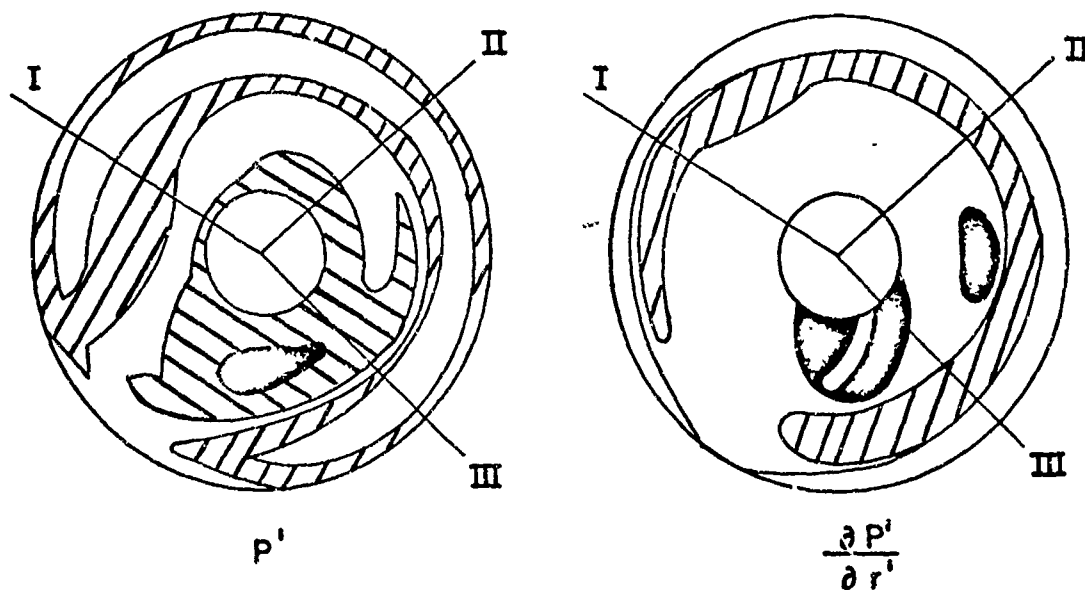
FIG. 28   DATA POINTS FOR CALCULATION OF ω_θ
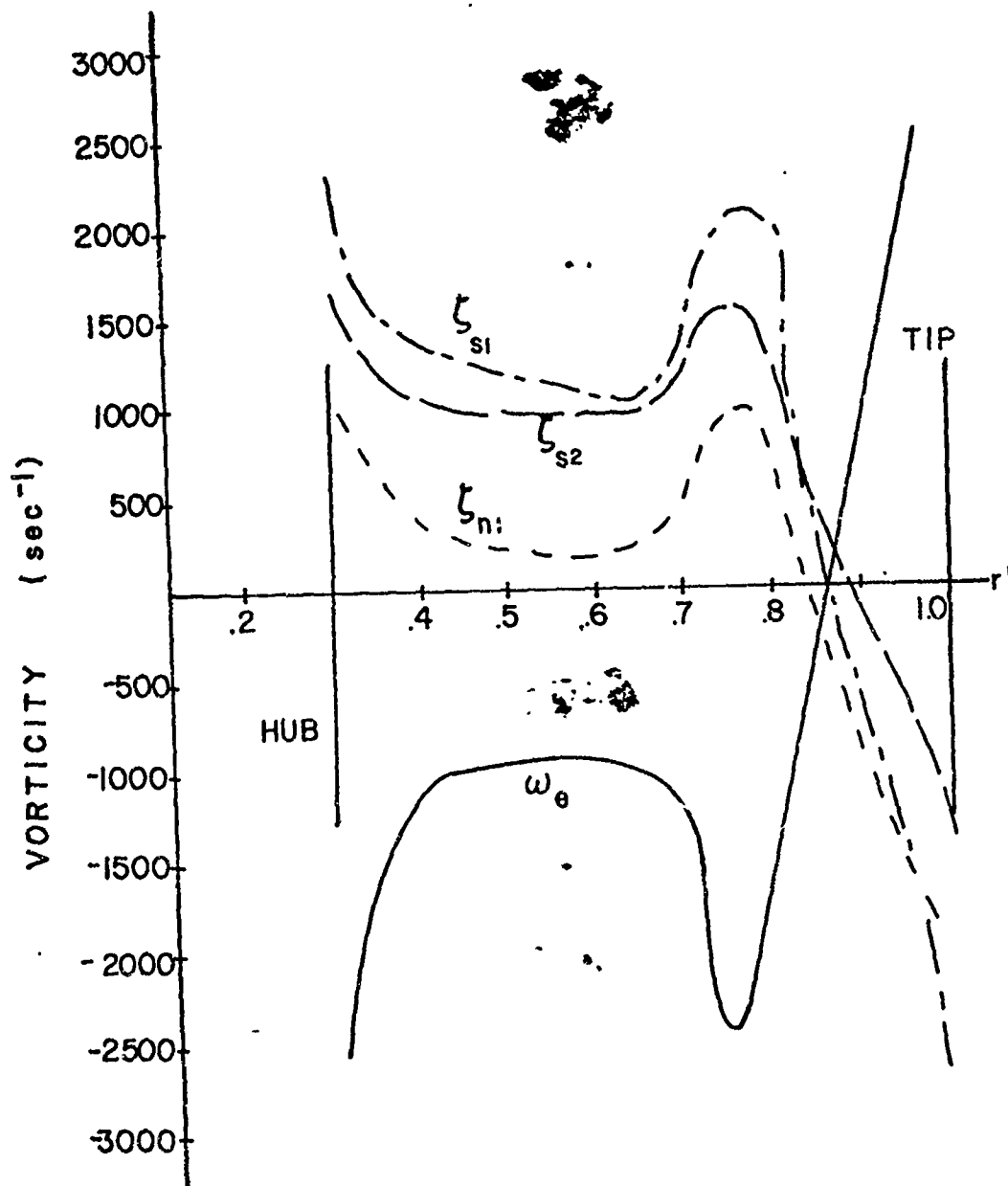
FIG. 29   VORTICITY COMPONENTS AT RADIAL   I

Secondary circulations as a function of span at the blade row exit plane were calculated using Eqns. (31), (32), and (33); see Appendix E. The area under curve "A" in Fig. 30 represents distributed secondary circulation. The area under curve "B" is trailing filament circulation, and the area under "C" is shed circulation. These latter two are the circulations due to the vortex-sheet. The magnitudes of these components are found by integration over dr'.

$$R \int_{.3}^{.9} \left(\frac{d\Gamma_1}{dr} \right) dr' = 32.1 \quad ft^2/sec$$

where R is the radius used for non-dimensionalizing.

Concerning the results in Table V, distributed secondary circulation, Γ_1, represents a loss in kinetic energy. Blade-lift circulation is approximately equal to 30 ft^2/sec; therefore the ratio of these two is about 1 to 1. In order to evaluate the actual effect Γ_1 has on the compressor, a solution to Poisson's Equation, as described previously, would be necessary. From this solution the exact strength of the trailing vortex-sheet could be determined. Subtracting trailing filament vorticity (or Γ_2) from the calculated strength of this vortex-sheet would yield the exact shed circulation. Equation (33) from which $\bar{\Gamma}_3$ in Table V has been calculated was found by Hawthorne to yield values higher than those found experimentally. However, this analysis is essentially an order-of-magnitude check, and Eqn. (33) is adequate. Since shed circulation is related to the spanwise variation in blade lift by

$$\Delta L = \rho W_\infty \Gamma_3$$

then

$$\frac{\Delta L}{L} \approx \frac{\Gamma_{shed}}{\Gamma_{lift}} \tag{34}$$
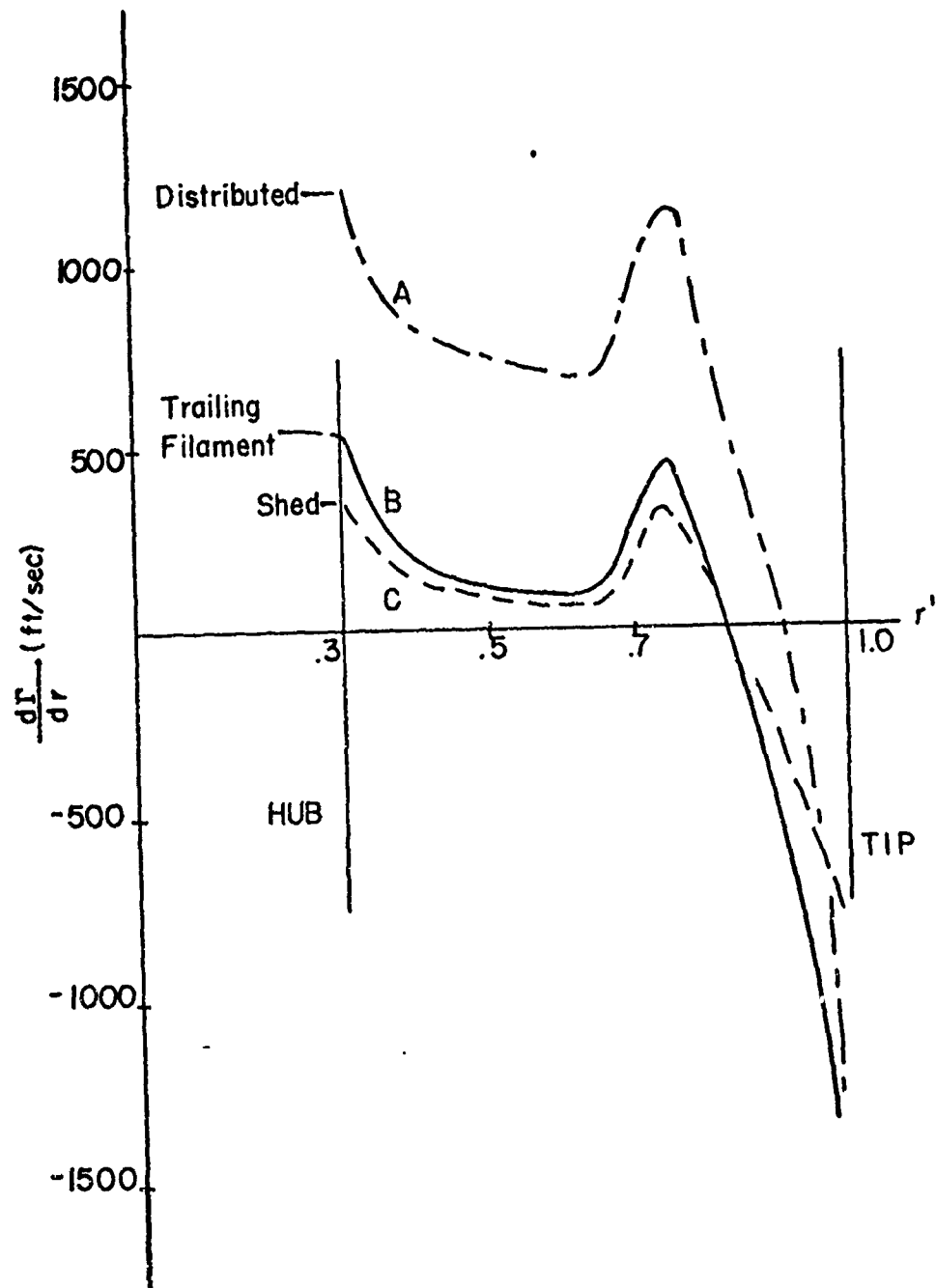
FIG. 30   EXIT SECONDARY CIRCULATION
COMPONENTS AT RADIAL   I

The circulation about one blade in the rotor under consideration for uniform inlet flow is approximately

$$\Gamma_{lift} = S(W_{u1} - W_{u2}) = 30 \text{ ft}^2/\text{sec}$$

The average value of positive shed circulation over the three circumferential data points considered, Radials I, II, and III, is

$$\frac{5.0 + 3.9 + 15.1}{3} = 8 \text{ ft}^2/\text{sec}$$

So the variation in lift from Eqn. (34) is

$$\frac{\Delta L}{L} = \frac{8}{30} \approx 25 \%$$

which represents unloading at the center span of the blade. For the negative shed circulation at the blade tip

$$\frac{-6.0 - 8.5 - 10.9}{3} = \frac{\Delta L}{L} = \frac{-8.8}{30} \approx 30 \%$$

If the compressor blading is operating near stall it certainly seems plausible that a change of 25 to 30 per cent in lift could trigger stall.

Table V Magnitudes of Circulation Components

	Radial I		Radial II		Radial III	
	Limits (r')	Value (ft²/sec)	Limits (r')	Value (ft²/sec)	Limits (r')	Value (ft²/sec)
Γ_1	.3 - .9	+32.1	.3 - .9	+30.6	.3 - .5	-4.2
	.9 - 1.0	-5.6	.9 - 1.0	-9.0	.5 - .9	+39.5
					.9 -1.0	-12.3
Γ_2	.3 - .825	+7.1	.3 - .475	-3.8	.3 - .525	-11.6
	.825 - 1.0	-9.7	.475 - .85	+5.6	.525 - .825	+21.4
			.85 - 1.0	-12.0	.825 - 1.0	-15.4
Γ_3	.3 - .825	+5.0	.3 - .475	-.3	.3 - .525	-8.24
	.825 - 1.0	-6.9	.475 - .85	3.9	.525 - .825	+15.1
			.85 - 1.0	-8.5	.825 - 1.0	-10.9

V. SUMMARY AND REVIEW

Figures 31 and 32 are presented as a review and outline of the
preceding theory for analyzing the effect of inlet flow distortion on
an axial-flow turbomachine. Data from total-pressure maps, $\partial P_T/\partial r$ and
$\partial P_T/\partial \theta$, consitute the initial known quantities. All pertinent assump-
tions and simplifying restrictions are included in the chart as they
apply. The resulting determination of ω_z through a consistent order-
of-magnitude analysis implies complete definition of the velocity field
ahead of the compressor with the exception of the ambiguity in sign of
ω_z. This is significant in that a three-dimensional flow field has been
determined from a two-dimensional pressure map at the expense of intro-
ducing an error of order ϵ^2. Continuing in Fig. 32, the analysis next
relates portions of several existing theories on secondary flows in
cascades and turbomachines to the maps of radial and circumferential
vorticity. This yields an estimate of the strength of the secondary
flows caused by inlet flow distortion. The large value for $\Delta L/L$ which
is calculated suggests that the linear cascade theories used are not
adequate for the accuracy required in deriving a stall criterion. Some
necessary considerations for further refinement of the theory which were
not considered in this analysis are (1) blade twist, (2) three-dimensional
effects and interaction between normal secondary flows with distortion
induced flows, and (3) changes in vorticity with passage through the
blade row.
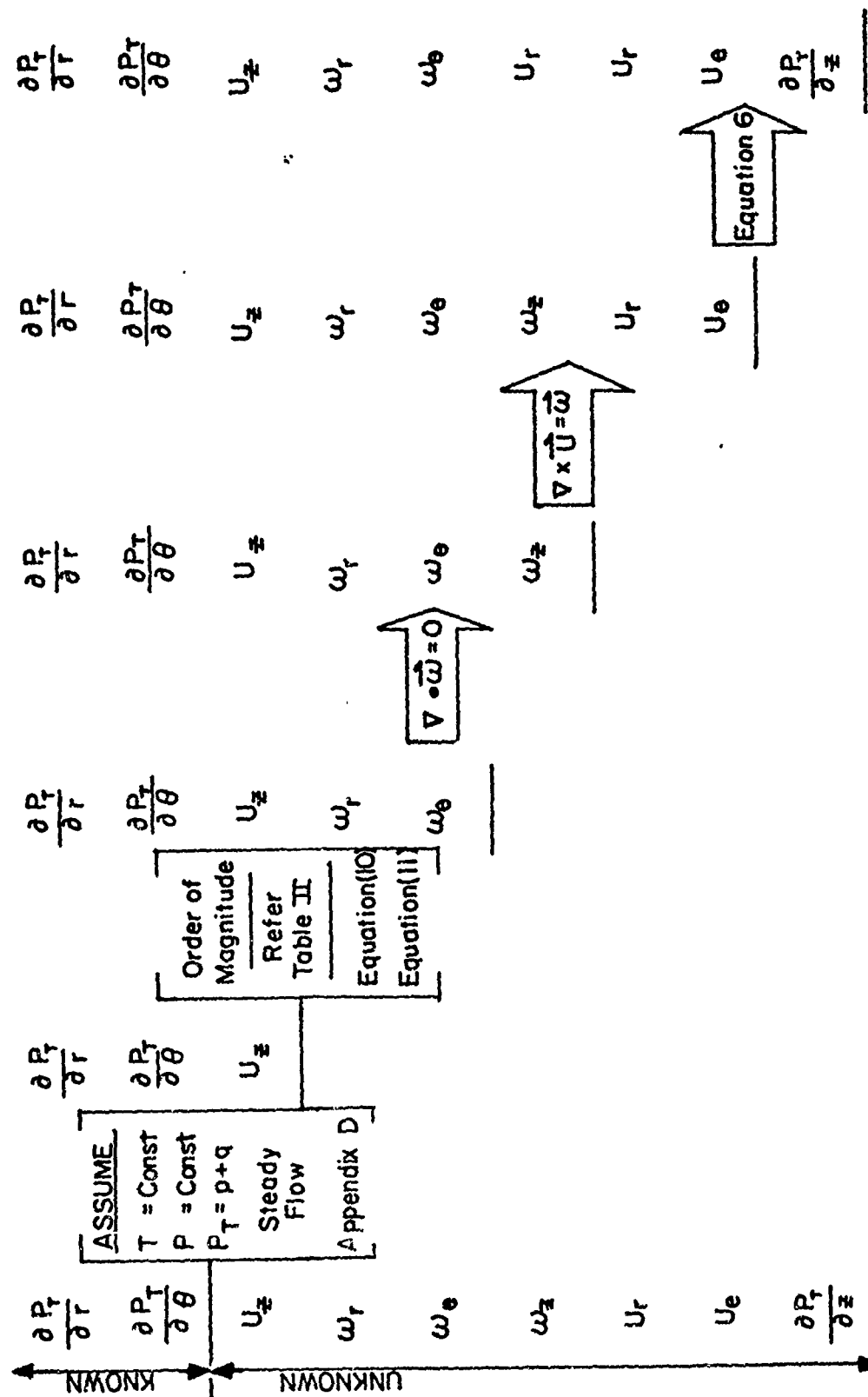
FIG. 31 FLOW DIAGRAM FOR ANALYSIS; STEADY FLOW
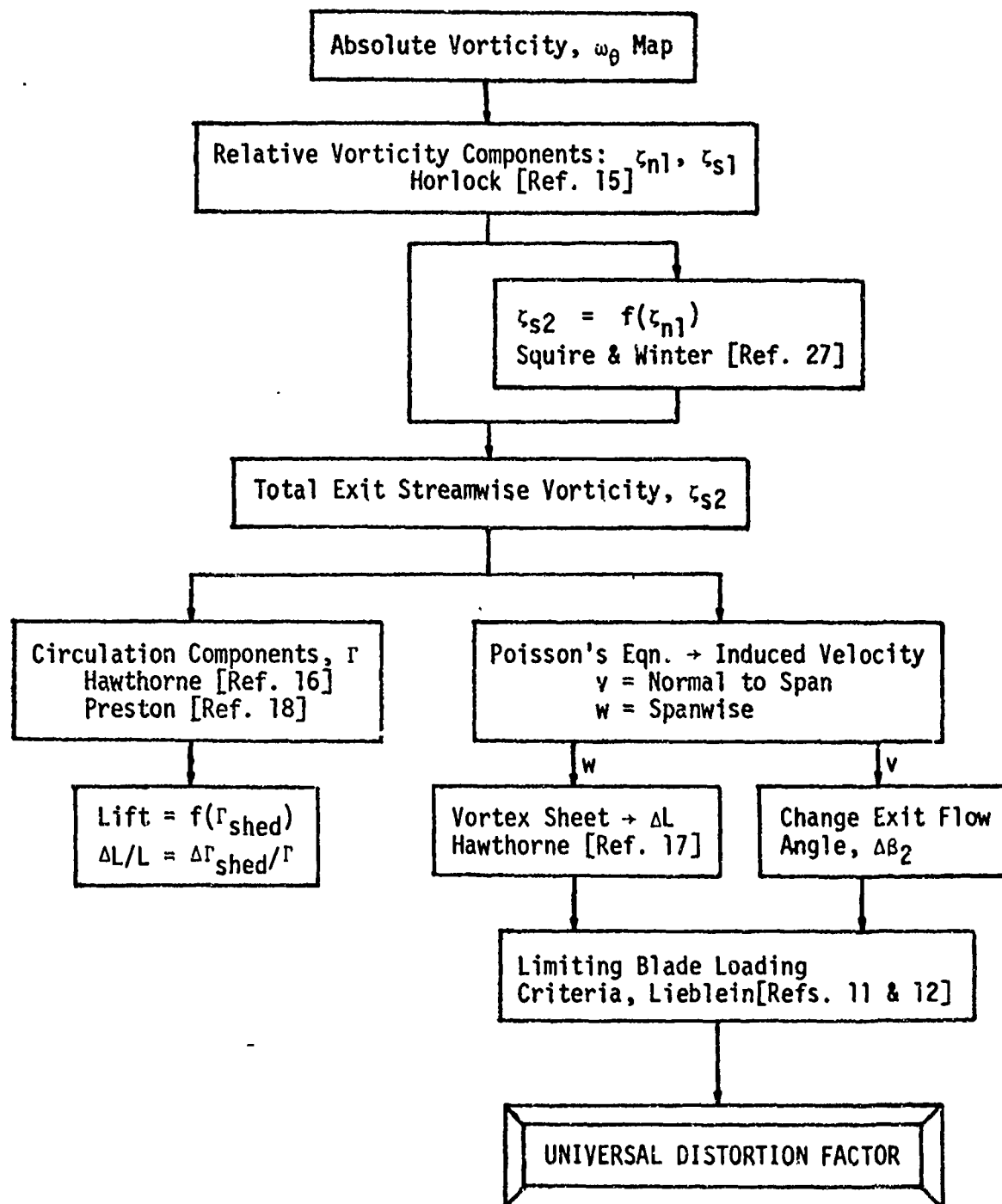
Fig. 32. Composite Theory for Analyzing Vorticity Maps

VI. CONCLUSIONS

This analysis is the first attempt at relating total-pressure distortion maps to the internal aerodynamics of a turbomachine. Separating the inlet distortion into components of radial and circumferential vorticity introduced flexibility in treating the problem as well as maintained a comprehensible physical picture of the aerodynamical situation. For the data analyzed herein, radial vorticity was found to be less significant to degradation of compressor performance than was circumferential vorticity since the radial vorticity was coupled to the dynamic response of the blading. This would require an unsteady analysis. The relative significance of $\vec{\omega}_r$ and $\vec{\omega}_\theta$ in this analysis does not necessarily apply in general. The effect of axial vorticity, $\vec{\omega}_z$, must be included in further work.

The size of the calculated shed circulation from a blade indicates distortion induced secondary flows are of sufficient size to seriously affect the compressor's operation. With further refinement to the present theory, secondary flows could be evaluated to a degree of accuracy capable of predicting stall through the mechanism of shed circulation or changes in exit flow angles. A solution to Poisson's Equation would provide the needed accuracy with which to use appropriate blade-loading criteria in defining inlet-distortion stall criteria. Although stall normally originates somewhere downstream of the first few stages, the distortion must be treated as it passes through each individual stage. The present theory deals only with the first blade row; however, it is one row closer to the origin of the stall and has eliminated a certain degree of uncertainty. This theory may be extended to

succeeding stages in the compressor by the technique illustrated in
Fig. 26.

Finally, in working toward a universal distortion factor, the
effects of other types of inlet distortion, i.e. total-temperature and
molecular weight, must be included. These extensions to the present
theory should provide reliable and comprehensive stall-inducing
distortion criteria.

APPENDIX A

ORDER OF MAGNITUDE ANALYSIS

Part I Preparation of Total-Pressure Data

The following data and calculations apply to the experiments performed on a J85-GE-13 turbojet as described in Ref. 2, $\alpha = 0^0$ stall point. Some data were also obtained from Ref. 24.

Subscripts:
- 0 - Free stream
- 1 - Compressor face
- 2 - Rotor exit, first stage
- T - Stagnation quantity

$$\bar{P}_{T1} = 1549 \text{ psf}$$

$$\bar{P}_1 = 1380 \text{ psf} \quad \text{(Static)}$$

$$\bar{T}_{T1} = 532^\circ R$$

$$M_\infty = 2.5$$

Compressor Inlet flow area, $A_1 = 185 \text{ in}^2$

Figure A-1 is a pressure contour map of $P_{T1}/\bar{P}_{T0}$ reproduced from Ref. 2. For our purposes, this must be converted to P' which is defined as $P_{T1}/\bar{P}_{T1}$.

Pressure Recovery of Inlet = .77

$$\frac{\bar{P}_{T1}}{\bar{P}_{T0}} \approx .77$$

$$\frac{P_{T1}}{\bar{P}_{T1}} = \frac{P_{T1}}{\bar{P}_{T0}} \cdot \frac{\bar{P}_{T0}}{\bar{P}_{T1}}$$

$$\frac{P_{T1}}{\bar{P}_{T1}} = \frac{P_{T1}}{\bar{P}_{T0}} \cdot \frac{1}{.77} \tag{A-1}$$
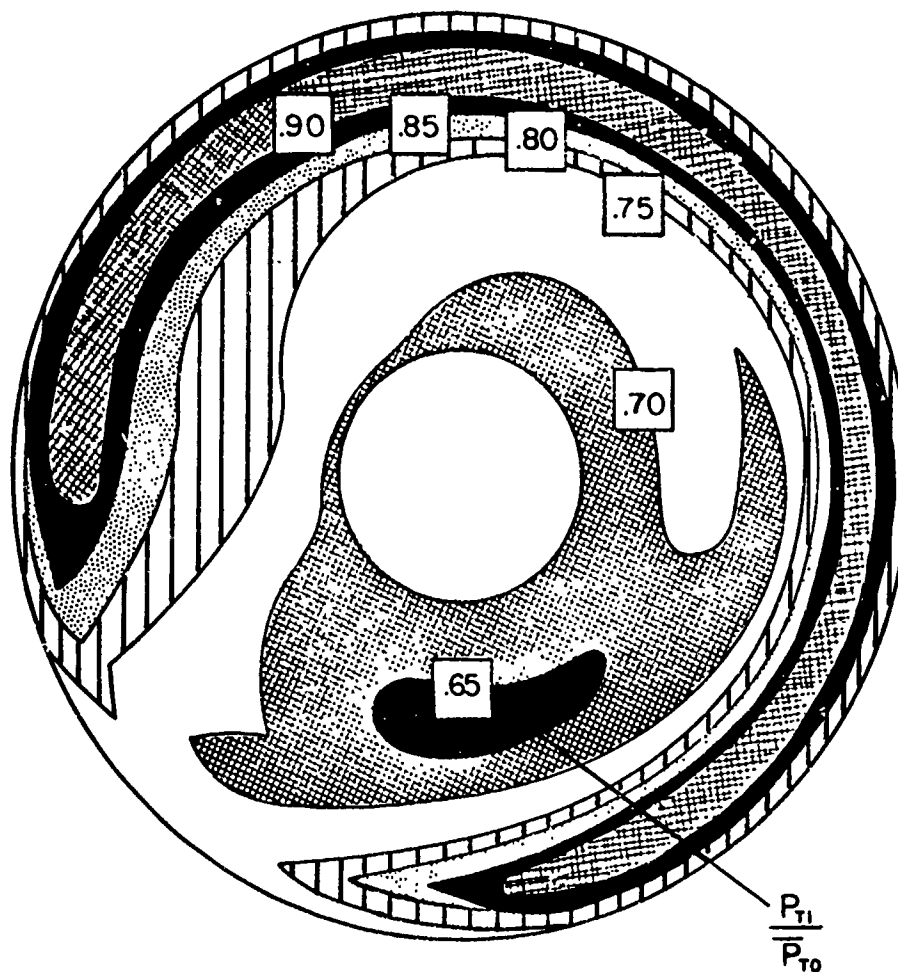
FIG. A-I PEAK INSTANTANEOUS PRESSURE
CONTOURS, J85 (from Ref. 2)

Application of Eqn. (A-1) to Fig. A-1 yields the desired pressure contours, Fig. A-2. Figures A-3 through A-11 are instantaneous pressure contours (P') taken from experiments conducted on a TF-30 engine [Ref. 23]. The radial lines at the centers represent compressor rotation.

$$RPM \simeq 10,000$$

$$\text{time between Figs.} = \left(\frac{60}{10^4} \quad \frac{Sec}{Rev}\right)\left(\frac{1}{32} \quad \frac{Rev}{Seg}\right)$$

$$= .1875 \times 10^{-3}$$

$$\simeq .2 \text{ ms.}$$

Elapsed time (A-3 → A-12) ≃ 1.5 ms.

Figure A-11 is the frame prior to engine surge.

$$\overline{P}_S = 1440 \text{ psf}$$

Estimated Inlet Values

$$\overline{M} = .4$$

$$\overline{P}_T = \overline{P}_S \left(1 + \frac{\gamma-1}{2} \overline{M}^2\right)^{\frac{\gamma}{\gamma-1}}$$

$$\overline{P}_T = 1610 \text{ psf}$$

79
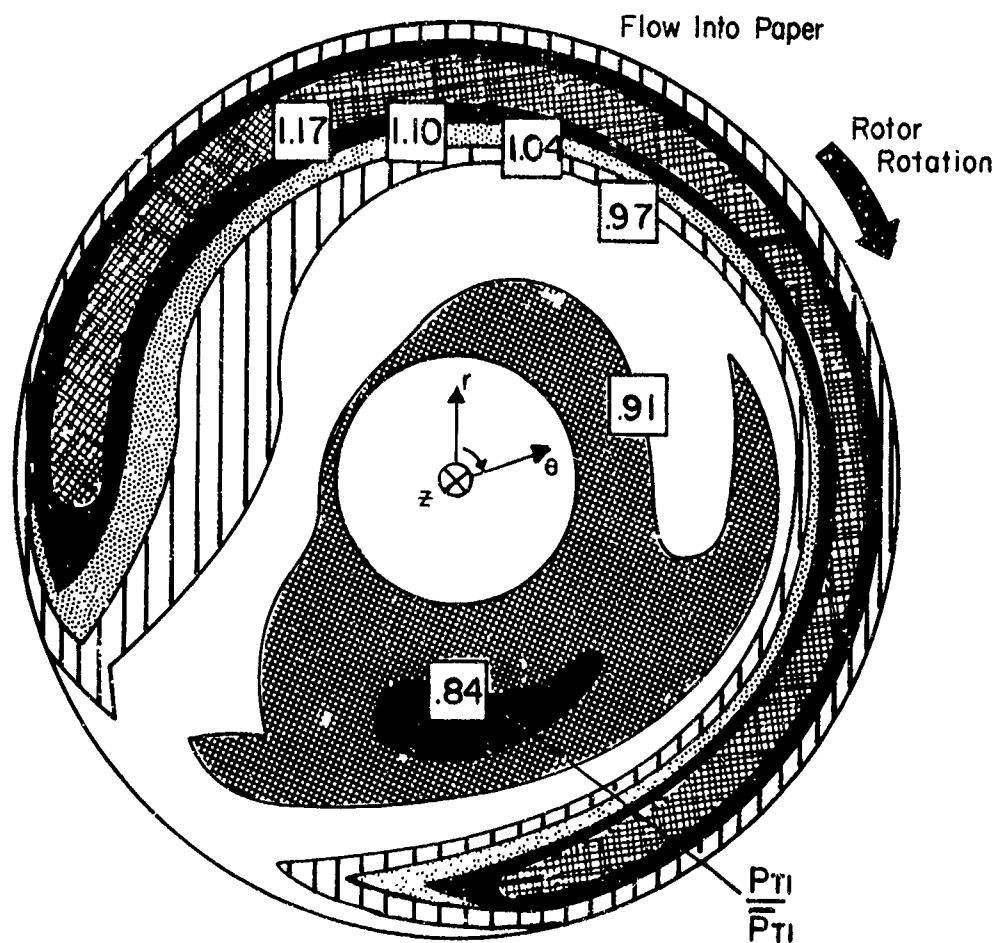
FIG. A-2   TRANSFORMED   PRESSURE
CONTOURS
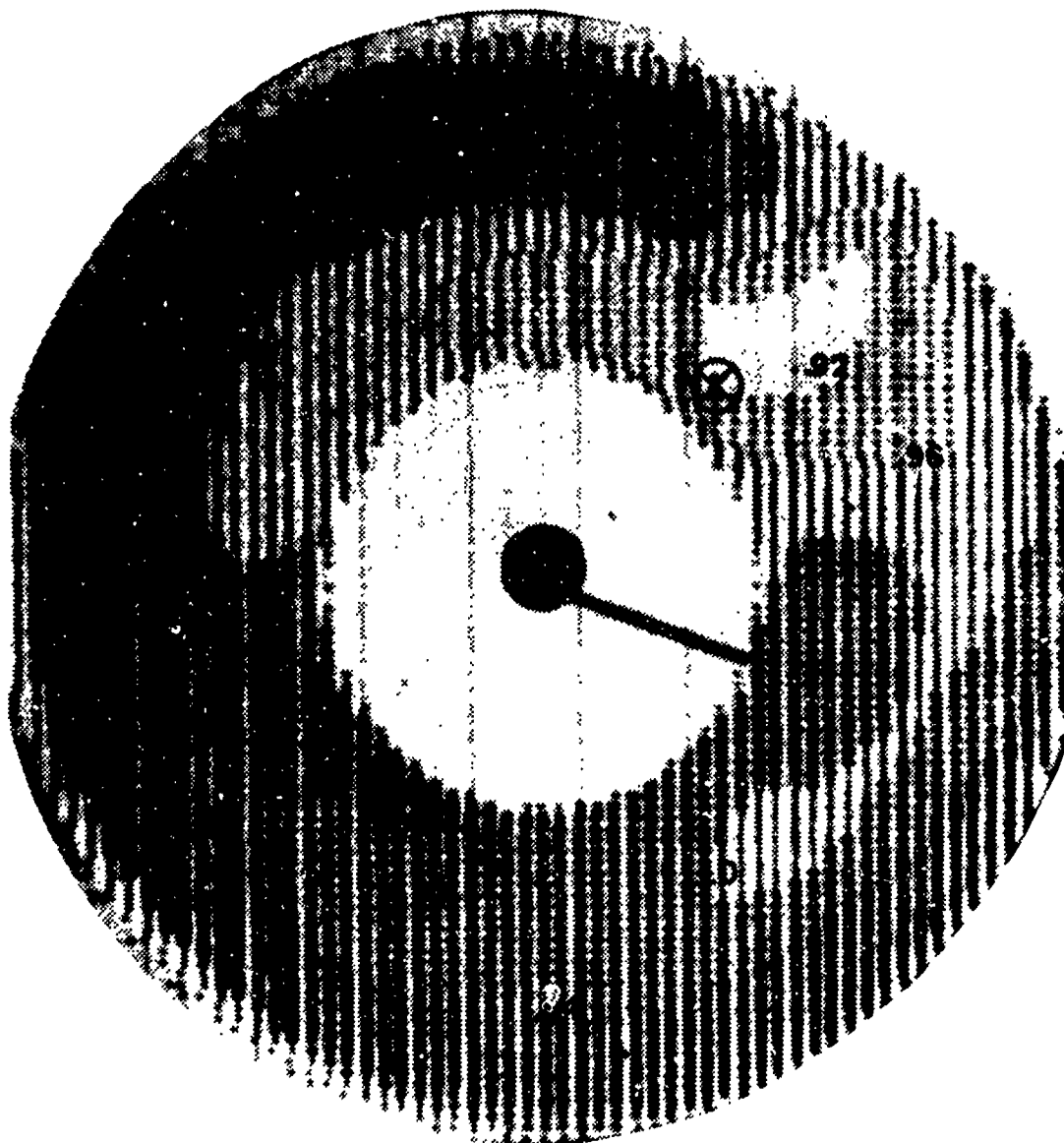
FIG. A-3   FRAME ONE OF INSTANTANEOUS
            PRESSURE CONTOURS SEQUENCE, TF-30
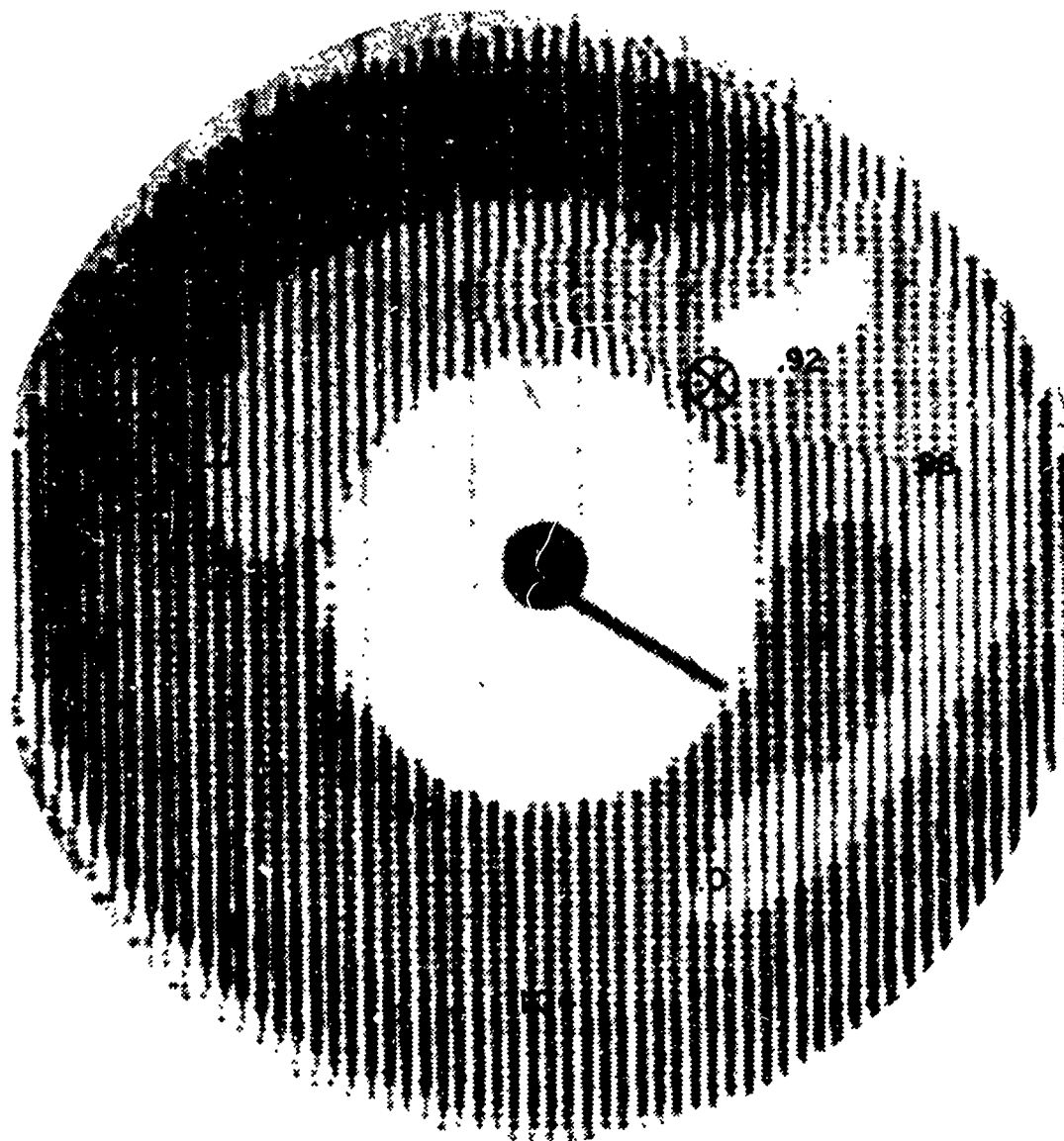
FIG. A-4   FRAME   TWO   OF   INSTANTANEOUS
PRESSURE   CONTOURS,   TF - 30
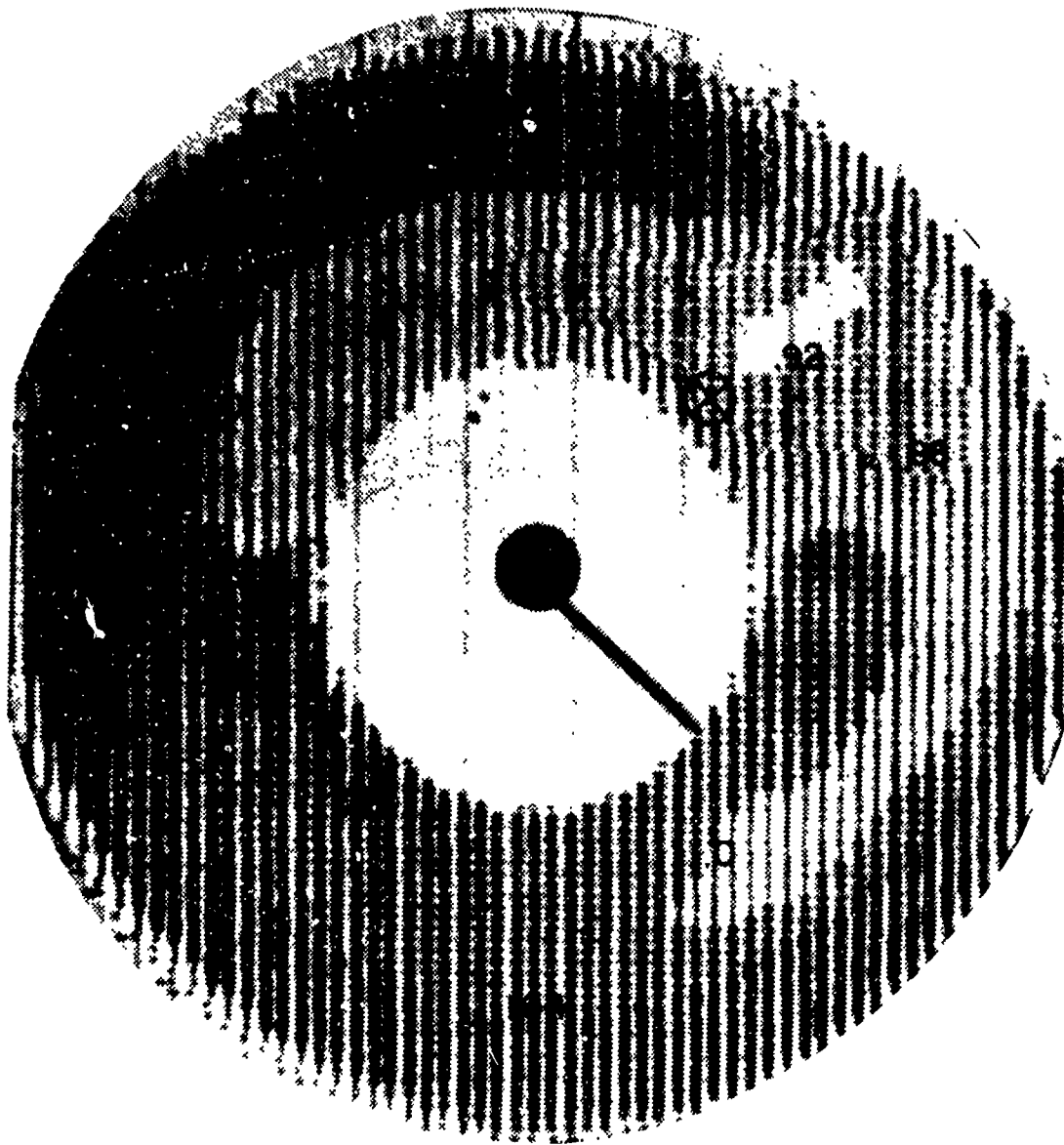
FIG. A-5 FRAME THREE OF INSTANTANEOUS
PRESSURE CONTOURS SEQUENCE, TF-30
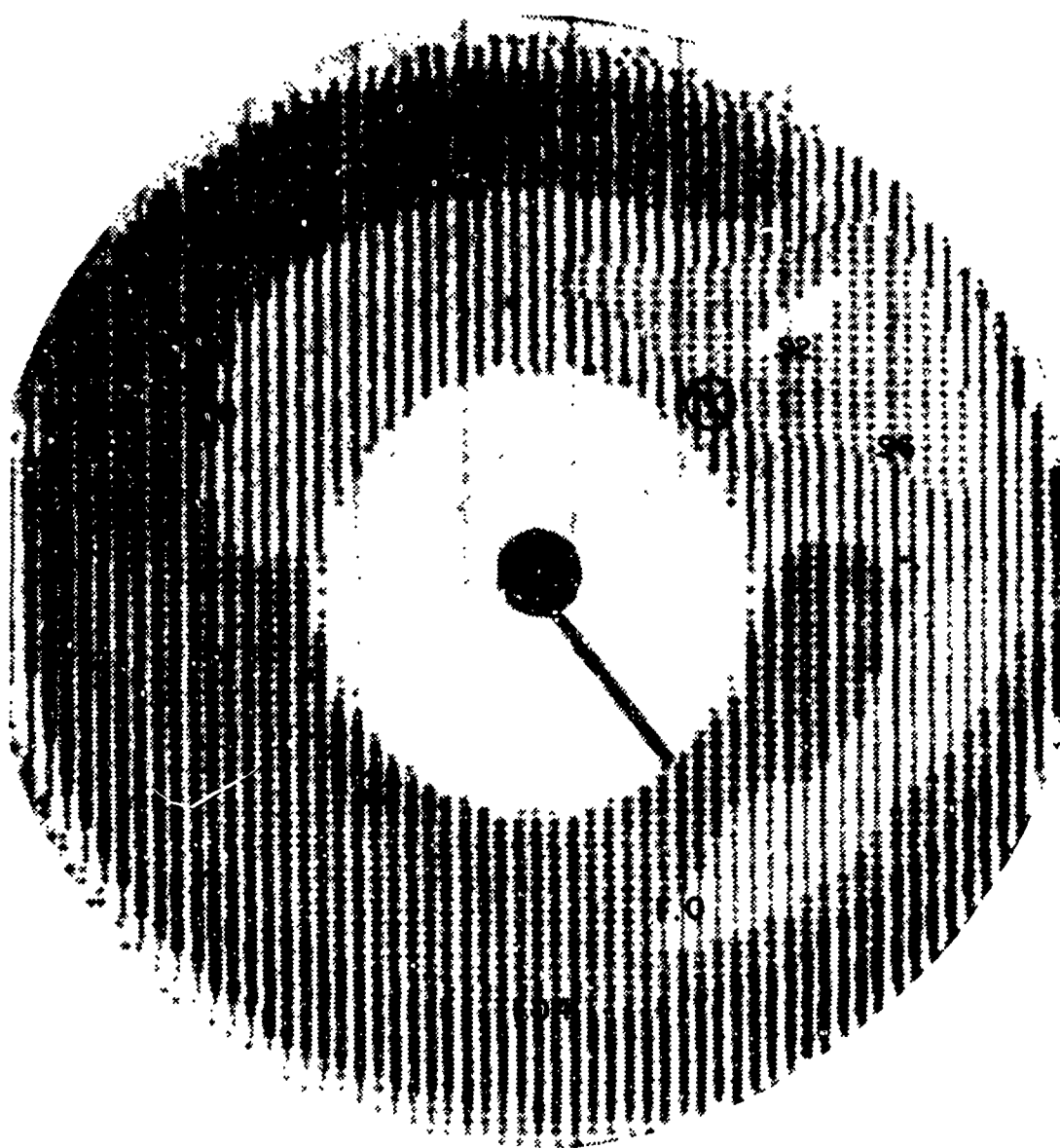
FIG. A-6   FRAME   FOUR   OF INSTANTANEOUS
PRESSURE CONTOURS SEQUENCE, TF-30
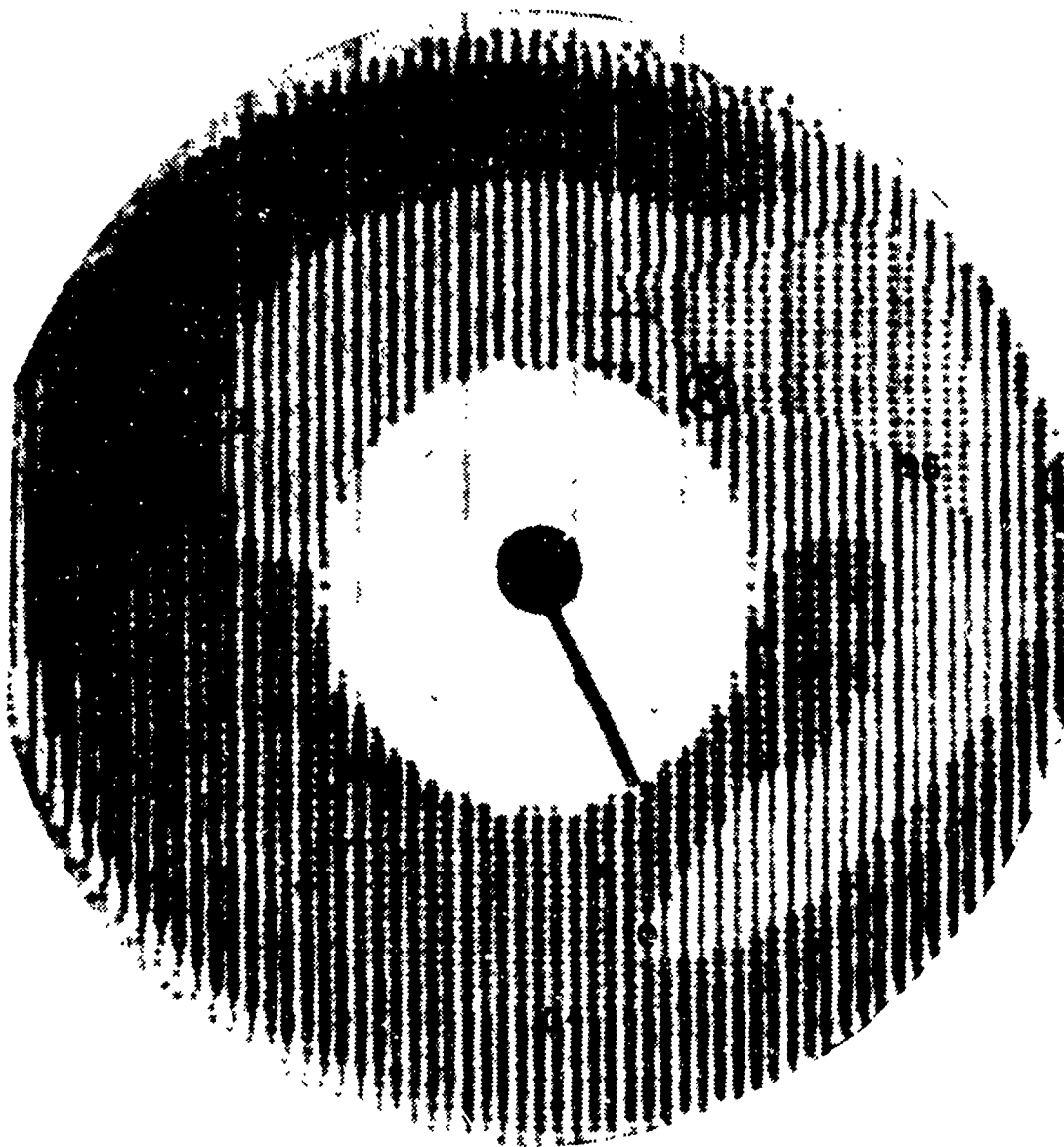
FIG. A-7   FRAME FIVE OF INSTANTANEOUS
            PRESSURE CONTOURS SEQUENCE, TF-30
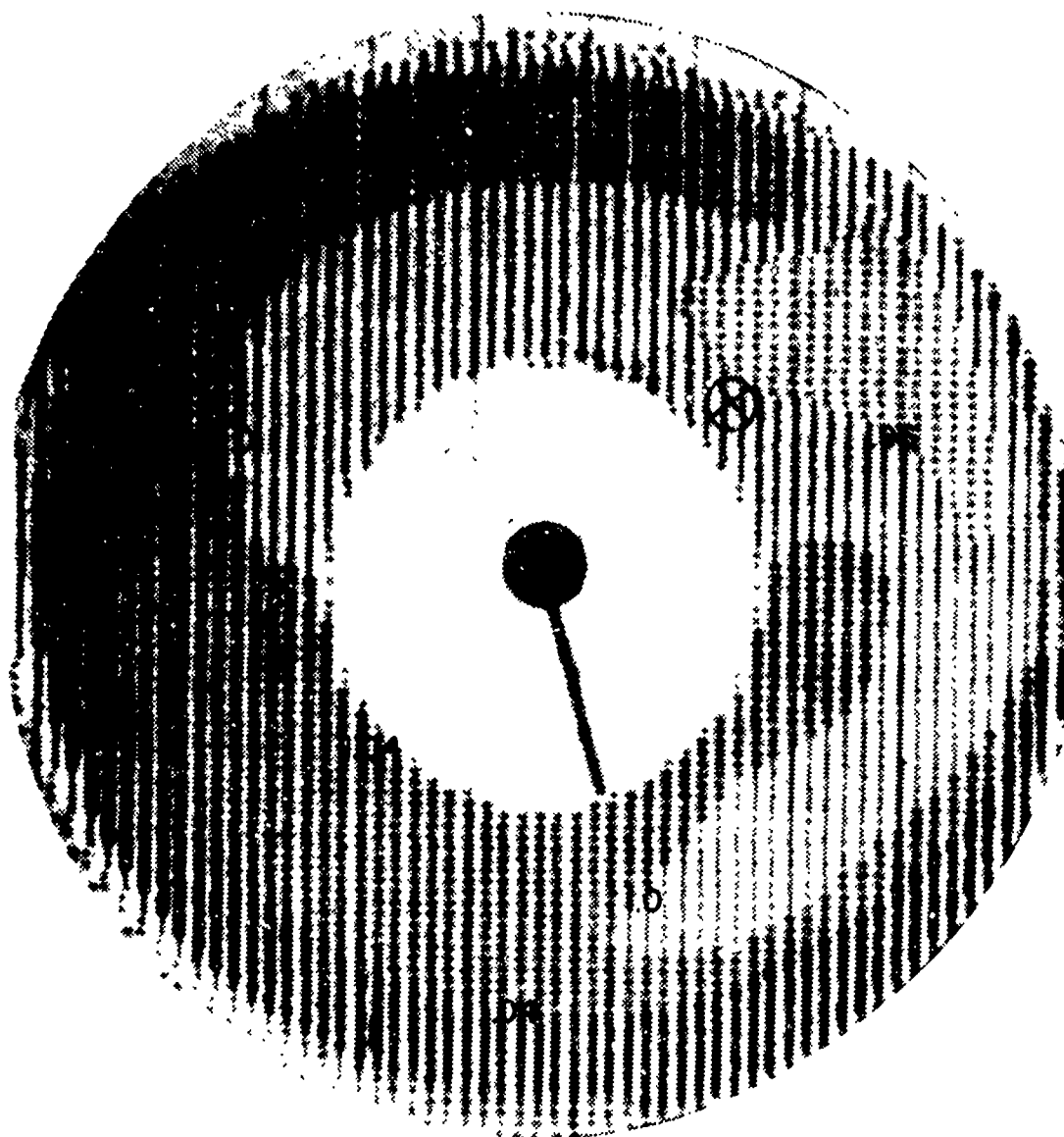
FIG. A-8   FRAME SIX OF INSTANTANEOUS
            PRESSURE CONTOURS SEQUENCE, TF-30
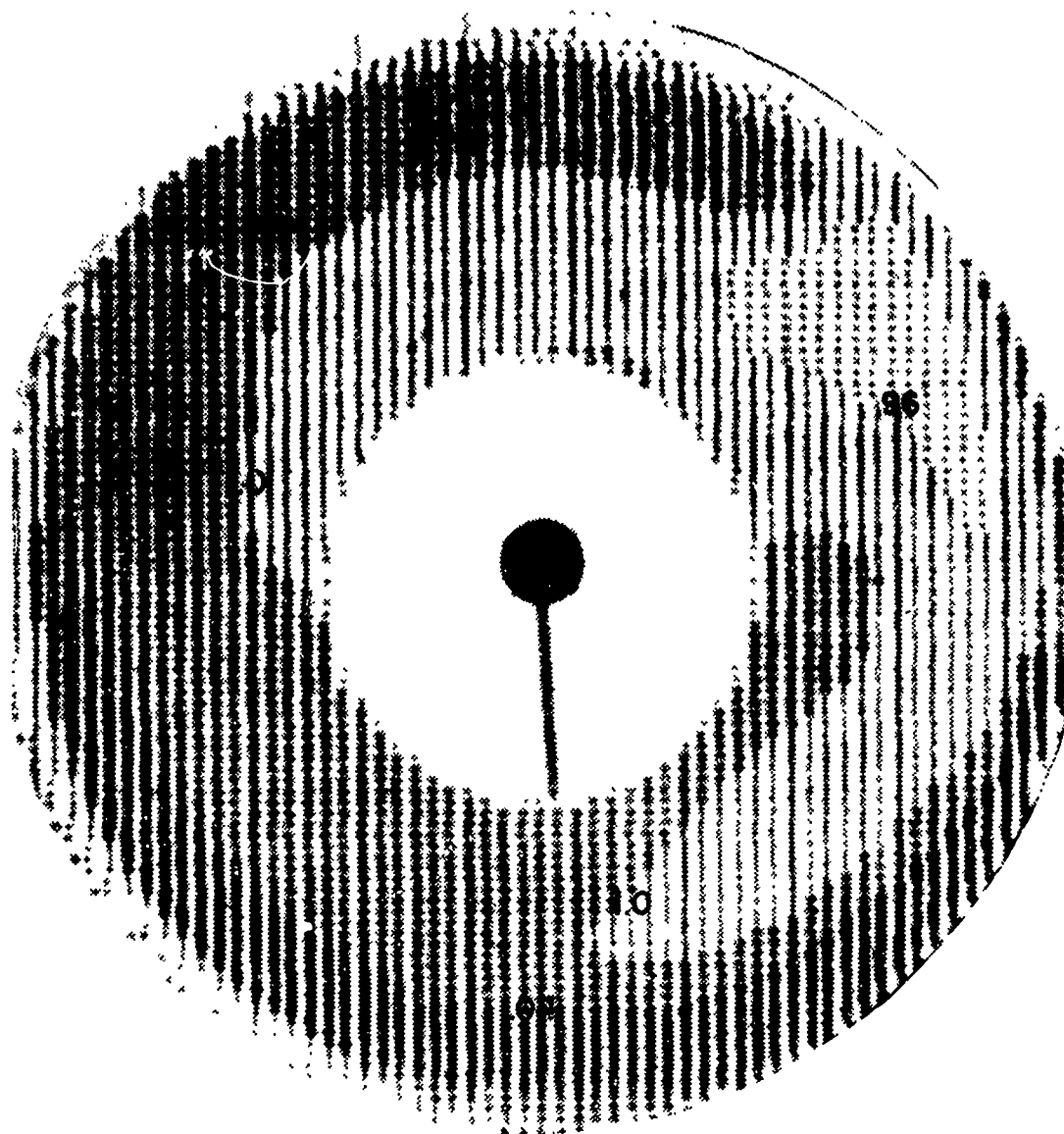
FIG. A-9   FRAME SEVEN   OF INSTANTANEOUS
           PRESSURE CONTOURS SEQUENCE, TF- 30
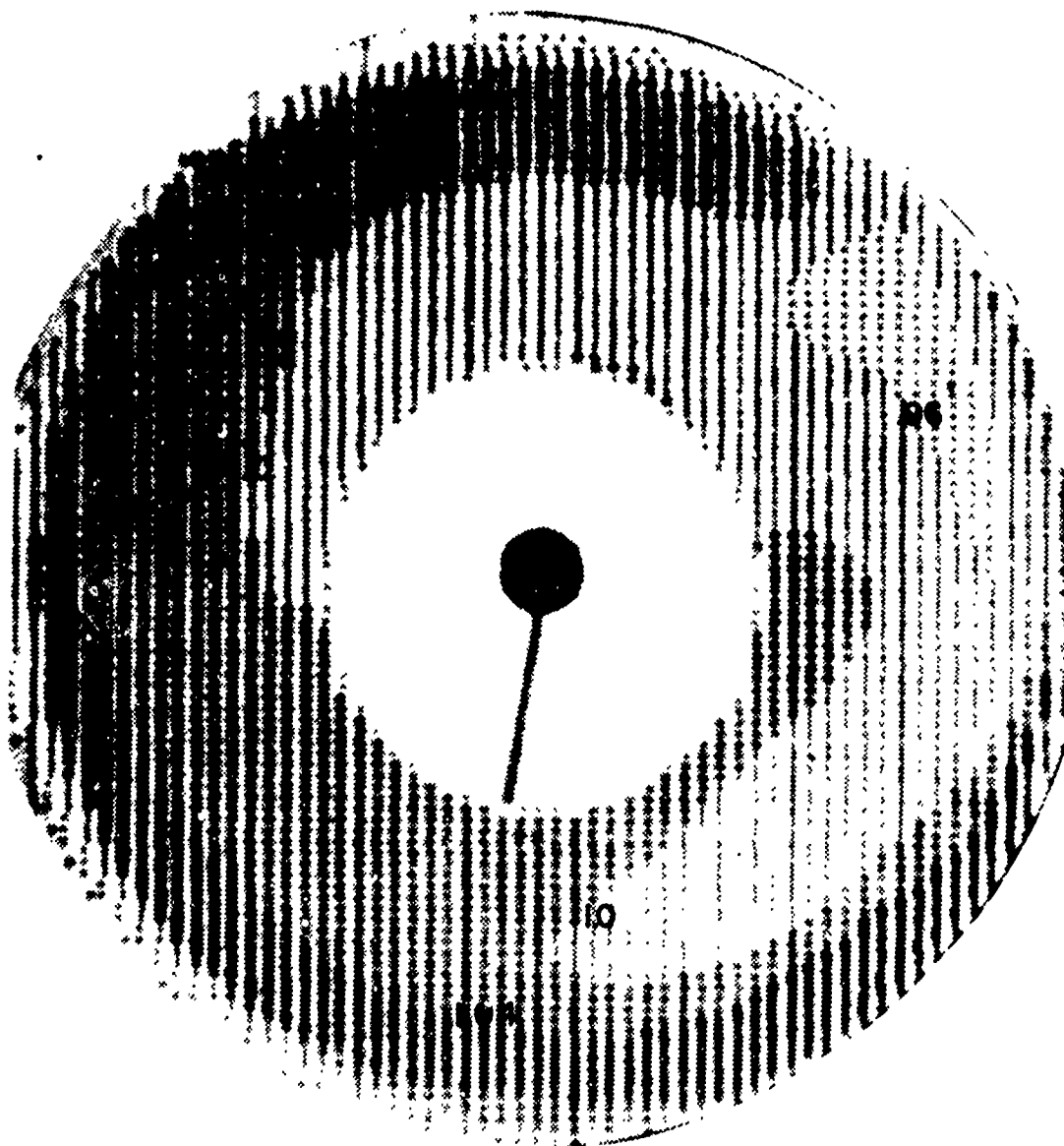
FIG. A-10   FRAME EIGHT OF INSTANTANEOUS
PRESSURE CONTOURS SEQUENCE, TF-30
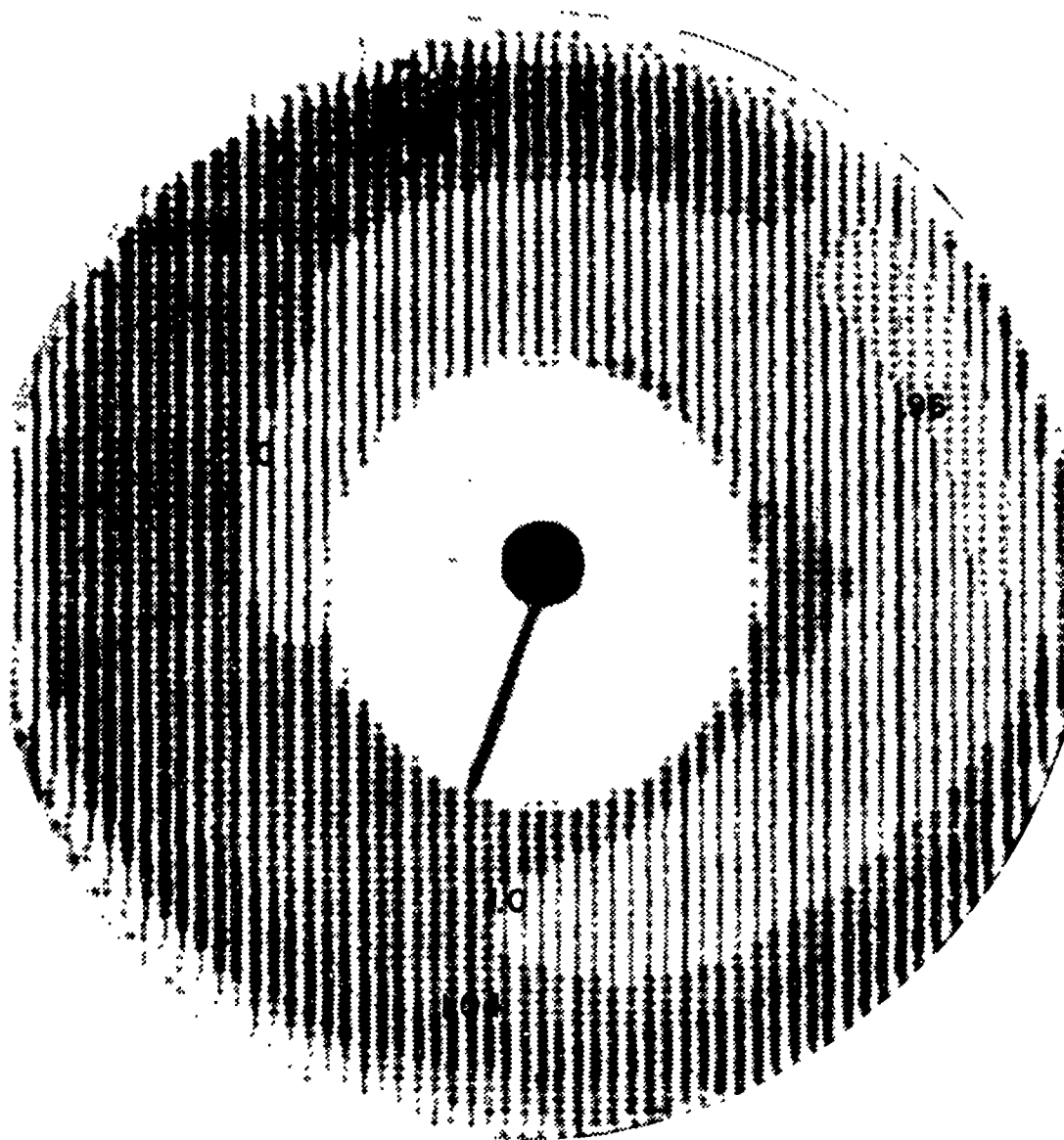
FIG. A-11 FRAME NINE OF INSTANTANEOUS
PRESSURE CONTOURS SEQUENCE, TF-30

Part II Pressure Fluctuations in the Z Direction

In the case of <u>steady flow</u>, ΔP_T is present only when dissipation occurs. Some causes of such dissipation in an inlet are shock waves, flow separation, obstructions, and boundary layers. These examples are illustrated in Fig. A-12.

Boundary Layer

Shock Wave

(a)   Oscillating Shock Wave

Flow Separation

Boundary Layer

(b)   Wall Effects

Strut
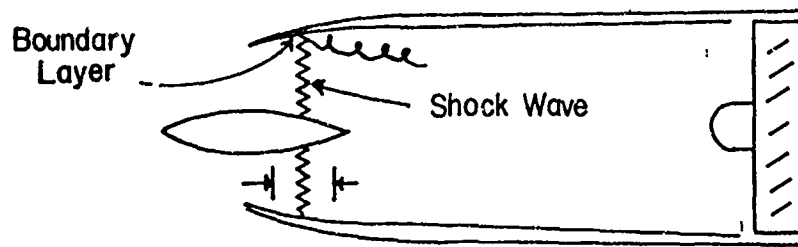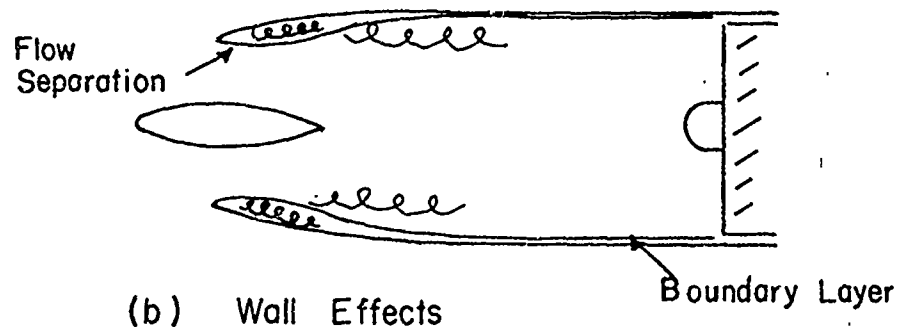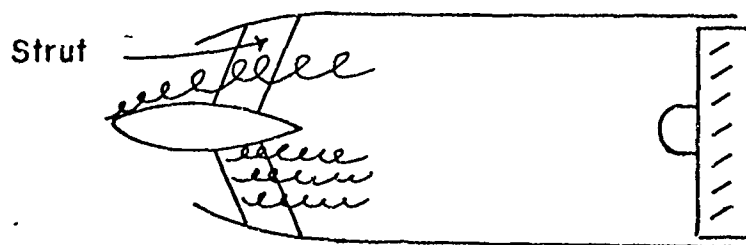
(c)   Obstructions

FIG. A-12   SOURCES OF DISSIPATION
WITHIN   INLETS

The stagnation pressure gradient is present only in the vicinity of dissipation. Therefore in steady flow, $\partial P'/\partial z'$ is zero at the compressor face if the dissipation is located upstream as shown in Fig. A-13.
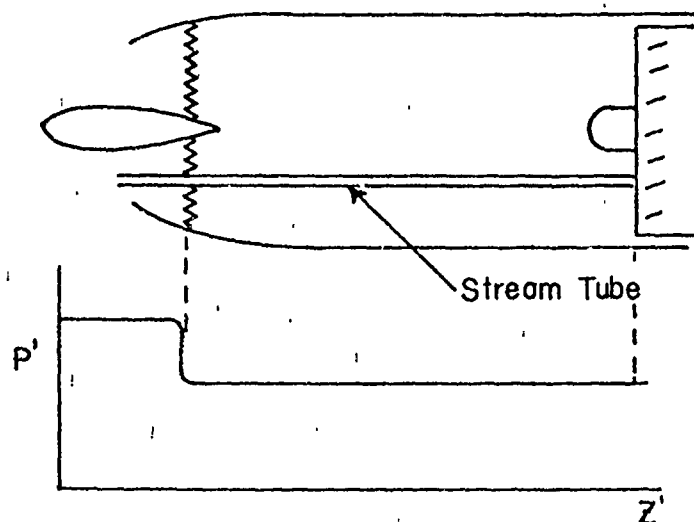
FIG. A-13   PRESSURE HISTORY FOR
STEADY   INLET   FLOW

For underlined unsteady flow, pressure gradients are again caused by dissipation. If there were a standing shock wave in the inlet, unsteady flow could cause this to oscillate in the axial direction. This is called "shock wave twitter" and can be self excited in oscillation. This is depicted in Fig. A-14.
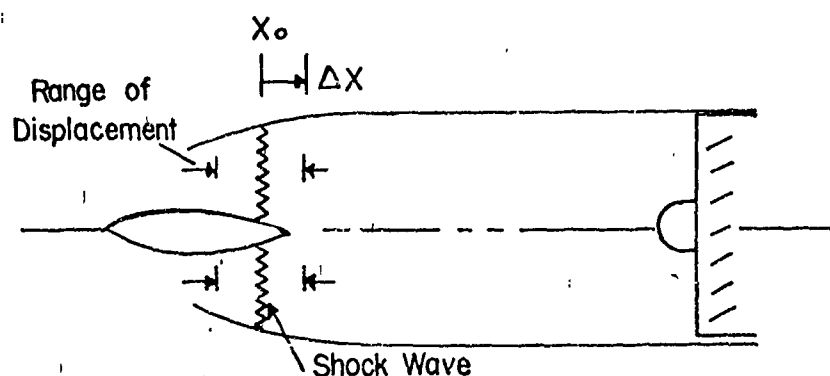
FIG. A-14   SHOCK-WAVE   TWITTER

The changing geometry seen by this oscillating shock-wave causes pressure pulses to be generated as shown in Fig. A-15. A/A* is the area ratio as a function of x. The second quadrant is local Mach number as a function of area ratio, A/A*. The third quadrant is the stagnation pressure ratio for a shock at M. Finally, the fourth quadrant yields the derivative of P_T with respect to x.
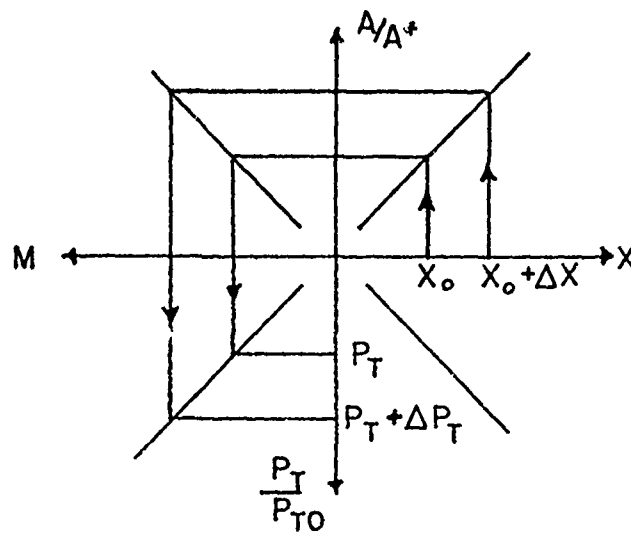
FIG. A-15   TOTAL PRESSURE FLUCTUATIONS
FROM OSCILLATING SHOCK-WAVES

The resulting $\Delta P_T/\Delta x$, a function of diffuser design, can be evaluated at the compressor face by assuming an acoustic analysis with no wave reflections at the compressor. Figure A-16 is a plot of the pressure pulses (waves) in the x-t plane. The slope of the characteristics is equal to the reciprocal wave speed; curvature is due to the variable area at the center-body.
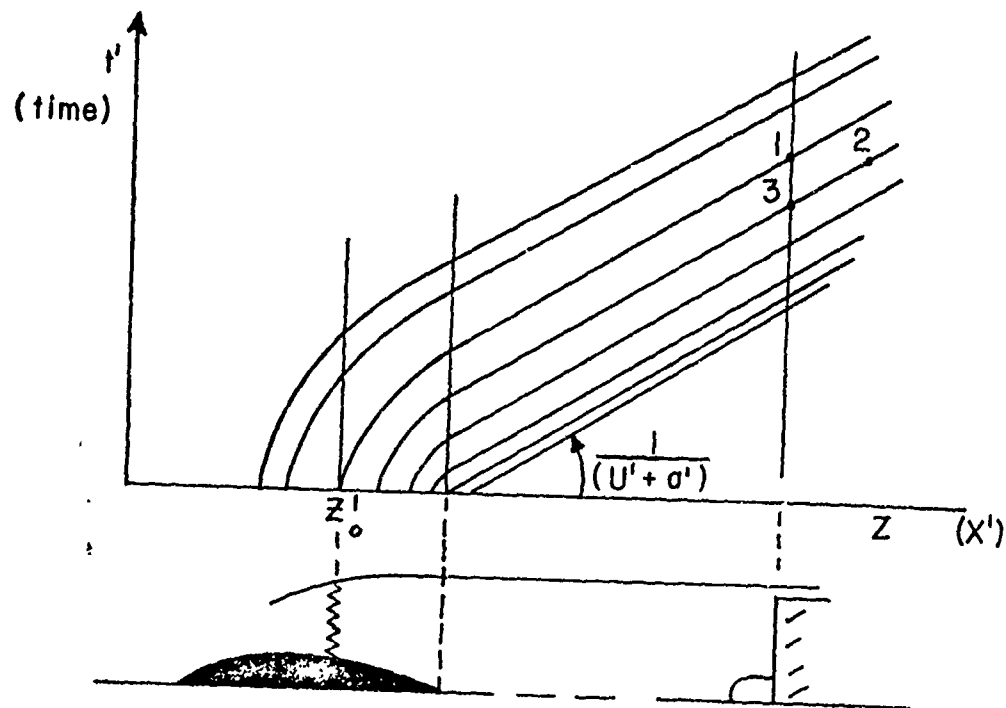
FIG. A-16   PRESSURE WAVES IN THE x-t PLANE
AS A RESULT OF SHOCK-WAVE TWITTER

Consider the three points labeled 1, 2, and 3 in Fig. A-16.

$$\frac{\partial P'}{\partial z'} = \frac{P_2' - P_1'}{z_2' - z_1'}$$

Since $P_3' = P_2'$

$$\frac{\partial P'}{\partial t'} = \frac{P_3' - P_1'}{t_3' - t_1'} = \frac{P_2' - P_1'}{t_3' - t_1'}$$

equating

$$\frac{\partial P'}{\partial t'} = \left(\frac{z_2' - z_1'}{t_3' - t_1'} \right) \frac{\partial P'}{\partial z'}$$

$$\frac{z_2' - z_1'}{t_3' - t_1'} = \frac{(z_2 - z_1)(2/D)}{(t_3 - t_1)(2\bar{a}/D)} = \frac{1}{\bar{a}} \frac{(z_2 - z_1)}{(t_3 - t_1)}$$

$$= \frac{1}{\bar{a}} (a + u) = a' + u'$$

therefore

$$\frac{\partial P'}{\partial z'} = \frac{1}{(a' + u')} \left(\frac{\partial P'}{\partial t'} \right)$$

and

$$\frac{\partial P_T}{\partial z} \qquad \frac{1}{(a + u)} \left(\frac{\partial P_T}{\partial t} \right) \tag{A-2}$$

The usefulness of Eqn. (A-2) can be demonstrated by application to a simple inlet/engine configuration with an oscillating shock wave present; see Fig. A-17. For brevity the following assumptions are made

        (1.) a = Constant

        (2.) Wave impedance of compressor matches wave impedance of duct

        (3.) U = constant

        (4.) No wave dispersion
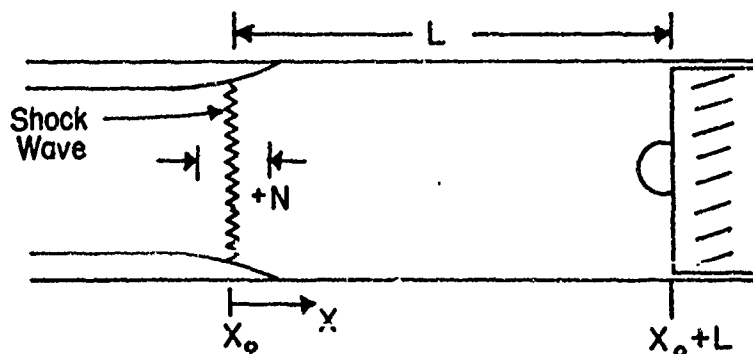
FIG. A-17   NOMENCLATURE

The shock wave, oscillating within $\pm N$, produces pressure waves which are represented as a sine wave function.

$$x - x_0 = N \sin (\omega t)$$

$$\frac{\partial x}{\partial t} = \omega N \cos (\omega t)$$

within ΔN

$$\frac{\partial P_T}{\partial t} = \frac{\partial x}{\partial t} \cdot \frac{\partial P_T}{\partial x}$$

$$= \omega N \cos (\omega t) \left(\frac{\partial P_T}{\partial x} \right)_{x_0}$$

Using a wave transit time equal to $L/(a+u)$ with $a =$ wave speed relative to the gas, the unsteady pressure at the compressor face becomes

$$\frac{\partial P_T}{\partial t} \bigg|_{x_0+L} = \omega N \cos \omega \left(t - \frac{L}{a+u}\right) \frac{\partial P_T}{\partial x} \bigg|_{x_0}$$

Combining this with Eqn. (A-2) yields

$$\frac{\partial P_T}{\partial z} \bigg|_{face} = \frac{\omega N \cos \omega \left(t - \frac{L}{a+u}\right)}{u + a} \left(\frac{\partial P_T}{\partial x} \right)$$

Non-dimensionalized the preceding equation becomes

$$\frac{\partial P'}{\partial z'} = \frac{(\omega/\Omega)(\Omega N/\bar{a}) \cos \left[\frac{\omega}{\Omega} \left(t' + \frac{1}{a' + u'} \frac{L\Omega}{\bar{a}}\right)\right]}{u'} \left(\frac{\partial P'}{\partial x'} \right)$$

where Ω is rotor angular speed.

This is one method of relating pressure fluctuations at the compressor face ($\partial P'/\partial z'$) with the pressure waves generated by inlet/shock-wave interaction.

APPENDIX B

CONVERSION OF P_T MAP TO VORTICITY - J85

Pressure data taken directly from Fig. B-1 are listed in Table B-I. From these data the curves in Fig. B-2 are generated. Slopes taken from these curves, which are tabulated in Table B-II, provide a means for constructing the circumferential vorticity map in Fig. 11. A similar procedure is performed in generating the radial vorticity map in Fig. 10. Data are contained in Tables B-III and B-IV and Fig. B-3.
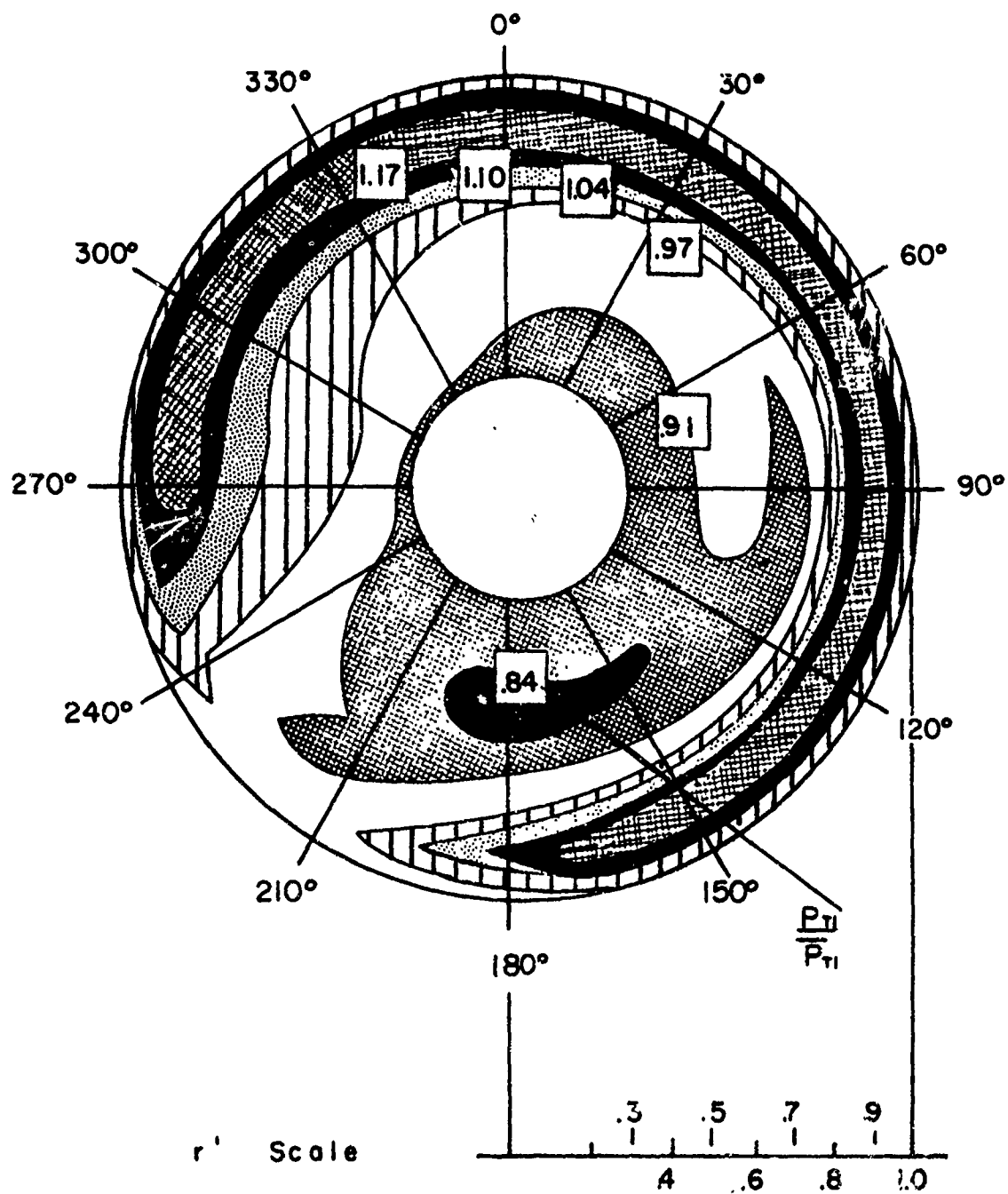
FIG. B-I   PRESSURE DATA AND SCALES FOR J85

97

Table B-I Pressure Data Taken in Radial Direction from J85
Total-Pressure Map

0°		30°		60°		90°		120°		150°	
r'	P'	r'	P'	r'	P'	r'	P'	r'	P'	r'	P'
.4	.91	.47	.91	.46	.91	.44	.91	.71	.91	.47	.84
.68	.97	.7	.97	.75	.97	.62	.91	.75	.97	.55	.84
.72	1.04	.74	1.04	.79	1.04	.72	.91	.79	1.04	.68	.91
.78	1.10	.79	1.10	.82	1.10	.75	.97	.82	1.10	.75	.97
.81	1.17	.81	1.17	.84	1.17	.79	1.04	.84	1.17	.78	1.04
.92	1.17	.92	1.17	.92	1.17	.82	1.10	.92	1.17	.80	1.10
.95	1.04	.95	1.04	.95	1.04	.85	1.17	.95	1.04	.82	1.17
						.92	1.17			.92	1.17
						.95	1.04			.95	1.04

180°		210°		240°		270°		300°		330°	
r'	P'	r'	P'	r'	P'	r'	P'	r'	P'	r'	P'
.4	.84	.82	.91	.42	.91	.3	.91	.29	.91	.3	.91
.6	.84			.9	.97	.43	.97	.47	.97	.6	.97
.7	.91			.95	.97	.65	1.04	.68	1.04	.71	1.04
.78	.97					.75	1.10	.76	1.10	.76	1.10
.82	1.04					.79	1.17	.80	1.17	.8	1.17
.86	1.10					.92	1.17	.92	1.17	.92	1.17
.90	1.10					.95	1.04	.97	1.04	.95	1.04
.92	1.04										
.97	.97										
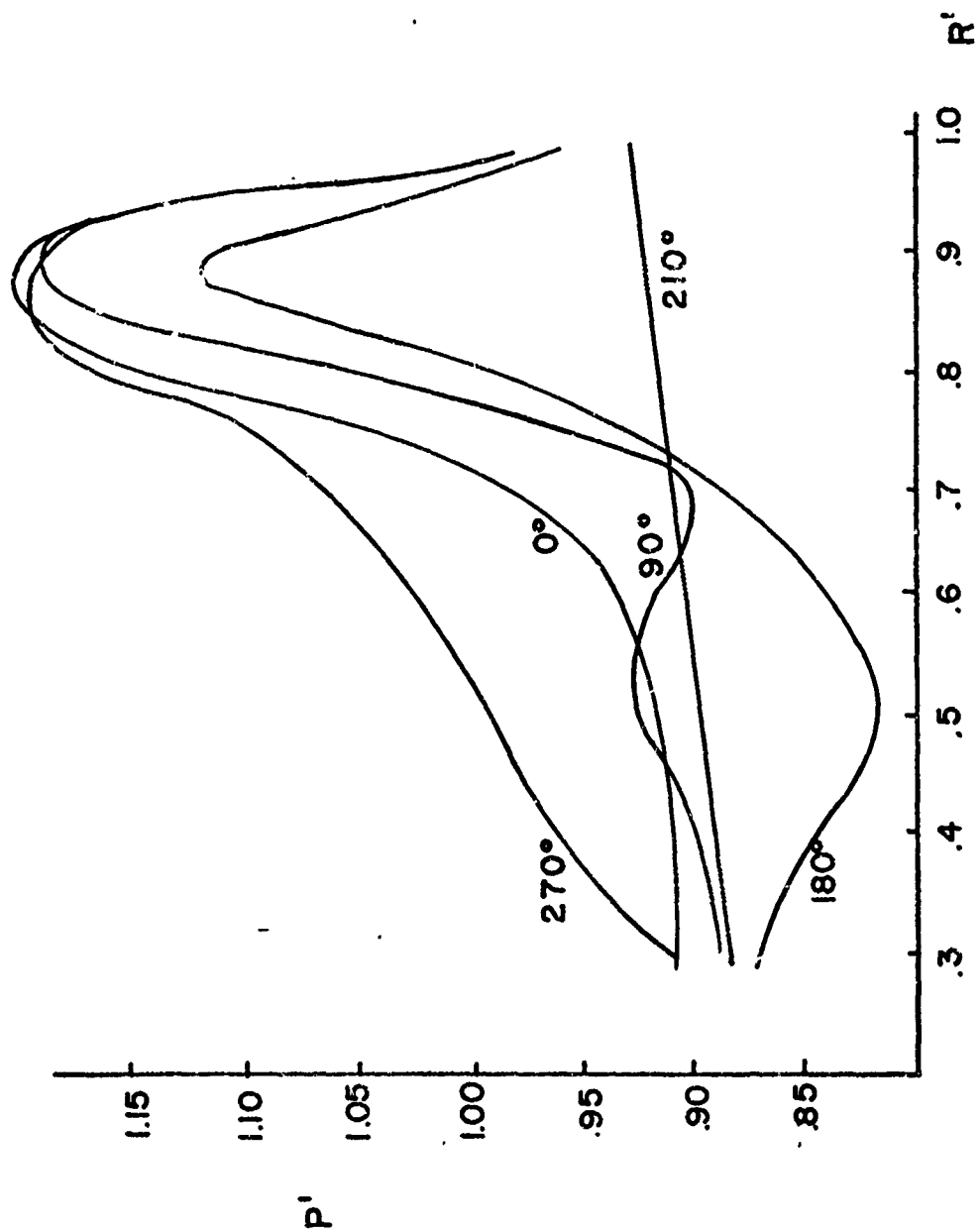
FIG. B-2   P' vs R'
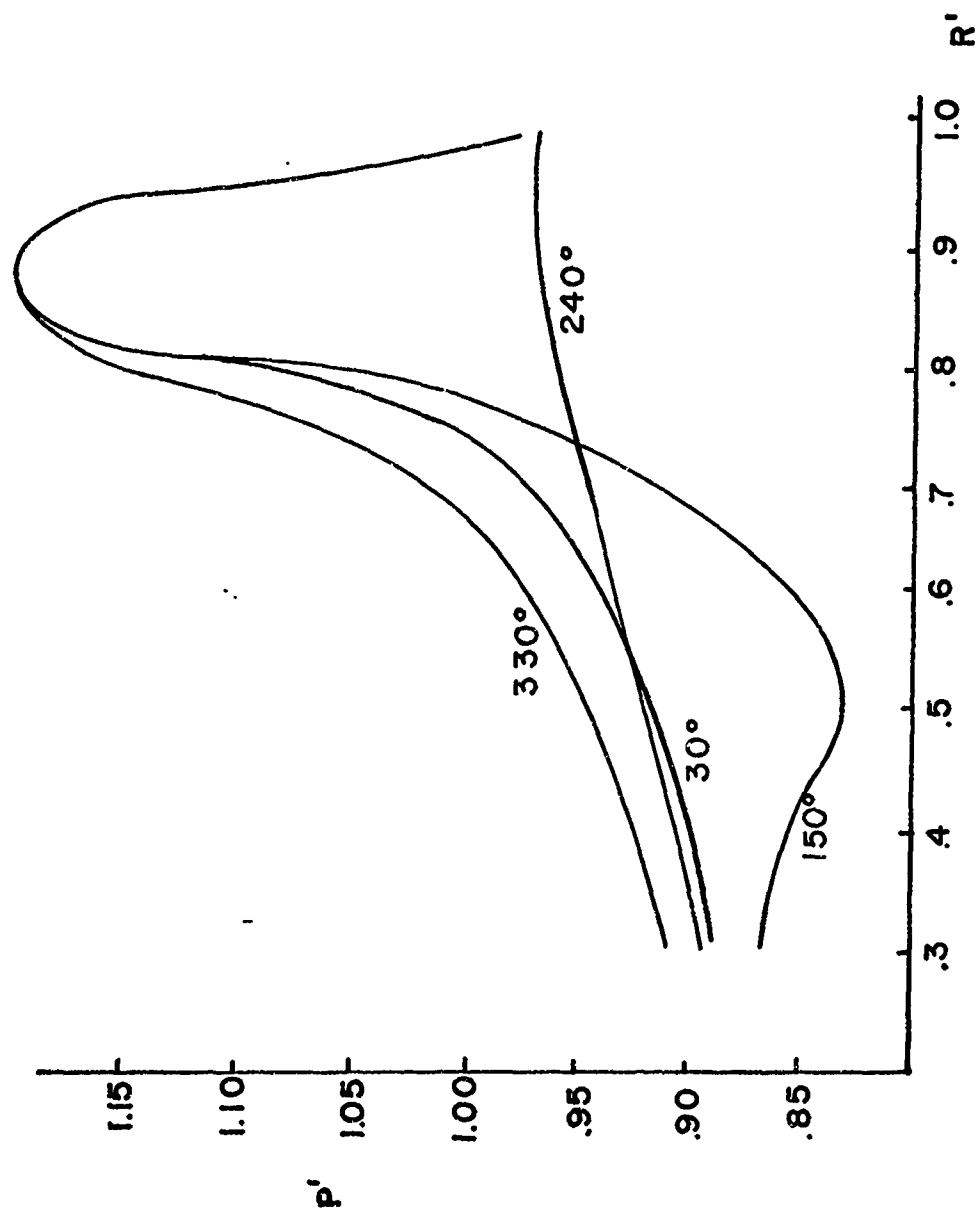
FIG. B-2 (cont.)
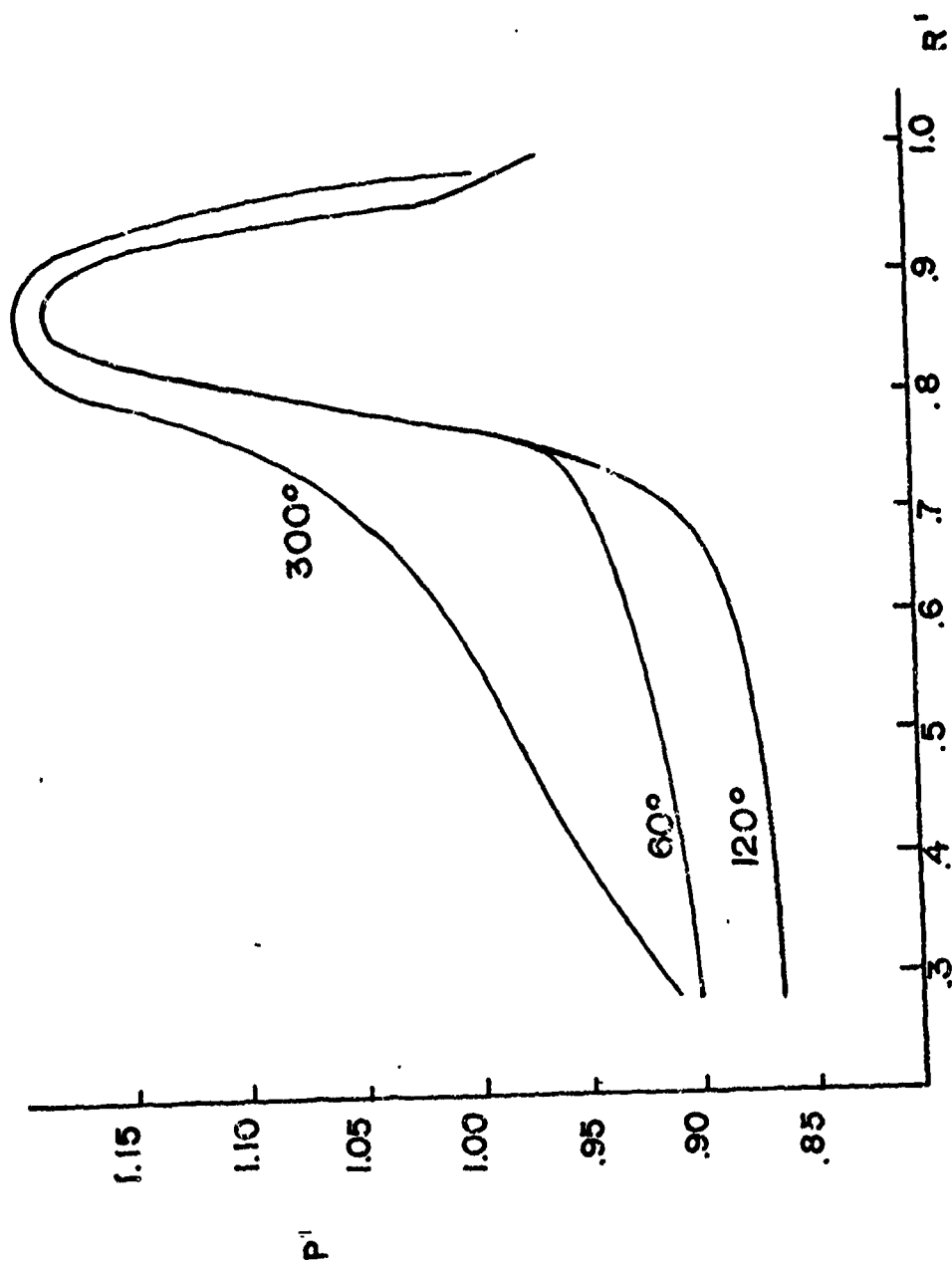
FIG. B-2 (cont)

Table B-II   Pressure Gradients Obtained from Slopes in Fig. B-2

0°		30°		60°		90°		120°		150°	
r'	∂P'/∂r'	r'	∂P'/∂r'	r'	∂P'/∂r'	r'	∂P'/∂r'	r'	∂P'/∂r'	r'	∂P'/∂r'
.4	0	.4	.13	.4	.07	.32	.045	.4	.03	.3	-.22
.5	.09	.5	.16	.5	.12	.38	.17	.5	.06	.3	-.22
.6	.28	.6	.26	.6	.135	.44	.26	.6	.1	.5	-.22
.7	.9	.7	.5	.7	.25	.52	0	.68	.33	.51	0
.76	1.8	.76	1.4	.74	.56	.6	-.26	.72	1.08	.54	.3
.78	2.6	.79	5	.8	2.3	.62	-.27	.8	3	.6	.53
.80	1.6	.8	6	.82	4.5	.66	0	.82	2.5	.7	.73
.82	.83	.82	1.1	.86	.55	.7	.29	.84	1.08	.76	1.5
.84	.37	.86	0	-.89	0	.72	1.2	.86	.4	.79	4.0
.87	0	.9	-.72	.92	-.6	.75	2.0	.89	0	.8	7
.9	-.6	.94	-2.7	.94	-2.7	.8	2.0	.9	-.26	8.2	1.3
.94	-2.7	.96	-3	.96	-3.0	.83	6.0	.92	-.6	.86	0
.96	-3.0					.85	.9	.94	-2.7	.9	-.72
						.87	.2	.96	-3.0	.94	-2.7

180°		210°		240°		270°		300°		330°	
r'	$\partial P'/\partial r'$	r'	$\partial P'/\partial r'$	r'	$\partial P'/\partial r'$	r'	$\partial P'/\partial r'$	r'	$\partial P'/\partial r'$	r'	$\partial P'/\partial r'$
.34	-.25	.3	.07	.3	.13	.32	.505	.4	.35	.4	.15
.4	-.35	.3	.07	.3	.13	.4	.38	.5	.26	.6	.33
.48	-.12	1.0		│	│	.5	.28	.6	.35	.7	.88
.51	0			.9	.13	.6	.35	.7	.55	.76	1.9
.6	.37			.92	0	.7	.52	.74	.8	.78	2.1
.7	.7			.94	-.15	.76	1.6	.78	2.3	.8	1.08
.78	1.7			│	│	.78	.56	.8	1.3	.82	.6
│	│			1.0	-.15	.8	.44	.82	.65	.84	.23
.86	1.7					.85	0	.85	0	.86	0
.88	0					.89	-.37	.9	-.7	.9	-.72
.9	-2.5					.92	-.6	.92	-1.3	.94	-2.7
.96	-1.2					.94	-2.7	.94	-2.7	.96	-3.
						.96	-3.0	.96	-3.		

Table B-III   Pressure Data Taken in Circumferential Direction from J85 Total-Pressure Map

r' = .38		r' = .46		r' = .54		r' = .61		r' = .69		r' = .77	
θ (rad)	P'	θ (rad)	P'	θ (rad)	P'	θ (rad)	P'	θ (rad)	P'	θ (rad)	P'
4.26	.91	4.19	.91	1.81	.91	1.69	.91	0	.97	0	1.04
6.17	.91	4.48	.97	2.35	.84	2.41	.84	1.25	.91	.872	.97
		5.23	.97	3.14	.84	3.19	.84	2.79	.91	2.09	.97
		.174	.91	4.10	.91	3.98	.91	3.84	.91	2.96	.97
				4.41	.97	4.36	.97	4.31	.97	3.40	.91
				5.48	.97	5.72	.97	4.59	1.04	3.87	.91
								5.13	1.04	4.27	.97
										4.48	1.04

r' = .85				r' = .93	
θ (rad)	P'	θ (rad)	P'	θ (rad)	P'
.174	1.17	3.70	.91	3.03	1.17
.785	1.10	3.92	.91	3.19	1.10
1.39	1.04	4.22	.97	3.37	1.04
2.0	1.10	4.39	1.04	3.58	.97
2.26	1.17	4.52	1.10	4.10	.97
2.61	1.17	4.71	1.17	4.27	1.04
2.87	1.10	4.88	1.17	4.45	1.10
3.14	1.04	5.23	1.17	4.57	1.17
3.40	.97	6.11	1.17		
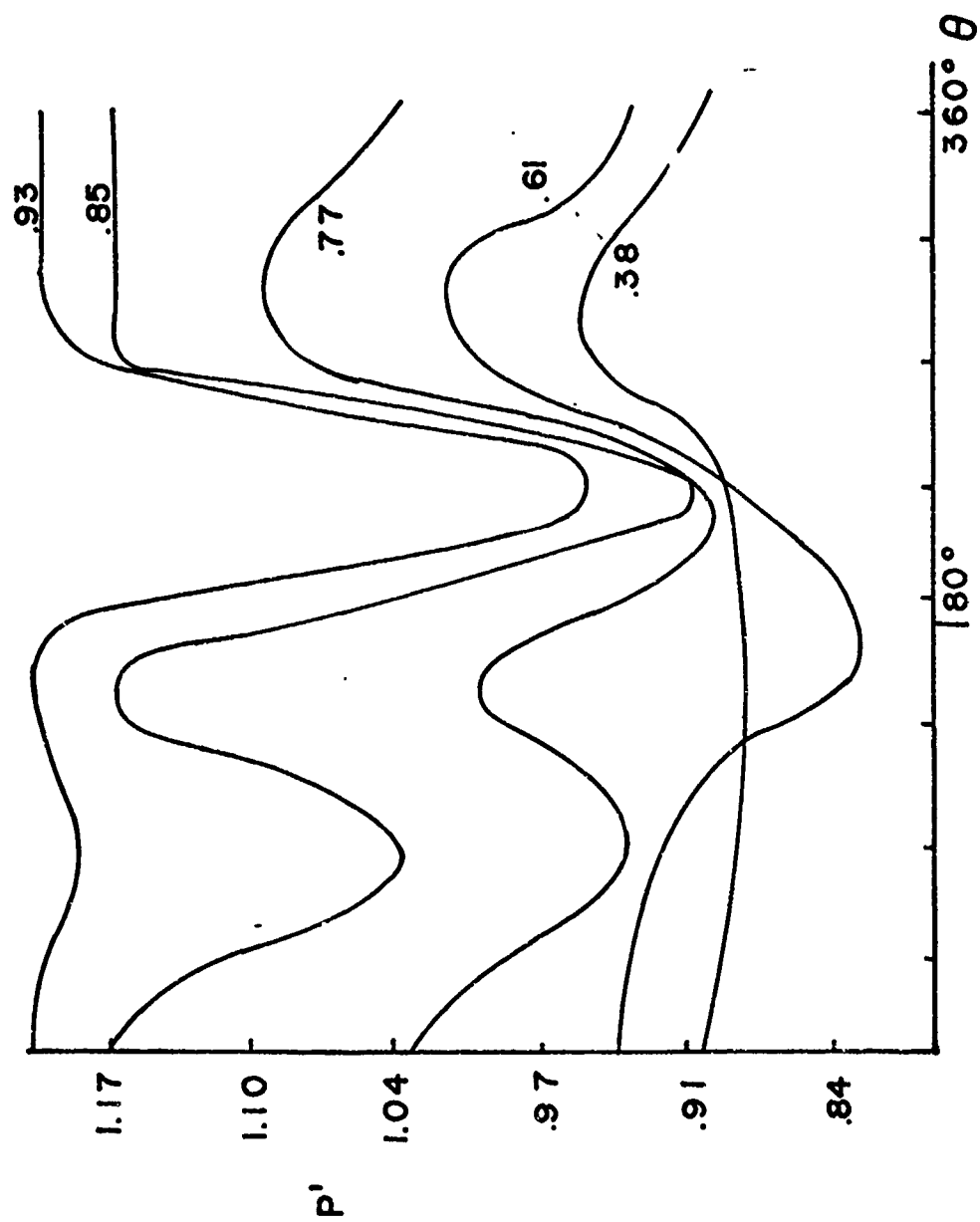
FIG. B-3   P' VS θ
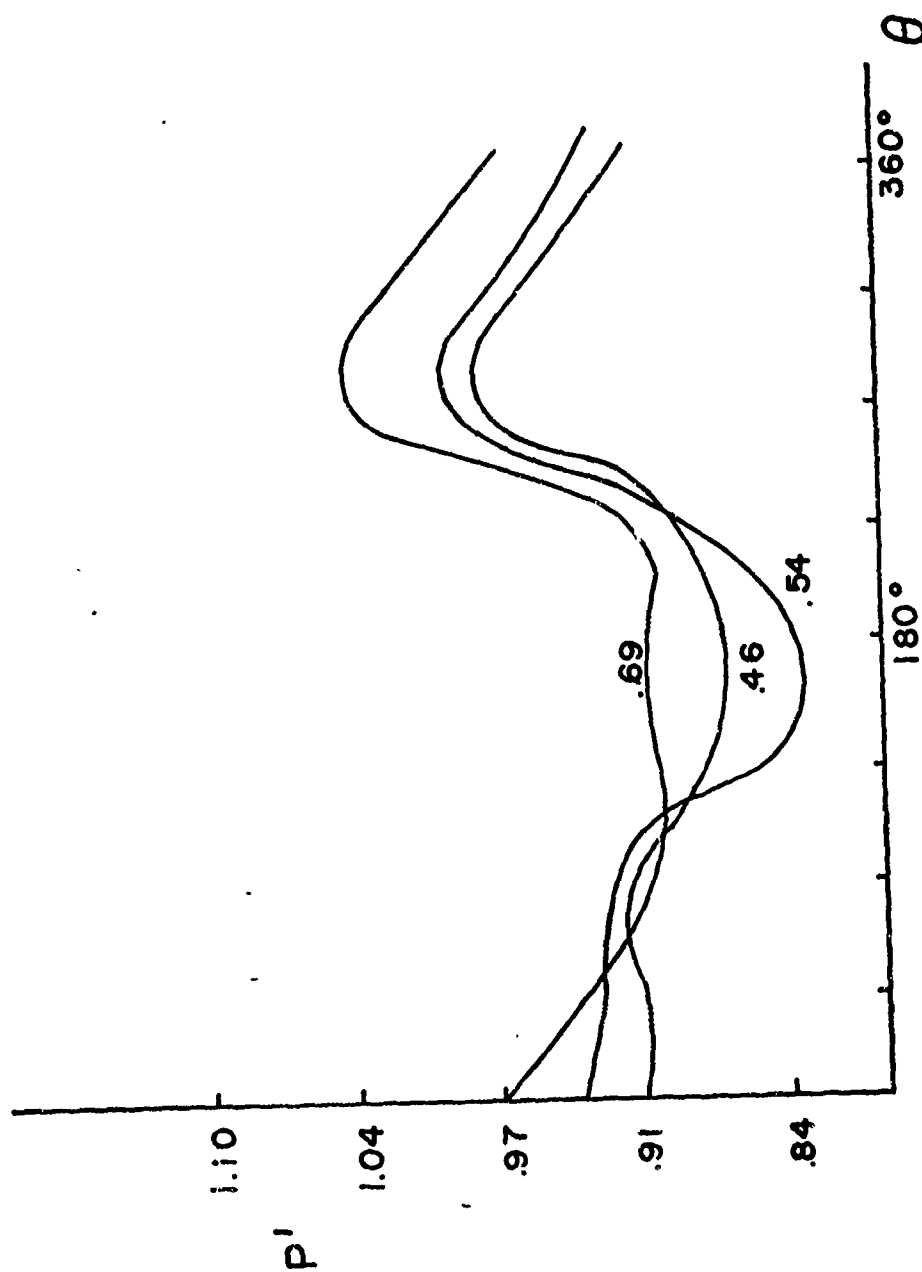
FIG. B-3 (cont.)

Table B-IV Pressure Gradients Obtained from Slopes in Fig. B-3

$r' = .38$		$r' = .46$		$r' = .54$		$r' = .61$		$r' = .69$		$r' = .77$		$r' = .85$		$r' = .93$	
θ	$\frac{1}{r'}\frac{\partial P'}{\partial \theta}$	θ	$\frac{1}{r'}\frac{\partial P'}{\partial \theta}$	θ	$\frac{1}{r'}\frac{\partial P'}{\partial \theta}$	θ	$\frac{1}{r'}\frac{\partial P'}{\partial \theta}$	θ	$\frac{1}{r'}\frac{\partial P'}{\partial \theta}$	θ	$\frac{1}{r'}\frac{\partial P'}{\partial \theta}$	θ	$\frac{1}{r'}\frac{\partial P'}{\partial \theta}$	θ	$\frac{1}{r'}\frac{\partial P'}{\partial \theta}$
0°	-.067	0°	-.066	0°	-.038	0°	-.009	0°	-.077	0°	-.10	0°	0	0°	0
57°	-.025	29°	0	57°	-.015	57°	-.032	57°	-.077	57°	-.121	23°	-.114	34°	-.014
137°	0	57°	+.029	80°	-.015	115°	-.131	80°	-.043	80°	0	46°	-.33	57°	-.028
172°	+.011	69°	0	103°	-.140	149°	-.26	103°	0	126°	+.113	57°	-.126	80°	0
230°	+.008	92°	-.120	115°	-.164	158°	0	115°	+.014	143°	0	80°	0	115°	-.028
252°	+.322	103°	-.105	137°	-.123	172°	+.054	160°	0	166°	-.208	103°	+.141	149°	0
275°	+.072	115°	-.091	149°	0	206°	+.141	172°	-.02	183°	-.156	126°	+.425	160°	-.057
286°	0	149°	0	172°	+.063	229°	+.437	183°	-.242	206°	0	143°	0	172°	-.402
298°	-.081	172°	+.011	229°	+.187	252°	+.175	200°	0	229°	+.147	149°	-.094	206°	-.402
309°	-.122	229°	+.127	252°	+.256	275°	+.069	218°	+.096	246°	+.312	155°	-.33	212°	-.086
332°	-.164	246°	+.455	264°	+.102	292°	0	229°	+.155	264°	+.235	212°	-.33	223°	0
344°	-.136	264°	+.154	281°	0	309°	-.113	252°	+.35	275°	+.095	218°	0	235°	+.201
		281°	0	298°	-.086	321°	-.328	264°	+.106	286°	+.015	229°	+.156	240°	+.43
		286°	-.075	332°	-.102	344°	-.092	275°	0	298°	0	252°	+.52	264°	+.43
		298°	-.154	0°	-.046			286°	-.032	309°	-.026	264°	+.52	286°	+.021
		344°	-.111					298°	-.077	320°	-.1	278°	+.094	296°	0
								360°	-.077	344°	-.1	275°	0		
												344°	0		

107

Application of Gauss' Divergence Theorem is performed in the follow-
ing manner. A grid such as is shown in Fig. B-4 is placed over a
vorticity map.
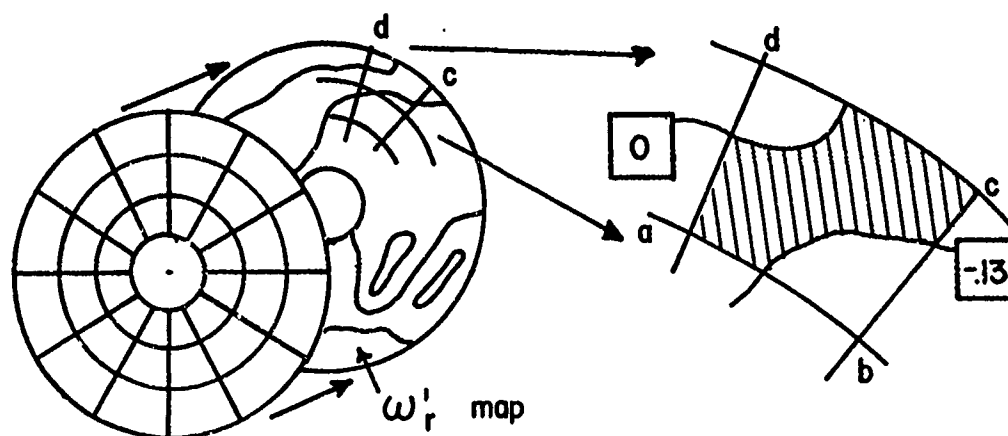
FIG. B-4   METHOD OF DIVERGENCE
APPLICATION

The net ω_r' passing through region abcd is equal to

$$[(-.13)(\tfrac{ab}{2}) + (\tfrac{0-.13}{2})(\tfrac{ab}{2})] - [(\tfrac{.13-0}{2})(\tfrac{2}{5}\,cd) + (\tfrac{0-.13}{2})(\tfrac{3}{5}\,cd)] = \omega_r'\Big|_{net}$$

Net flux of ω_θ' is calculated in a similar manner using the same grid
over an ω_θ' map. The sum of flux of ω_r' and ω_θ' is then equal to
$\omega_z'(ab\cdot cd)$ so that

$$\omega_z' = \frac{\omega_z'(ab\cdot cd)}{Area(abcd)}$$

This procedure is performed on each of the 36 segments so that a complete
ω_z' map can be drawn. These data are contained in Table B-V. If the sum

of net flux of ω_r' and ω_θ' is negative, then the net flux of ω_z' must be positive. There is an ambiguity of algebraic sign which cannot be resolved without additional data or information. One evaluates $\vec{\omega}'\cdot\vec{n}$.

Table B-V Net Fluxes of Vorticity in Three Coordinate Directions

Region	ω_θ'	ω_r'	ω_z'	Region	ω_θ'	ω_r'	ω_z'
1	-.0138	-.0273	+.374	19	+.025	-.086	+.555
2	0	0	0	20	-.025	-.024	+.527
3	0	0	0	21	+.1875	-.011	-3.14
4	0	0	0	22	+.09	+.013	-.937
5	-.045	0	+.483	23	0	-.032	+.344
6	0	0	0	24	0	-.0248	+.43
7	0	0	0	25	-.0675	+.066	0
8	+.08	-.02	-.645	26	0	+.042	-.45
9	0	0	0	27	0	+.011	-.195
10	0	0	0	28	0	+.038	-.346
11	+.08	-.03	-.54	29	0	+.008	-.086
12	0	-.038	+.68	30	0	-.003	+.05
13	0	0	0	31	+.06	-.0274	-.296
14	-.03	-.0377	+.728	32	-.045	-.026	+.764
15	+.198	-.034	-2.93	33	0	-.012	+.214
16	-.057	-.048	+.955	34	0	-.027	+.245
17	-.01	-.059	+.74	35	-.045	-.008	+.595
18	+.022	0	-.39	36	0	-.003	+.05

APPENDIX C

ESTIMATION OF SOME J85 PARAMETERS

Subscripts: T - Stagnation Quantity

           0 - Freestream ahead of Compressor

           1 - Compressor Face

           2 - Rotor Exit, first stage

           m - Mean radius

Data obtained from Ref. 24:

$$\bar{P}_{T1} = 1549 \text{ psf}$$

$$\bar{P}_1 = 1380 \text{ psf}$$

$$T_{T1} = 532°R$$

Data obtained from Ref. 2 and Ref. 34:

$$\theta = \frac{T_T}{518.7°R} \qquad \text{(Corrected Total-Temperature)}$$

$$\delta = \frac{P_T}{2116 \text{ psf}} \qquad \text{(Corrected Total-Pressure)}$$

$$N^* = 16,500 \text{ RPM} \qquad \text{(Rated Engine Speed)}$$

$$W_{corr} = \frac{W\sqrt{\theta}}{\delta} = 15 \text{ KG/sec} = 33.5 \text{ lbs/sec} \qquad \text{(Corrected Mass Flow Rate)}$$

$$\text{Percentage Corrected Engine Speed} = \frac{N}{N^*}\sqrt{\theta} \times 100 = 86.9$$

$$D_1 = 16.1 \text{ inches} \qquad \text{(Compressor Face Outside Diameter)}$$

$$D_{1 \text{ hub}} = 4.8 \text{ inches}$$

$$A_1 = 155 \text{ in}^2 \qquad \text{(Entrance Flow Area)}$$

$$N = 31 \qquad \text{(Number of blades in first row)}$$
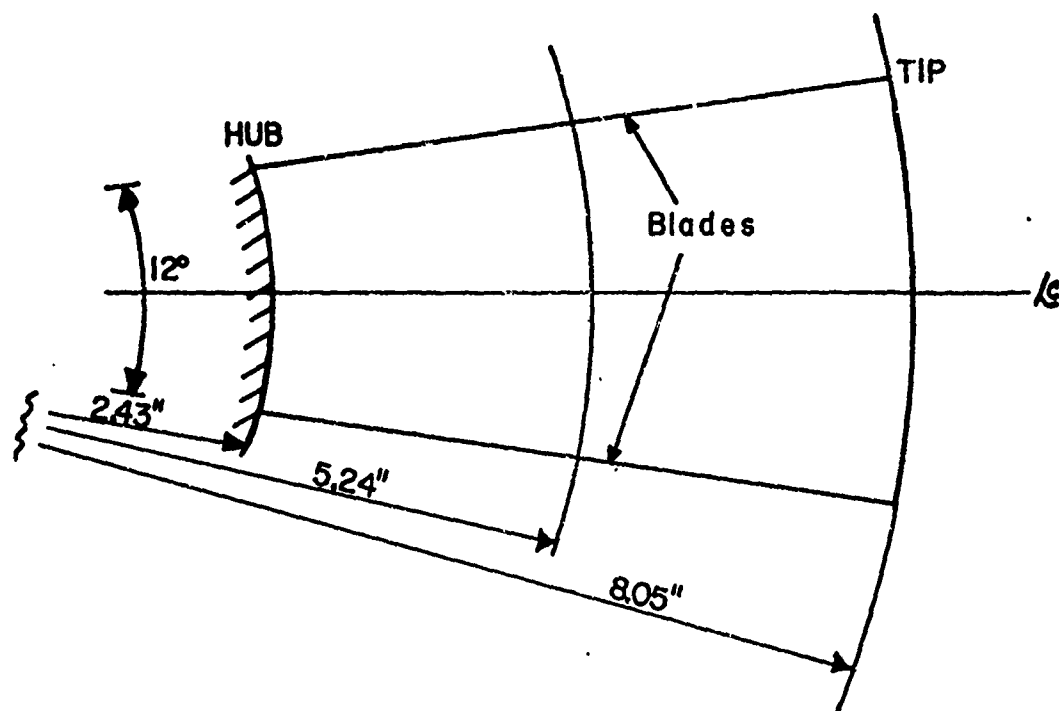
FIG. C-1   BLADE   PASSAGE   DIMENSIONS

Calculated Parameters

$$\frac{\overline{P}_{T1}}{\overline{P}_1} = (1 + \frac{\gamma-1}{\gamma} M^2)^{\frac{\gamma}{\gamma-1}}$$

$$\frac{1549}{1380} = 1.125 = (1 + .2M^2)^{3.5}$$

$$\underline{\overline{M}_1 = .414}$$

$$\frac{T_{T1}}{T_1} = 1 + \frac{\gamma-1}{2} M^2$$

$$T_1 = T_{T1} \Big/ 1 + \frac{\gamma-1}{2} M^2$$

$$\underline{\overline{T}_1 = 514°R}$$

112

$$\bar{a} = \sqrt{\gamma R T_1}$$

$$\bar{a} = 49.02 \sqrt{514}$$

$$\underline{\bar{a} = 1110 \text{ ft/sec}}$$

$$\bar{U}_z = \bar{M}\,\bar{a}$$

$$\bar{U}_z = (.414)(1110 \text{ ft/sec})$$

$$\underline{\bar{U}_z = 460 \text{ ft/sec}}$$

$$\bar{\rho}_1 = \frac{\bar{P}_1}{R T_1}$$

$$\bar{\rho} = \frac{1380 \text{ lbs/ft}^2}{(1715.6 \frac{\text{ft-lbs}}{\text{slug}^\circ R})(514^\circ R)}$$

$$\underline{\bar{\rho} = .001565 \text{ slugs/ft}^3}$$

As a check on these figures, another method may be used.

$$W = \frac{W_{cor}\,\delta}{\sqrt{\theta}} = \frac{(33.5 \text{ lbs/sec})\left(\frac{1549}{2116}\right)}{\sqrt{532/518}}$$

$$\underline{W = 24.15 \text{ lbs/sec}}$$

$$W = \rho A_1 U_z$$

$$U_z = \frac{W}{\rho A_1}$$

$$= \frac{(24.15 \text{ lbs/sec})(144 \text{ in}^2/\text{ft}^2)}{(.001565 \frac{\text{slugs}}{\text{ft}^3})(155 \text{ in}^2)(32.2 \frac{\text{lbs}}{\text{slug}})}$$

$$\underline{U_z = 462 \text{ ft/sec}}$$

Estimation of β_1
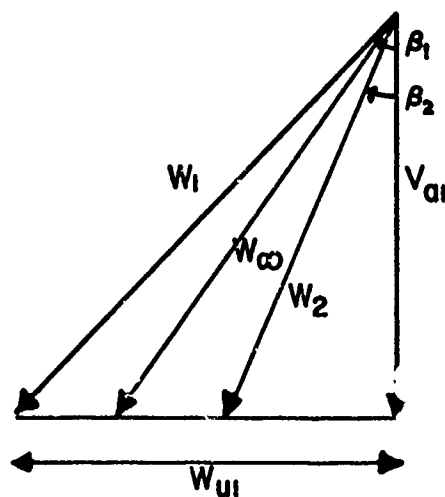
FIG. C-2   VELOCITIES AHEAD OF ROTOR

W → Relative Velocity

V → Absolute Velocity

$$\beta_1 = \tan^{-1}\left(\frac{W_{u1}}{V_a}\right) = \tan^{-1}\left(\frac{\pi \cdot D \cdot RPM}{V_a}\right)$$

$$D_M \approx .875 \text{ ft}$$

$$\text{Ang. Speed} = \frac{(86.9)(16500)}{\sqrt{T_T/518.7} \times 100} = 14,200 \text{ RPM}$$

$$W_{u1} = \pi \left(.875 \frac{ft}{rev}\right) \left(\frac{14200}{60} \frac{rev}{sec}\right)$$

$$W_{u1} = 650 \text{ ft/sec} \qquad \text{Mean Radius}$$

$$\beta_1 = \tan^{-1}\left(\frac{650}{460}\right) \qquad \beta_1 = 55° \quad \text{Mean Radius}$$

114

Estimation of β_2

Individual stage characteristics and loss data for the J85 are not available. The following data are from Ref. 34:

> Compressor of Free-Vortex Design
> Lieblein Diffusion Parameter, $D < .5$
> Solidity $(\sigma) = 1.14$ $\Big\}$ First Stage Rotor
> Axial Velocity Ratio $= .96$

$$D = (1 - \frac{W_2}{W_1}) + \frac{\Delta W_u}{2\sigma W_1} \qquad \text{(Ref. 10)}$$

$$W_2 = V_{a2}/\cos \beta_2 = .96 \, V_{a1}/\cos \beta_2$$
$$= 442/\cos \beta_2 = 546$$

$$W_{u2} = V_{a2} \tan \beta_2 = .96 \, V_{a1} \tan \beta_2$$
$$= 442 \tan \beta_2$$

$$W_1 = V_a/\cos \beta_1 = 802 \text{ ft/sec}$$

$$.5 = (1 - \frac{442/\cos \beta_2}{802}) + \frac{(650 - 442 \tan \beta_2)}{(2)(1.14)(802)}$$

$$\underline{\beta_2 = 36° \text{ minimum}}$$

$$\underline{W_{u2} = 320 \text{ ft/sec}}$$

Since the loading limit is $D < .5$, 36° can be considered a minimum for β_2, and the maximum turning angle becomes

$$\Delta \beta = \beta_1 - \beta_2 = 55° - 36°$$
$$= 19°$$
$$\underline{\varepsilon = .332 \quad \text{radians}}$$

APPENDIX D

CALCULATION OF ABSOLUTE VORTICITY

Radial Vorticity:

$$\omega_r' = \frac{1}{\gamma P' U_z'} \left(\frac{1}{r'} \frac{\partial P'}{\partial \theta} \right) \tag{11}$$

$$\gamma = 1.4$$

$$P' = \frac{P_{T1}}{\bar{P}_{T1}}$$

$$U_z' = \frac{U_z}{\bar{a}} = \frac{U_z}{\bar{U}_z/\bar{M}} = \bar{M}\frac{U_z}{\bar{U}_z}$$

$$= \bar{M}\left(\frac{(P_T - P_S)(2/\rho)}{(\bar{P}_T - P_S)(2/\rho)}\right)^{1/2} = \bar{M}\left(\frac{P_T - 1380}{1549 - 1380}\right)^{1/2}$$

$$= \bar{M}\left(\frac{P_T}{169} - 8.17\right)^{1/2}$$

$$= \bar{M}\left(\frac{P_T}{\bar{P}_T} \cdot \frac{\bar{P}_T}{169} - 8.17\right)^{1/2} = \bar{M}\left(9.17\frac{P_T}{\bar{P}_T} - 8.17\right)^{1/2}$$

$$U_z' = \bar{M}\sqrt{9.17P' - 8.17}$$

$$\omega_r' = \frac{\omega_r D}{2\bar{a}}$$

Substituting into Eqn. (11)

$$\omega_r = \frac{2\bar{a}}{1.4\,D\,P'\,\bar{M}\sqrt{9.17P' - 8.17}}\left(\frac{1}{r'}\frac{\partial P'}{\partial \theta}\right)\frac{ft/sec}{ft}$$

Recall:　$\bar{a}$ = 1110 ft/sec

$D = \frac{16.1}{12}$ ft

$\bar{M}$ = .414

$$\omega_r = \frac{2854.9}{P' \sqrt{9.17P' - 8.16}} \left(\frac{1}{r'} \frac{\partial P'}{\partial \theta} \right) \, \text{sec}^{-1} \qquad (D\text{-}1)$$

Circumferential Vorticity

$$\omega_\theta = \frac{-2854.9}{P' \sqrt{9.17P' - 8.16}} \left(\frac{\partial P'}{\partial r'} \right) \, \text{sec}^{-1} \qquad (D\text{-}2)$$

Equation (D-2) is used to convert the contours in Fig. 11 to absolute vorticity for subsequent calculation of secondary circulation. Tabulated results are contained in Table D-I.

Table D-I Absolute Vorticity for Three Circumferential Positions

on ω_θ' Map

r'	r (in)	Radial I			Radial II		
		P'	$\partial P'/\partial r'$	ω_θ (sec^{-1})	P'	$\partial P'/\partial r'$	ω_θ (sec^{-1})
.3	2.43	.91	.35	-2554.9	.9	.05	-520
.325	2.63	.93		-1770.8		.05	
.35	2.83	.94		-1567.6		.05	
.375	3.03	.95		-1416.3		.05	
.4	3.23	.96		-1297.8		.05	
.425	3.43	.97		-1201.6		.06	-624.1
.45	3.63	.98		-1121.4	.9	.075	-780.1
.475	3.83	.99		-1053.2	.91	.09	-656.9
.5	4.03	.99		-1053.2	.91	.1	-729.9
.525	4.23	1.0		-994.2	.91	.11	-802.9
.55	4.43	1.0		-994.2	.92	.13	-767.3
.575	4.63	1.01		-942.5	.92	.14	-826.3
.6	4.83	1.01		-942.5	.93	.15	-758.9
.625	5.03	1.02		-896.7	.93	.17	-860.1
.65	5.23	1.03		-855.7	.94	.20	-895.7
.675	5.43	1.04	.35	-818.8	.94	.23	-1030.1
.7	5.63	1.05	.75	-1682.7	.95	.25	-1011.6
.725	5.83	1.06	1.0	-2156.2	.97	.5	-1716.6
.75	6.04	1.08	1.2	-2402.2	1.0	1.0	-2840.7
.775	6.24	1.10	1.2	-2243.5	1.04	1.5	-3509.2
.8	6.44	1.17	1.0	-1522.4	1.10	2.0	-3739.2
.825	6.64	1.18	.75	-1112.4	1.17	1.5	-2283.6
.85	6.84	1.19	0	0	1.18	.5	-741.6
.875	7.04	1.20	-.25	352.6	1.20	0	0
.9	7.24	1.18	-.75	1112.4	1.18	-.5	+741.6
.925	7.44	1.17	-1.0	1522.4	1.17	-1.0	1522.4
.95	7.65	1.14	-1.5	2480.2	1.1	-3.0	5608.9
.975	7.85	1.1	-3.0	5608.9	1.05	-3.2	7179.8
1.0	8.05						

Table D-I (continued)

r'	/ r (in)		Radial III	
		P'	$\partial P'/\partial r'$	ω_θ (sec^{-1})
.3	2.43	.9	-.2	+2080.3
.325	2.63			
.35	2.83			
.375	3.03			
.4	3.23			
.425	3.43			
.45	3.63			
.475	3.83			
.5	4.03		-.2	+2080.3
.525	4.23		0	0
.55	4.43		+.3	-3120.5
.575	4.63		.4	-4160.7
.6	4.83		.5	-5200.8
.625	5.03		.5	-5200.8
.65	5.23	.90	.5	
.675	5.43	.90	.5	
.7	5.63	.91	.5	-3649.9
.725	5.83	.94	1.0	-4478.9
.75	6.04	.97	1.5	-5149.8
.775	6.24	1.0	2.0	-5681.4
.8	6.44	1.04	2.3	-5380.8
.825	6.64	1.17	1.7	-2588.0
.85	6.84	1.18	0	0
.875	7.04	1.2	-.3	+423.2
.9	7.24	1.18	-.75	+1112.4
.925	7.44	1.17	-1.5	+2283.6
.95	7.65	1.04	-3.0	+7018.4
.975	7.85	1.0	-3.2	+9090.3
1.0	8.05			

APPENDIX E

CALCULATION OF CIRCULATION FROM ω_θ MAP FOR J85

$$\zeta_{S1} = + 2\Omega \cos \beta_1 - \omega_\theta \sin \beta_1 \tag{28}$$

$$= + 2 \left(236.6 \frac{Rev}{Sec}\right) \cos 55° - \omega_\theta \sin 55°$$

$$\zeta_{S1} = + 271.4 - .8191 \omega_\theta \tag{E-1}$$

$$\zeta_{n1} = - 2\Omega \sin \beta_1 + \omega_\theta \cos \beta_1 \tag{29}$$

$$= 2 \left(236.6 \frac{Rev}{Sec}\right) \sin 55° + (\cos 55°) \omega_\theta$$

$$\zeta_{n1} = - 387.6 - .573 \omega_\theta \tag{E-2}$$

$$\zeta_{S2} = + \zeta_{S1} - 2\varepsilon\zeta_{n1} \tag{29}$$

$$= (271.4 - .8191 \omega_\theta) + 2(.3316 \text{ rad})(387.6 + .573 \omega_\theta)$$

$$\zeta_{S2} = 528.4 - .439 \omega_\theta \tag{E-3}$$

$$\frac{d\Gamma_1}{dr} = \zeta_{S2} \, S \cos \beta_2 \tag{31}$$

$$S = \frac{1.095 \text{ in}}{12 \text{ in/ft}} = .09125 \text{ ft}$$

$$\beta_2 = 36°$$

$$\frac{d\Gamma_1}{dr} = .0738 \, \zeta_{S2} \quad \text{ft/sec} \tag{E-4}$$

120

$$\frac{d\Gamma_2}{dr} = S \, \zeta_{n1}\left(\frac{1}{2} \, \frac{\sin 2\beta_2 - \sin 2\beta_1}{\cos \beta_1} - 2\epsilon \cos \beta_2\right) \tag{32}$$

$$\beta_1 = 55°$$

$$\epsilon = .3316$$

$$\frac{d\Gamma_2}{dr} = .0480 \, \zeta_{n1} \quad \text{ft/sec} \tag{E-5}$$

$$\frac{d\Gamma_3}{dr} = S \cos \beta_1 \, \zeta_{n1} \, (\tan \beta_2 - \tan \beta_1) \tag{33}$$

$$\frac{d\Gamma_3}{dr} = .0336 \, \zeta_{n1} \tag{E-6}$$

Tabulated results for Eqns. (E-1) through E-6) using previously determined data are contained in Tables E-I, E-II, and E-III.

Table E-I Relative Vorticity and Circulation Components at Radial I

r'	ω_θ (sec^{-1})	ζ_{S1} (sec^{-1})	ζ_{n1} (sec^{-1})	ζ_{S2} (sec^{-1})	$d\Gamma_1/dr$ (ft/sec)	$d\Gamma_2/dr$ (ft/sec)	$d\Gamma_3/dr$ (ft/sec)
.3	−2554.9	+2364.1	+1076.3	+1650	+121.7	51.2	+36.3
.325	−1770.8	+1721.8	+627.0	+1305.7	+96.3	29.8	+21.1
.35	−1567.6	+1555.4	+510.6	+1216.5	+89.7	24.5	+17.2
.375	−1416.3	+1431.4	+423.9	+1150.1	+84.8	20.1	+14.3
.4	−1297.8	+1334.4	+356.0	+1098.1	+81.0	16.9	+12.0
	−1201.6	+1255.6	+300.9	+1055.9	+77.9	14.3	+10.1
.45	−1121.4	+1189.9	+254.9	+1020.6	+75.3	12.1	+8.5
	−1053.2	+1134.0	+215.8	+990.7	+73.1	10.3	+7.3
.5	−1053.2	+1134.0	+215.8	+990.7	+73.1	10.3	+7.3
	−994.2	+1085.7	+182.0	+964.8	+71.2	8.6	+6.14
.55	−994.2	+1085.7	+182.0	+964.8	+71.2	8.6	+6.14
	−942.5	+1043.4	+152.4	+942.1	+69.5	7.2	+5.12
.6	−942.5	+1043.4	+152.4	+942.1	+69.5	7.2	+5.12
	−896.7	+1005.8	+126.2	+922.0	+68.0	6.0	+4.2
.65	−855.7	+972.3	+102.7	+904.0	+66.7	4.8	+3.5
	−818.8	+942.0	+81.5	+887.8	+65.5	3.9	+2.75
.7	−1682.7	+1649.6	+576.5	+1267.1	+93.5	27.4	+19.4
	−2156.2	+2037.5	+847.9	+1474.9	+108.8	40.3	+28.7
.75	−2402.2	+2239.0	+988.8	+1582.9	+116.8	47.0	+33.3
	−2243.5	+2109.0	+897.9	+1513.2	+111.6	42.6	+30.3
.8	−1522.4	+1518.3	+484.7	+1196.7	+88.3	23.0	+16.3
	−1112.4	+1182.5	+249.8	+1016.7	+75.0	11.8	+8.4
.85	0	+271.4	−387.6	+528.4	+38.9	−18.4	−13.0
	352.6	−17.4	−589.6	+373.6	+27.5	−28.0	−19.8
.9	1112.4	−639.7	−1025.0	+40.0	+2.9	−48.8	−34.5
	1522.4	−975.5	−1259.9	−139.9	−10.3	−60.0	−42.5
.95	2480.2	−1760.1	−1808.7	−560.4	−41.3	−86.0	−61.0
	5608.9	−4322.8	−3601.4	−1933.9	−142.7	−171.5	−121.0
1.0							

Table E-II Relative Vorticity and Circulation Components at Radial II

r'	ω_θ (sec^{-1})	ζ_{S1} (sec^{-1})	ζ_{n1} (sec^{-1})	ζ_{S2} (sec^{-1})	$d\Gamma_1/dr$ (ft/sec)	$d\Gamma_2/dr$ (ft/sec)	$d\Gamma_3/dr$ (ft/sec)
.3	-520	+697.3	-89.6	+756.6	+55.8	-4.26	-3.0
	-520						
.35	-520						
	-520						
.4	-520						
	-624.1	+782.3	-29.9	+802.3	+59.2	-1.4	-1.0
.45	-780.1	+910.3	+59.3	+870.8	+64.2	+2.8	+1.9
	-656.9	+809.4	-11.1	+816.7	+60.2	-.5	-.3
.5	-729.2	+869.2	+30.6	+848.8	+62.6	+1.4	+1.0
	-802.9	+929.0	+72.4	+880.8	+65.0	+3.4	+2.4
.55	-767.3	+899.8	+52.0	+865.2	+63.8	+2.4	+1.7
	-826.3	+948.2	+85.8	+891.1	+65.7	+4.0	+2.8
.6	-758.9	+893.0	+47.2	+861.5	+63.5	+2.2	+1.6
	-860.1	+975.9	+105.2	+905.9	+66.8	+5.0	+3.5
.65	-895.7	+1005.0	+125.6	+921.5	+68.0	+5.9	+4.2
	-1030.1	+1115.1	+202.6	+980.6	+72.3	+9.6	+6.8
.7	-1011.6	+1100.0	+192.0	+972.4	+71.7	+9.1	+6.4
	-1716.1	+1677.0	+595.7	+1281.7	+94.5	+28.3	+20.0
.75	-2840.7	+2598.2	+1240.1	+1775.4	+131.0	+59.0	+41.7
	-3509.2	+3145.7	+1623.1	+2068.9	+152.6	+77.2	+54.6
.8	-3738.6	+3334.5	+1755.1	+2170.0	+160.1	+83.5	+59.1
	-2283.6	+2141.8	+920.9	+1530.9	+112.9	+43.8	+31.0
.85	-741.6	+878.8	+37.3	+853.9	+63.0	+1.7	+1.2
	0	+271.4	-387.6	+528.4	+38.9	-18.4	-13.0
.9	+741.6	-336.0	-812.5	+202.8	+14.9	-38.6	-27.3
	+1522.4	-975.5	-1259.9	-139.9	-10.3	-59.9	-42.4
.95	+5608.9	-4322.8	-3601.4	-1933.9	-142.7	-171.4	-121.3
	+7179.8	-5609.5	-4501.6	-2623.5	-193.6	-214.2	-151.7
1.0							

Table E-III Relative Vorticity and Circulation Components at Radial III

r'	ω_θ (sec^{-1})	ζ_{S1} (sec^{-1})	ζ_{n1} (sec^{-1})	ζ_{S2} (sec^{-1})	$d\Gamma_1/dr$ (ft/sec)	$d\Gamma_2/dr$ (ft/sec)	$d\Gamma_3/dr$ (ft/sec)
.3	+2080.3	-1432.5	-1579.6	-384.8	-28.4	-75.1	-53.2
.35							
.4							
.45							
.5							
	0	+271.4	-387.6	+528.4	+38.9	-18.4	-13.0
.55	-3120.5	+2827.4	+1400.4	+1898.2	+140.0	+66.6	+47.1
	-4160.7	+3679.4	+1996.4	+2354.9	+173.7	+95.0	+67.2
.6	-5200.8	+4531.3	+2592.4	+2811.5	+207.4	+123.3	+87.3
.65							
.7	-3649.9	+3261.0	+1703.7	+2130.7	+157.2	+81.0	+57.4
	-4478.9	+3940.0	+2178.8	+2494.6	+184.1	+103.7	+73.4
.75	-5149.8	+4489.6	+2563.2	+2789.1	+205.8	+122.0	+86.3
	-5681.4	+4925.0	+2867.8	+3022.5	+223.0	+136.5	+96.6
.8	-5380.8	+4678.8	+2695.5	+2800.5	+213.3	+128.3	+90.8
	-2588.0	+2391.2	+1095.3	+1664.5	+122.8	+52.1	+36.9
.85	0	+271.4	-387.6	+528.4	+38.9	-18.4	-13.0
	+423.2	-75.2	-630.0	+342.6	+25.2	-29.9	-21.3
.9	+1112.4	-639.7	-1025.0	+40.0	+2.9	-48.7	-34.5
	+2283.6	-1599.0	-1696.1	-474.1	-34.9	-80.7	-57.1
.95	+7018.4	-5477.3	-4408.1	-2552.6	-188.3	-209.8	-148.5
	+9090.3	-7174.4	-5596.3	-3462.2	-255.5	-266.3	-188.5
1.0	-						

LIST OF REFERENCES

1. Brimelow, Brian, Performance Matching of the Propulsion System, SAE preprint 680712, Aeronautics and Space Engineering and Manufacturing Meeting, Los Angeles, Calif., Oct. 7-11, 1968.

2. AIAA Paper No. 71-667, Instantaneous and Dynamic Analysis of Supersonic Inlet-Engine Compatibility, by J. E. Calogeras, P. L. Burstadt, and R. E. Coltrin, June 1971.

3. NASA TMX-1928, Experimental Investigation of the Effects of Pulse Pressure Distortions Imposed on the Inlet of a Turbofan Engine, by L. M. Wenzel, November 1969.

4. AIAA Paper No. 70-632, Distortion and Turbulence Interaction, A Method for Evaluating Engine/Inlet Compatibility, by E. A. Van Deusan and V. R. Mardoc, June 1970.

5. Plourde, G. A. and Brimelow, B., Pressure Fluctuations Cause Compressor Instability, paper presented at the Airframe/Propulsion Combatibility Symposium, Wright-Patterson AFB, Ohio, 25 June 1969

6. AIAA Paper No. 70-624, Analysis of In-Flight Pressure Fluctuations Leading to Engine Compressor Surge in an F-111A Airplane for Mach Numbers to 2.17, by F. W. Burcham, Jr. and D. L. Hughes, June 1970.

7. AIAA Paper No. 69-488, The Flight Investigation of Pressure Phenomena in the Air Intake of an F-111A Airplane, by D. R. Bellman and D. L. Hughes, 1969.

8. Hawthorne, W. R., and others, Aerodynamics of Turbines and Compressors, p. 277-296 and p. 342-367, Princeton University Press, 1964.

9. Valensi, J., "Experimental Investigation of the Rotating Stall in a Single-Stage Axial Compressor," J. Aero. Sci., v. 25, p. 1-10, January 1958.

10. NACA RM E53D01, Diffusion Factor for Estimating Losses and Limiting Blade Loadings in Axial-Flow-Compressor Blade Elements, by S. Lieblein, F. C. Schwenk, and R. L. Broderick, 1953.

11. Lieblein, S. "Loss and Stall Analysis of Compressor Cascades," J. Basic Eng., p. 387-400, September 1959.

12. Lakshminarayana, B. and Horlock, J. H., "Review: Secondary Flows and Losses in Cascades and Axial-Flow Turbomachines," Int'l. J. Mech. Sci., v. 5, p. 287-307, 1963.

13. Woods, J. R., Jr., _The Analytical Treatment of Secondary Flows and Associated Losses in Axial-Flow Turbomachines_, a paper prepared at the Naval Postgraduate School, Monterey, Calif., 10 December 1971.

14. Horlock, J. H., Louis, J. F., Percival, P. M. E. and Lakshminarayana, B., "Wall Stall in Compressor Cascades," Trans. _ASME J. Basic Eng._, p. 637-648, September 1966.

15. Horlock, J. H., "Annulus Wall Boundary Layers in Axial Compressor Stages," Trans. _ASME J. Basic Eng._, p. 55-65, March 1963.

16. Hawthorne, W. R.,"Rotational Flow Through Cascades, Part I. The Components of Vorticity," _Quart. J. Mech. Applied Math._, v. VIII, p. 266-279, 1955.

17. Hawthorne, W. R., Armstrong, W. D., "Rotational Flow Through Cascades, Part II. The Circulation About the Cascade," _Quart. J. Mech. Applied Math._ v. VIII, p. 280-292, 1955.

18. Preston, J. H., "A Simple Approach to the Theory of Secondary Flows," _Aero. Quart._, v. V, p. 218-234, September 1954.

19. Liepmann, H. W. and Roshko, A., _Elements of Gasdynamics_, p. 191-193, Wiley, 1958.

20. Carta, F. C., "Unsteady Normal Force on an Airfoil in a Periodically Stalled Inlet Flow," _Journal of Aircraft_, v. 4, p. 416-421, October 1967.

21. Ericsson, L. E. and Reding, J. P., "Unsteady Airfoil Stall, Review and Extension, _Journal of Aircraft_, v. 8, p. 609-616, 1971.

22. Carta, F. O., "Effect of Unsteady Pressure Gradient Reduction on Dynamic Stall Delay," _Journal of Aircraft_, v. 8, p. 839-841, 1971.

23. _New Communications Define Propulsion Stability_, movie by Pratt and Whitney Aircraft.

24. Private Communication, James E. Calogeras, NASA Lewis Research Center, Cleveland, Ohio, 1 November 1971.

25. AIAA Paper No. 72-37, _A Method For Analyzing Dynamic Stall_, by P. Crimi and B. L. Reeves, January 1972.

26. Ward, J. F., "Helicopter Rotor Differential Pressures and Structural Response Measured in Transient and Steady-State Maneuvers," _J. Am. Helicopter Soc._, v. 16, p. 16-25, January 1971.

27. Squire, H. B. and Winter, K. G., "The Secondary Flow in a Cascade of Airfoils in a Nonuniform Stream," _J. Aero. Sci._, v. 18, p. 271-277, April 1951.

28. Carter, A. D. S., "Three-Dimensional-Flow Theories for Axial Compressors and Turbines," Proc. Instn. Mech. Engrs., v. 159, p. 255-268, 1948.

29. Hausmann, G. F., "The Theoretical Induced Deflection Angle in Cascades Having Wall Boundary Layers," J. Aero. Sci., v. 15, p. 686-690, November 1948.

30. ARC Report No. 17,519, Some Formulae for the Calculation of Secondary Flow in Cascades, by W. R. Hawthorne, March 1955.

31. Smith, L. H., "Secondary Flow in Axial-Flow Turbomachinery," Trans. ASME., v. 77, p. 1065-1076, October 1955

32. Ehrich, F. F., "Secondary Flows in Cascades of Twisted Blades," J. Aero. Sci., v. 22, p. 51-60, January 1955.

33. Honda, M., "Theory of Shear Flow Through a Cascade," Proc. R. Soc., v. 265, p. 46-70, 1961.

34. Private Communication, Robert P. Zalis, General Electric Co., Lynn, Mass., 29 Dec. 1971.

BIBLIOGRAPHY

35. AFOSR-TR-58-89, Performance of Axial Compressors with Asymmetric Inlet Flows, by R. Katz, Guggenheim Jet Propulsion Lab., Pasadena, Calif., June 1958.

36. AIAA Paper No. 70-941, Inlet-Engine Compatability Analysis, by J. L. Campbell and S. Ellis, June 1970.

37. A.R.C. Reports and Memoranda No. 3136, Secondary Flow and Losses in a Compressor Cascade, by J. F. Louis, March 1958.

38. Bowditch, D. N., "Inlet-Engine-Nozzle Wind Tunnel Test Techniques," AGARD Conference Preprint No. 91 on Inlets and Nozzles for Aerospace Engines, September 1971.

39. Burcham, F. W. and Bellman, D. R., A Flight Investigation of Steady-State and Dynamic Pressure Phenomena in the Air-Inlets of Supersonic Aircraft, paper presented at 38th Meeting of AGARD, Sandefjord, Norway, September 1971.

40. Conference on Internal Aerodynamics 1967, Internal Aerodynamics, "Methods of Treating Three-Dimensional Flows in Cascades and Blade Rows," by W. R. Hawthorne. Institution of Mech. Eng., Cambridge, July 1967.

41. Conference on Internal Aerodynamics 1967, Internal Aerodynamics, "Rotating Stall in Axial Flow Compressors," by J. Fabri, Institution of Mech. Eng., Cambridge, July 1967.

42. Cornell Aero. Lab., Inc., AFAPL-TR-67-19, Analytical and Experimental Investigation of Rotating Stall Phenomena in Turbine Engine Compressors, by W. G. Brady, G. R. Ludwig, R. S. Rice, Jr., and E. F. Schroeder, Buffalo, N. Y., March 1967.

43. Cornell Aero. Lab., Inc., AFAPL-TR-70-26, An Investigation of Rotating Stall Phenomena in Turbine Engine Compressors, by G. R. Ludwig, J. P. Nenni, and R. S. Rice, Jr., Buffalo, N. Y., May 1970.

44. Cornell Aero. Lab., Inc., AFAPL-TR-65-115, Part I, Basic Studies of Rotating Stall and an Investigation of Flow-Instability Sensing Devices, by W. G. Brady and G. R. Ludwig, Buffalo, N. Y., October 1965.

45. Csanady, G. T., Theory of Turbomachines, McGraw-Hill, 1964.

46. Ehrich, F. F. and Detra, R. W., "Transport of the Boundary Layer in Secondary Flow," J. Aero. Sci., p. 136-138, February 1954.

47. Ehrich, F., "Circumferential Inlet Distortions in Axial Flow Turbomachinery," J. Aero. Sci., v. 24, p. 413-417, June 1957.

48. Eichenberger, H. P., "Note About Secondary Flow in Cascades," J. Aero. Sci., v. 19, p. 137-138, February 1952.

49. Greenspan, H. P., The Theory of Rotating Fluids, p. 18-23, Cambridge Univ. Press, 1968.

50. Gregory-Smith, D. G., "An Investigation of Annulus Wall Boundary Layers in Axial-Flow Turbomachines," J. Eng. Power, v. 92, p. 369-376, October 1970.

51. Griepentrog, H., "Secondary Flow Losses in Axial Compressors," AGARD Lecture Series No. 39 on Advanced Compressors, May 1970.

52. Hawthorne, W. R. and Armstrong, W. D., "Shear Flow Through a Cascade," Aero. Quart., v. VII, p. 247-274, November 1956.

53. Hawthorne, W. R., "Secondary Circulation in Fluid Flow," Proc. Roy. Soc., v. 206, p. 374-387, May 1951.

54. Herzig, H. Z., and Hansen, A. G., "Visualization Studies of Secondary Flows With Applications to Turbomachines," Trans. ASME., vol. 77, no. 3, p. 249-266, April 1955.

55. Horlock, J. H., Axial Flow Compressors, Butterworths, 1958.

56. Huppert, M. C. and Benser, W. A., "Some Stall and Surge Phenomena in Axial Flow Compressors," J. Aero. Sci., v. 20, p. 835-845, December 1953.

57. Iura, T. and Rannie, W. D., "Experimental Investigation of Propagating Stall in Axial-Flow Compressors," Trans. ASME, v. 76, p. 463-471, April 1954.

58. Jansen, W. and Moffatt, W. C., "The Off-Design Analysis of Axial-Flow Compressors," J. Eng. Power, v. 89, p. 453-462, October 1967.

59. Kemp, N. H. and Sears, W. R., "Aerodynamic Interference Between Moving Blade Rows," J. Aero. Sci., v. 20, p. 585-597, September 1953.

60. Kimzey, W. F. and McIlveen, M. W., Analysis and Synthesis of Distorted and Unsteady Turbo Engine Inlet Flow Fields, paper presented at AIAA Seventh Propulsion Joint Specialist Conference, Salt Lake City, Utah, June 1971.

61. Lakshminarayana, B. and Horlock, J. H., "Effect of Shear Flows on the Outlet Angle in Axial Compressor Cascades - Methods of Prediction and Correlation With Experiments," Trans. ASME J. Basic Eng., v. 89, p. 191-200, March 1967.

62. Loos, H. G. and Zwaaneveld, J., "Secondary Flow in Cascades," J. Aero. Sci., v. 19, p. 646-647, September 1952.

63. Marble, F. E., "Propagation of all in a Compressor Blade Row," J. Aero. Sci., v. 22, p. 541-55, August 1955.

64. NASA TMX-2239 Experimental Investigation of the Effect of Screen-Induced Total Pressure Distortion on Turbojet Stall Margin, by J. E. Calogeras, C. M. Mehalic, and P. L. Burstadt, Lewis Research Center, Cleveland, Ohio, March 1971.

65. Schlichting, H. and Das, A., "On the Influence of Turbulence Level on the Aerodynamic Losses of Axial Turbomachines," Flow Research On Blading, edited by L. S. Dzung, p. 243-274, Brown, Boveri and Co. Limited, 1970.

66. Sears, W. R., "On Asymmetric Flow in an Axial-Flow Compressor Stage," J. App. Mech., v. 20, p. 57-62, March 1963.

67. Seidel, B. S., "Asymmetric Inlet Flow in Axial Turbomachines," J. Eng. Power, p. 18-28, January 1964.

68. Smith, A. G., "On the Generation of the Streamwise Component of Vorticity for Flows in Rotating Passages," Aero. Quart., p. 369-383, November 1957.

69. Stephenson, J. M., "Secondary Flow in Cascades," J. Aero. Sci., v. 18, p. 699-700, October 1951.

70. Vavra, M. H., Aero-Thermodynamics and Flow in Turbomachines, Wiley, 1960.

71. Von Karman, T. and Tsien, H., "Lifting-Line Theory For A Wing In Non-Uniform Flow," <u>Quart. J. App. Math.</u>, v. III, p. 1-11, April 1945.

72. Wislicenus, G. F., <u>Fluid Mechanics of Turbomachinery</u>, McGraw-Hill, 1947.

73. Wright Air Development Center Tech. Rep. 59-75, Parts I and II, <u>Research on Rotating Stall in Axial Flow Compressors</u>, by R. A. Hartunian, Cornell Aero. Lab., Inc., Buffalo, N. Y., January 1959.

74. Yeh, H., "An Actuator Disc Analysis of Inlet Distortion and Rotating Stall in Axial Flow Turbomachines," <u>J. Aero. Sci.</u>, v. 26, p. 739-753, November 1959.